

**Fragility Assessment of RC Structure
using Incremental Dynamic Analysis Considering
Variability of Ground Motion, Damping and Soil
Parameters**

By

GAGANDEEP SINGH

(ENGG01201801013)

Bhabha Atomic Reseach Centre, Mumbai

*A thesis Submitted to the
Board of Studies in Engineering Sciences*

*In Partial Fulfillment of Requirements
for the Degree of*

MASTER OF TECHNOLOGY

of

HOMI BHABHA NATIONAL INSTITUTE

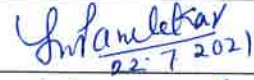
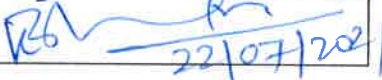


July, 2021

Homi Bhabha National Institute

Recommendations of the Thesis Examining Committee

As members of the Thesis examining Committee, we recommend that the thesis prepared by **Gagandeep Singh** entitled "**Fragility Assessment of RC Structure using Incremental Dynamic Analysis Considering Variability of Ground Motion, Damping and Soil Parameters**" be accepted as fulfilling the thesis requirement for the Degree of Master of Technology.

	Name	Signature
Member – 1	Dr. R.R. Rakesh	
Member – 2	Dr. Praveen Kumar	
Examiner	-	
Guide/Convenor	Dr. Smt. Y.M. Parulekar	 22.7.2021
Technical Advisor	Shri. Sumit T Bhamare	
Chairman	Dr. Kapilesh Bharghava	 22/07/2021

Final approval and acceptance of the thesis is contingent upon the candidate's submission of the final copies of the thesis to HBNI.

I hereby certify that I have read this thesis prepared under my direction and recommend that it may be accepted as fulfilling the thesis requirement.

Date: 20.7.2021

Place: RSD, BARC



Signature of Guide

Name of Guide: Dr. Smt. Y.M.Parulekar

DECLARATION

I, hereby declare that the investigation presented in the thesis has been carried out by me. The work is original and has not been submitted earlier as a whole or in part for a degree / diploma at this or any other Institution/university.


(GAGANDEEP SINGH)

ACKNOWLEDGEMENTS

I feel immense pleasure and privilege to express my deep sense of gratitude, and heartfelt sincere thankfulness towards my guide, Dr. Yogita Parulekar, Scientific Officer 'H', Structural and Seismic Engineering Section (SSES), Reactor Safety Division (RSD), Bhabha Atomic Research Centre (BARC) Mumbai & Professor, Homi Bhabha National Institute, Mumbai, for her invaluable guidance, constant supervision, continuous encouragement and support during this work. It is because of her great care and tender treatment that this project report could be brought to the present form within stipulated time frame.

I also extend my genuine thanks to Shri Srijit Bandyopadhyay Scientific Officer 'E', Structural and Seismic Engineering Section (SSES), Reactor Safety Division (RSD), Bhabha Atomic Research Centre (BARC), Mumbai, for his precious advice, ever extending co-operation and helping attitude during my project work.

I also would like to thank my Technological advisor Shri Sumit T Bhamare, Scientific Officer 'E' Engg- LWR group, for supporting me at various stages to undertake this project.

Last but not the least, I express thanks to the Almighty for his blessings and giving me courage to complete the project with great satisfaction.

(GAGANDEEP SINGH)

TABLE OF CONTENTS

SYNOPSIS.....	ix
LIST OF FIGURES.....	x
LIST OF TABLES.....	xiii
LIST OF ABBREVIATIONS.....	xiv
1 INTRODUCTION.....	1
1.1 General	1
1.2 Objective	2
1.3 Plan of work	2
1.4 Organization of thesis.....	3
2 LITERATURE SURVEY.....	5
2.1 General	5
2.2 Review of literature for IDA	8
2.3 Review of Literature for Fragility analysis	13
2.4 Other Literature	17
2.5 Summary of Literature Survey.....	17
2.6 Gap areas	18
3 MODAL ANALYSIS AND NONLINEAR STATIC PUSHOVER ANALYSIS	19
3.1 Details of structure	19
3.2 Material properties	24
3.3 Modeling of various structural and non-structural elements:.....	24
3.4 Modeling of hinges.....	24
3.5 Moment-curvature relationship.....	27
3.6 Modeling of masonry infill	32
3.7 Modal analysis.....	34
3.8 Non-linear static pushover analysis.....	38

3.9	Discussion on obtained pushover curves	40
3.10	Displacement ductility calculations	44
3.10.1	For X direction (Fixed support):	45
3.10.2	For Y direction (Fixed support):	46
3.10.3	Importance of bilinear idealization:	49
3.11	Concluding remarks	49
4	INCREMENTAL DYNAMIC ANALYSIS	51
4.1	General information on analysis procedures	51
4.2	Modeling of damping	51
4.2.1	Caughey damping	53
4.3	Soil structure interaction	56
4.4	Ground motion selection	58
4.5	Nonlinear time history analysis	61
4.5.1	Pivot hysteresis model	62
4.5.2	Assumptions of Pivot hysteresis model	63
4.5.3	Parameters for hysteretic response:	63
4.6	Incremental dynamic analysis (IDA)	69
4.6.1	Characteristics of IDA curves	71
4.7	Concluding remarks	91
5	FRAGILITY RELATIONSHIPS	92
5.1	Introduction	92
5.2	Briefing on limit states	93
5.3	Test for distribution of data	93
5.4	Development of fragility curves	95
5.5	Discussion on fragility curves	98
5.6	Concluding remarks on fragility curves	101
6	CONCLUSION	103
7	FUTURE WORK	105
	REFERENCES	106

SYNOPSIS

This report summarizes the evaluation of fragility curves of a RC structure using incremental dynamic analysis approach considering variability of ground motion, soil and structural damping properties. A detailed literature on Fragility analysis and incremental dynamic analysis is reviewed and presented. A G+3 RC framed structure is modeled in SAP2000 software. The nonlinear dynamic behavior of frame members is modeled in the form of nonlinear springs inserted at the ends of frame members. Soil is modeled in the form of springs considering variability of soil properties as per provisions of ASCE-4-2016 [1]. Structural damping is varied as 4%, 5% and 7%. The variation in ground motion is considered using 11 real earthquake data and one design basis ground motion of a NPP. Pushover analysis of structure, calculations of displacement ductility, hysteretic model and Rayleigh damping is also discussed. Subsequently, nonlinear direct integration time history analysis is performed in SAP2000 software to evaluate response of the structure when subjected to series of earthquakes and IDA curves are obtained. These curves are then operated by fragility evaluation procedure to obtain fragility curves at different damage limit states and at 5%, 50 % and 95 % confidence levels for X and Y directions. From the fragility curves, it is concluded that the structure in study has 60% probability of reaching damage state of Immediate Occupancy in X direction and 50% probability of reaching damage state of Immediate Occupancy in Y direction for a given value of $0.4g S_a$.

LIST OF FIGURES

Figure 2.1: Different behavior of IDA curves	9
Figure 3.1 RC structure considered	19
Figure 3.2 Typical floor Plan of Building.....	20
Figure 3.3: Section X-X (Refer Figure 3.1).....	20
Figure 3.4: Typical plan of building in SAP2000.....	21
Figure 3.5: 3D view of SAP2000 model of building	21
Figure 3.6: Assignment of hinges to beams and columns	25
Figure 3.7: Force-displacement curve for hinge input.....	26
Figure 3.8: Moment curvature curve	27
Figure 3.9: Kent and Park model for concrete	28
Figure 3.10 Stress-strain curve for HYSD Fe500 steel (IS 456:2000)	28
Figure 3.11: M- ϕ curve for beam sections of RC frame under ‘hogging’ bending moment	30
Figure 3.12 Hinge property of beams B1 and B2 (as input to SAP2000)	30
Figure 3.13: M- ϕ curve for column C1 acting in Y direction	31
Figure 3.14: M- ϕ curve for column C1 acting in X direction	31
Figure 3.15: Equivalent strut representation for infill wall.....	33
Figure 3.16 Deformed shape of building for mode no. 1 (first mode X-direction).....	35
Figure 3.17 Deformed shape of building for mode no. 2 (Y direction).....	36
Figure 3.18 Deformed shape of building for mode no. 7 (Z direction)	36
Figure 3.19: Deformed shape of the frame for analysis in X-direction	39
Figure 3.20: Deformed shape of the frame for analysis in Y-direction	40
Figure 3.21: Pushover curves for fixed support.....	41

Figure 3.22: Pushover curves for 1.0G support	42
Figure 3.23: Pushover curves for X direction.....	42
Figure 3.24: Pushover curves for Y direction.....	43
Figure 3.25: Pushover curves for X and Y direction for all support cases	43
Figure 3.26 Bilinear idealization -X direction for fixed Support.....	45
Figure 3.27 Bilinear idealization -X direction for fixed Support(FEMA 356).....	46
Figure 3.28: Bilinear idealization -Y direction for fixed support	47
Figure 3.29: Bilinear idealization Y direction for fixed support (FEMA 356).....	47
Figure 4.1: Normalized response spectra for 12 time histories for 4% damping	60
Figure 4.2: Normalized response spectra for 12 time histories for 5% damping	60
Figure 4.3: Normalized response spectra for 12 time histories for 7% damping	61
Figure 4.4: Pivot point designations	64
Figure 4.5: Moment-rotation curve for link X direction.....	67
Figure 4.6: Moment-rotation curve for link Y direction.....	67
Figure 4.7 Force deformation curve for link element for 0.4g scale factor X direction.....	68
Figure 4.8: Force deformation curve for link element for 1.8g scale factor, X direction.....	68
Figure 4.9: Force deformation curve for link element for 0.4g scale factor direction.....	69
Figure 4.10: IDA curves for 2 ground motion records for fixed support for 7% damping	72
Figure 4.11: Flattened IDA curves for 2 time histories	73
Figure 4.12: IDA curve for Whittier Narrows TH with different Damping for fixed support	74
Figure 4.13: IDA curve for Loma Gilroy2 TH with different damping cases	75
Figure 4.14: IDA curve for TH-Coyote for all 12 cases (X direction)	78
Figure 4.15: IDA curve for TH-Kobe for all 12 cases (X direction)	79

Figure 4.16: IDA curve for TH-El Centro for all 12 cases (X direction)	80
Figure 4.17: IDA curve for TH Chi-chi for all 12 cases (X direction)	81
Figure 4.18: IDA curve for TH-Imperial Valley for all 12 cases (X direction).....	82
Figure 4.19: IDA curve for TH-Loma Gilroy2 for all 12 cases (X direction)	83
Figure 4.20: IDA curve for TH-Mammoth Lake for all 12 cases (X direction)	84
Figure 4.21: IDA curve for TH-Nahaani for all 12 cases (X direction)	85
Figure 4.22: IDA curve for TH-Northridge for all 12 cases (X direction)	86
Figure 4.23: IDA curve for TH-Parkfield for all 12 cases (X direction)	87
Figure 4.24: IDA curve for TH-Tarapur DBE for all 12 cases (X direction)	88
Figure 4.25: IDA curve for TH-Whittier Narrows for all 12 cases (X direction).....	89
Figure 4.26: IDA curves for all cases for X direction.....	90
Figure 5.1: Histogram for data distribution of spectral acceleration values	94
Figure 5.2: Q-Q plot for logarithm of first mode spectral acceleration values.....	94
Figure 5.3: Sample fragility curve [44].....	97
Figure 5.4: Fragility curves for Y direction for IO(2% drift)	98
Figure 5.5: Fragility curves for Y direction for LS (4% drift).....	99
Figure 5.6: Fragility curves for Y direction for CP (6% drift).....	99
Figure 5.7: Fragility curves for X direction for IO(2% drift)	100
Figure 5.8: Fragility curves for X direction for LS(4% drift).....	100
Figure 5.9: Fragility curves for X direction for CP(6% drift).....	101

List of Tables

Table 3.1: Geometric data of the building	22
Table 3.2: Cross section of frame members.....	22
Table 3.3 Frequency and mass participation in different modes for fixed support	34
Table 3.4: Frequency for various support cases.....	37
Table 3.5: Comparison of fundamental modes frequencies for structure with fixed support	37
Table 3.6: Bilinear curve comparison for 4 support conditions for X direction.....	48
Table 3.7: Bilinear curve comparison for 4 support conditions for Y direction.....	48
Table 4.1 : Rayleigh coefficients for X direction	55
Table 4.2: Rayleigh coefficients for Y direction	55
Table 4.3: Soil Spring constants	56
Table 4.4: Foundation Soil Properties	57
Table 4.5: Spring stiffness	58
Table 4.6: Ground motion records	59
Table 4.7: Parameters for Pivot model	66
Table 5.1: Drift limits	93
Table 5.2: Median and standard deviation for X and Y direction	97

Abbreviations:

PGA: Peak Ground Acceleration

PGV: Peak Ground Velocity

IO: Immediate Occupancy

LS: Life Safety

CP: Collapse Prevention

S_a: Spectral Acceleration

IDA: Incremental Dynamic analysis

NLTHA: Non-Linear Time History Analysis

NLSPA: Non-Linear Static Pushover Analysis

1 INTRODUCTION

1.1 General

Nowadays, deterministic structural assessment methods are thought to be insufficient to define structural behavior under earthquake effect. This is mainly because of the uncertainty and randomness of variables in the analysis for earthquake loads. It is thus essential to include probabilistic assessment into the analysis. Fragility analysis which is a system reliability analysis with correlated demands and capacity is required to be performed to establish the probabilistic characterization of the demands in different ways.

Fragility curves are derived from the statistical evaluation of the results of numerical analyses carried out on structural models. For large scale fragility analyses, demand and capacity can be determined using analytical method like Incremental Dynamic Analysis (IDA). IDA is a parametric non-linear dynamic analysis method used to estimate the structural performance under several ground motions and includes the development of one or more curves of a specific damage measure(DM) (i.e. maximum storey drift as a percentage) versus an intensity measure (IM) of the ground motion (peak ground or spectral acceleration). Thus, a probabilistic approach is used to conduct the vulnerability and risk assessment of structures. Generation of IDA curves can take into account various uncertainties such as variability in ground motion (demand), variability in damping, variability in modeling of the structure and variability in soil parameters. Till date researchers have incorporated variability of ground motion and carried out incremental dynamic analysis of various structures [2]. However, variability of energy dissipating capability and variation in soil parameters along with ground motion variability was not considered by them. The variability in soil parameters will lead to variability in soil structural interaction. Hence, there is a need to generate IDA curves for a structure considering variation in soil structure interaction,

structural damping and ground motion. After generation of numerous IDA curves considering all these variability parameters, fragility curves are needed to be generated. Different limit states are defined as per FEMA-440 guidelines based on various damage measures such as interstorey drift, roof displacement, roof drift etc. The fragility curves are required to be derived at different limit states of the structure.

In this project a simple three storied reinforced concrete (RC) framed structure is proposed to be studied using fragility analysis considering variability in ground motion, damping and soil structure interaction.

1.2 Objective

The objective of the project is to perform incremental dynamic analysis on a RC framed structure considering the nonlinearity in its frame elements till the collapse of the structure. It is aimed to generate several IDA curves for different real earthquake time histories, with different values of damping of the structure and taking into account the soil uncertainties. Lastly it is intended to generate fragility curves for the RC structure for different performance levels or damage measures of immediate occupancy, life safety and collapse prevention.

1.3 Plan of work

The scope of work in the project is described as follows

- i. Numerical modeling of selected RCC structure in SAP2000 using frame elements.
- ii. Deriving moment-curvature relationships for beams and columns based on their cross section at junctions using Kent and Park model.
- iii. Assigning hinge properties to beam and columns using moment curvature relationship derived in step (ii).

- iv. Performing nonlinear static pushover analysis in SAP2000 using displacement controlled condition in both the directions.
- v. Based on the results of pushover analysis, assigning link elements (Based on Pivot model) to the hinges undergoing full deterioration (if any).
- vi. Performing Nonlinear time history analysis (NLTHA) using direct integration method in SAP2000 with variation in ground motion. In this study, 12 earthquake records were selected (11 records from the Pacific Earthquake Engineering Research (PEER) Center Strong Motion Database (2000) and 1 record of design basis earthquake of Tarapur Atomic Power Plant).
- vii. Carrying out NLTHA, taking into consideration the variation of damping properties of structure (3 nos. damping %) for each ground motion and for each damping taking into consideration the variation in soil properties with 0.5G, G and 2.0G as soil stiffness along with fixed support case.
- viii. Generating 144 numbers of IDA curves.
- ix. Developing fragility curves (considering lognormal distribution) at the limit states of immediate occupancy, life safety, and collapse prevention and generating them for different confidence levels (5%, 50% and 95%).

1.4 Organization of thesis

Chapter 1: INTRODUCTION deals with general introduction, need, importance and background of proposed study. It also presents the plan of work followed during the study.

Chapter 2: LITERATURE SURVEY initially deals with discussion on vulnerability analysis followed by discussion on fragility curves for risk assessment of building. Further, this chapter

includes discussion on works carried out by various researchers in the direction of fragility and IDA followed by summary of the literature survey and gap areas in the study.

Chapter 3: MODAL ANALYSIS AND NONLINEAR STATIC PUSHOVER ANALYSIS discusses the detailed model of the building explaining the geometric data of building, properties of materials and cross section of the beams and columns used. Modal analysis, nonlinear static pushover analysis results and displacement ductility calculations are also presented.

Chapter 4: INCREMENTAL DYNAMIC ANALYSIS briefs the procedure of incremental dynamic analysis (IDA) for twelve different ground motions, four different soil conditions and three different damping values followed by discussion on obtained IDA curves.

Chapter 5: FRAGILITY RELATIONSHIPS discusses the procedure for derivation of fragility curves from IDA data. The fragility curves obtained are presented for different limit state levels given by FEMA-356 at various confidence levels.

Chapter 6: CONCLUSIONS discusses the detailed conclusions of the work

Chapter 7: FUTURE WORK presents few points of the work which can be done in future.

2 LITERATURE SURVEY

2.1 General

Indian subcontinent is one of the earthquake prone regions of the world. The Bhuj earthquake in 2001 highlighted the vulnerability of Indian Buildings and the need for proper seismic risk assessment in India. Seismic risk assessment requires collaboration of various fields like seismology for hazard estimation, structural engineering for vulnerability of structures and for economic impact etc.

For seismic risk analysis simplified methods were used initially like expert opinion based methods (ATC 1985) [3] and vulnerability index based methods (Barbat et al.) [4] . The capacity spectrum based methods (CSBM) developed by S. A. Freeman [5] are also used for assessing seismic risk. The CSBM is based on nonlinear static pushover analysis. The vulnerability of buildings in CSBM methods is defined with help of fragility curves. Nonlinear dynamic analysis though time consuming but gives more realistic results in vulnerability estimation and it considers the uncertainty of ground motions.

Earlier predictions of risk assessment were mainly based on deterministic methods because of limitations of computer technology when it was very cumbersome to adopt all the inherent uncertainties in various sources. But now computation can include all those uncertain factors which have made probabilistic methods highly popular. Vulnerability assessment of buildings using fragility curves is widely practiced approach these days [6]. Fragility theory is a branch of structural reliability, which aims to assess the vulnerability of a structure subjected to some extreme load or hazard of known intensity. For seismic hazards, fragility analysis studies the probability that a structure exceeds a certain limit state for a given ground motion parameter.

Fragility curves are used in Seismic Probabilistic risk assessment i.e. SPRA. The Fragility relationships are a required input for commercial loss assessment software. Fragility curves help to identify the level of damage in structure which makes them an indispensable tool for probabilistic assessment [7].

Earlier forms of fragility curves were developed based on post damage data and expert opinions i.e. Empirical curves. Empirical methodologies suffer from lack of post-earthquake damage data and are based on judgment. The analytical methodologies can be employed in which a single structure believed to be representative of a class of buildings or a set of randomly generated buildings are modeled using finite element techniques, and tested against specific loading patterns or ground acceleration time histories [8] but recent developments in nonlinear analysis have enabled development of analytical fragility curves using analysis consistent with the design codes.

Seismic fragility can generally be expressed as:

$$\text{Fragility} = \Pr [D \geq C | IM] = \Pr [C - D \leq 0.0 | IM] \quad (2.1)$$

Where D implies demand parameter

C implies Capacity of structure

IM implies intensity measure

An adequate number of ground motions are necessary to conduct accurate seismic fragility analyses.

The fragility curves at different confidence levels are prepared i.e. 5%, 50% and 95%. The 95% confidence curve means that the analyst has 95% confidence that the true fragility curve lies to the right of 95% curve. Vertical axis on fragility curve is conditional probability of failure. Horizontal

axis is ground motion parameter like PGA (peak ground acceleration), average spectral acceleration.

The fragility curves are also affected by height of the building and the IM adopted. Considering PGA as the intensity measurement works well for 3 storey buildings. However, with the increase of the number of storeys, PGA may not be a good intensity measure to derive fragility curves. Despite PGA, S_a works better for all buildings. Structural vulnerability increases with the increase of the number of storeys [7].

As discussed by Rossetto and Elnashai (2005) [9], there is not a unique methodology for the development of fragility functions and therefore, the resulting curves will be conditional on the assumptions and techniques followed in the process and discrepancies coming due to the different approaches will consequently produce significant variations in the risk assessments, even when considering the exact same region, seismicity and type of structures.

There are 2 groups of methodologies: nonlinear dynamic analysis and nonlinear static analysis, each one having its own strengths and weaknesses. Application of nonlinear dynamic analysis reproduces the actual phenomenon by applying an acceleration time history at the base of the structure, which leads to more accurate results and uncertainty of ground motion can also be considered.

In this study, Incremental dynamic analysis has been adopted as nonlinear dynamic analysis. IDA is the first step in developing fragility curves. Incremental dynamic analysis (IDA) is a parametric analysis method which is basically similar to static pushover analysis (SPA). In SPA structure is subjected to increasing lateral load but in IDA, structure is subjected to changing ground motions derived from original motions by using scale factors and thus producing curves for response. Due

to this analogy IDA is also sometimes called as Dynamic Pushover Analysis [2]. Federal Emergency Management Agency (FEMA) [10] has also elaborated the procedure to derive IDA curves and establish global stability capacity in its guidelines [11]. IDA curves have also been used to ascertain the effect of corrosion on the performance level of RCC buildings [12].

In most of the research work the uncertainty in ground motion is realized by selecting a large number of ground motions from various regions. In this work 11 number of Earthquake motions are selected from all around the world and 1 design basis earthquake of NPP. Further for each ground motion scaling is performed as per fundamentals of IDA curve generation.

2.2 Review of literature for IDA

Vamvatsikos & Cornell, Incremental dynamic analysis, 2002 [2] Research paper on IDA explained the fundamentals of IDA curves- scale factor, Intensity measure and Damage Measure. The peculiarities of IDA curves like softening, hardening, discontinuity and non-monotonicity (Figure 2.1) were explained using SDOF oscillators and five steel moment resisting frames of different storeys with maximum up to 20 storey. The inclusion of probabilistic framework into IDAs, legitimacy of using scale factor for ground motion records, relationship between IDAs with R-factors and comparison of IDA curves with SPO (Static pushover analysis) curves were also addressed. The algorithm for generating IDA curves were discussed in the end mentioning stepping algorithm and their own developed Hunt & fill tracing algorithm. The hunt and fill algorithm is divided into hunt and fill phase. This algorithm hunts for final point on IDA curve satisfying the failure criteria by constantly increasing spacing of IMs. Then filling is performed to fill the gaps both demand wise and capacity wise to generate required adequate number of points for IDA curve.

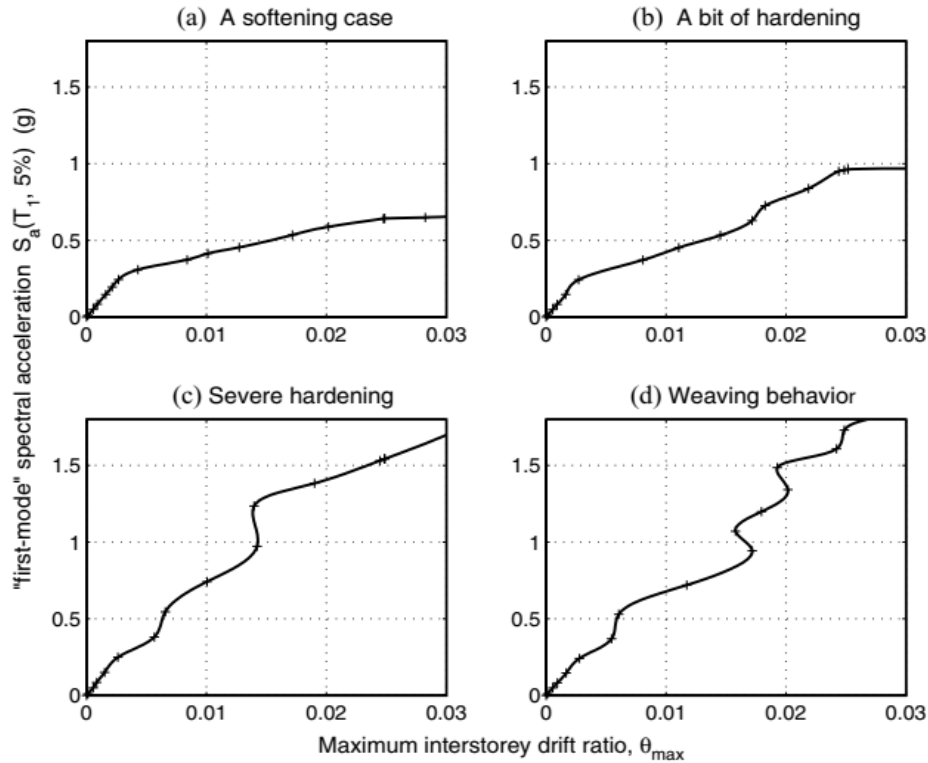


Figure 2.1: Different behavior of IDA curves

Vamvatsikos & Cornell, 2004 [13] Has given a thorough understanding of IDA from scratch using 9 storey steel moment resisting frame. The selection of ground motion suites, sensitivity of no. of runs, interpolation of IDA curves, calculation of mean annual frequency using PBEE framework are demonstrated. The relationship between median IDA curve and SPO (Static pushover curve) is drawn out. Selection of an IM level for each run is dependent upon tracing algorithm used. The superiority of Hunt and fill algorithm over stepping algorithm is also justified based on their sensitivity to algorithm parameters. The sensitivity to the record suite size is derived using bootstrap estimation technique.

Dolsek, 2009 [14] Extended the IDA by adopting a set of structural models (epistemic uncertainty) in addition to set of ground motion records (aleatory uncertainty) in generating IDA curves. The procedure of using Latin Hypercube sampling in selecting sets of structural models was explained

thoroughly. The number of sets of structural models considered changed the results. It was found that input random variables were properly sampled if the size of set of structural models is larger than size of set of input random variables. IDA curves were also generated using variability in ground motion records only and it was observed on comparing that epistemic uncertainty does not have significant influence on the seismic response parameters in the range far from collapse. But near collapse their accounting into IDA process is highly recommended.

Vamvatsikos & Fragiadakis, Incremental dynamic analysis for estimating seismic performance sensitivity and uncertainty, 2010 [15] Performed IDA on a 9 storey steel moment resisting frame to study the model parameter uncertainty. Uncertainty was established in the moment-rotation relationship of beam plastic hinges. Six properties of this moment-rotation curve like Yield moment, post-yield hardening ratio, end of hardening rotation, slope of descending branch, residual moment capacity and ultimate rotation were used as uncertain parameters. The model parameter uncertainty was propagated to seismic behavior using Monte Carlo simulation using LHS (Latin Hypercube Sampling), point estimate method and first-order second moment (FOSM) techniques. Results indicated that Monte Carlo provided best estimates but simpler techniques of FOSM and PEM (Point Estimate Method) did not result in much error. Therefore, FOSM and PEM are suitable for uncertainty propagation. It was concluded that median-parameter model need not always produce median seismic demand and capacity with accuracy. SRSS rule for combining aleatory and epistemic uncertainty produced almost accurate estimates of total dispersion for some of limit states but produced significant errors for other limit states.

Azarbakht & Dolsek, Progressive incremental dynamic analysis of first mode dominated structures, March 2011 [16] Proposed progressive incremental dynamic analysis to predict summarized IDA curves (i.e. 16th, 50th and 84th fractiles) in situation where number of ground

records is too large for computation analysis. This is based on the behavior of summarized IDA curves which do not change with increase in records after analysis of certain number of ground motion records. The difference between progressive and normal IDA is that the former uses precedence list of ground motion records. This precedence list is first established and then optimized. This basically involves first developing a simple SDOF (single degree of freedom) representation of complex MDOF (Multi degree of freedom) model. For this simple model IDA is performed for all records and summarized IDA curves are generated. Then using proposed procedure precedence list of records is established and IDA curves for original model are computed only for selected number of records in order of list. When the required tolerance in prediction of summarized IDA curves is achieved, the analysis is terminated.

Yalciner, Sensoy, & Eren , 2012 [12] Performed incremental dynamic analysis to predict the time dependent seismic performance level of a building under the effect of corrosion. Three time instants 0 (non-corroded), 25years and 50 years were considered. Three combined effects of corrosion (loss in rebar cross sectional area, reduction in concrete compressive strength and bond slip relationships) were considered in deriving fragility curves. Plastic hinge properties were derived from predicted time dependent moment curvature relationships. The fragility curves derived revealed the considerable effect of bond strength on seismic performance level.

Zhu & Qiu, 2014 [17] Carried out seismic performance evaluation of SC (Self-centering) SMA (Shape memory alloy) isolators using IDA of a prototype highway bridge with SMA isolators. The SMA based isolators and Prototype Bridge was designed as per DBD (displacement based design) approach. Nitinol SMA's were used in this study. Stress-strain characteristics were derived as per modified Wilde model. Highway model was idealized as an equivalent SDOF in DBD approach assuming mass of pier is relatively small compared to deck. The suitability of this SDOF model

was studied by comparing its seismic IDA curves with that of MDOF model and it was observed that SDOF approach is suitable only under low seismic intensity levels. This study concluded that SMA isolators are quite effective in preventing superstructure of highway-bridge and can minimize post-earthquake residual deformation.

Banerjee, Pramanik, & Roy, 2016 [18] Highlighted the seismological inconsistency of using scale factors for scaling records in IDA and cumbersome nature of ground motion selection in MSA (multiple strip analysis). The authors proposed a new method that involves time domain spectral matching of real accelerograms by selecting CMS (conditional mean spectrum) associated with different return periods. Real accelerograms are intensified by spectrally matching them to CMS of different return periods. Synthetic motions were also generated and matched with CMS. The fragility curves generated using proposed method showed smaller variation between IDA and MSA based median estimates as compared to conventional approach. Even the dispersion in different IMs was lower than conventional approach.

Hosseinpour & Abdelnaby, 2017 [19] Derived fragility curves for 3, 7 and 12 storey RC frame building subjected to as recorded seismic sequences with fiber based modeling approach. The effect of main shocks, complete sequence, aftershocks with damage from main shocks and without previous damage was considered in deriving fragility curves. The study concluded that increasing number of storeys increases vulnerability of structure. Also aftershocks with damage from previous events showed highest probability of exceedence. The vertical component of earthquake showed no effect on fragility curves. The curves were derived with IM as S_a and PGA. It was concluded that PGA worked well for 3 storey building but for higher storeys, S_a is better choice.

2.3 Review of Literature for Fragility analysis

Shinozuka, Feng, Naganuma, & Lee, 2000 [6] Developed empirical fragility curves of bridges using post damage data collected after 1995 Kobe earthquake event. Also analytical fragility curves were developed using dynamic analysis. PGA was chosen as the IM. Both curves were developed assuming two parameter lognormal distribution and parameters were calculated using maximum likelihood function. The statistical procedure of goodness of fit and the confidence interval estimation for calculated parameters for developed curves were explained in detail. The development of combined fragility curves for representing family of bridges was also covered.

Erberik & Elnashai, 2004 [20] Performed fragility analysis of medium rise flat-slab building with masonry infill walls. The ten different ground motions records were used with criteria that elastic spectrum from these curves be compatible with code prescribed spectrum. Because of difference in behavior of flat slab buildings, limit states defined were different from conventional moment resisting frames. Four limit states- slight, moderate, extensive and complete were assigned to building in terms of inter-storey drift. Material uncertainty was accounted with Latin hypercube sampling. Spectral displacement was used as IM (Intensity measure) or Hazard parameter. The fragility curves developed were compared with those of Moment resisting frames and it was concluded that applicability of vulnerability curves of moment resisting frames for flat slab structures is non-conservative.

Erberik M. A., 2008 [8] Developed reference seismic fragility curves using building database of Turkey. These reference curves were then used to investigate the influence of sampling techniques, sample size, type of hysteresis model and limit state definition on fragility curves. PGV was used

as IM. Buildings considered were classified as low rise and mid-rise. The buildings were modeled as equivalent SDOF system with 3 structural parameters: period, strength ratio and post-yield to initial stiffness ratio which were obtained for each building after performing bilinear idealization on capacity curves obtained from SAP2000. It was observed that fragility curves were highly sensitive to degradation characteristics and definition of limit states. The sample size and simulation techniques hardly made any appreciable difference in fragility curves. In the end the fragility curves derived were used to predict damage to the buildings in database. The actual damage data from 1999 earthquake in Turkey was compared with predicted one. The result showed that derived curves were slightly overestimated but the results were good for crude estimation.

Liel, Haselton, Deierlein, & Baker, 2009 [21] Proposed a simplified procedure to incorporate structural modeling parameter uncertainties into collapse assessment. The developed procedure combines capabilities of Monte Carlo and response surface methods. Using sensitivity analysis, the effect of each random variable on structural response is determined by varying a single modelling parameter and reevaluating the structure's performance. The results of sensitivity analysis provides response surface. Then, Monte Carlo method is used to sample the modal random variables and structural response is predicted by response surface. The outcome of the method was fragility curves. Applying this method on RC frames, it was concluded that exclusion of modeling uncertainties is always non-conservative. It can affect the median of response fragility by as much as 20%.

Asgarian, Yahyai, Mirtaheri, Samani, & Alanjari, 2010 [22] Performed seismic fragility analysis of 435m high Tehran telecommunication tower. The structure was modeled as 2D fiber beam element as well as 3D elastic and inelastic multi-axial element based model. The results of 2D model were almost matching 3D model which showed the structure can be simplified

analytically without accuracy limitations. Both S_a and PGA were selected as IM and the results showed higher dispersion for the IDA curves of PGA. Since for long structures higher modes have significant participation, the limitation of using S_a was also highlighted.

Lee & su, 2012 [23] proposed a simple coefficient based method to approximate first modal spectral acceleration values of low rise masonry in filled RC Buildings. Experimental results of shake table tests were collected and through regression analysis three equations were proposed. 1st equation relates PGA to interstorey drift ratio, 2nd equation relates PGA to period shift factor. The period shift factor gives the effect of period lengthening with increase in intensity of ground shaking. The last equation relates PGA to spectral acceleration. These all equations along with standard equations to estimate fundamental time periods of structure were used to estimate values of spectral acceleration and interstorey drift ratio. On basis of these equations fragility curves for standard models were estimated which showed good correlation with experimental results. The method proposed provides a good alternative to bypass huge computations involved in arriving at fragility curves.

K. Mondal, Ghosh, & N. Pujari, 2016 [24] Performed seismic fragility analysis of primary containment structure of 700MWe Indian PHWR and compared different methods for fragility evaluation. Containment shell was idealized as 2D stick model in open sees platform. PGA (preferred in Nuclear Industry) was used as IM. 24 earthquake records were used in analysis. Regression and maximum likelihood methods were discussed in detail. Discrete Fragility values using IDA data were compared with continuous estimation of fragility curve using conventional method (based on NSPA data), regression method, maximum likelihood method and a new proposed method. It was drawn out that likelihood method is computationally intensive but gives good estimate. The conventional method overestimates the fragility values. The regression method

is light in computation but fails to provide good estimates at higher intensity levels. The method given by authors is light in computation and also provide reasonably good estimate.

Liu, Chen, Yuan, & Shao, 2017 [25] Applied IDA procedure to perform fragility analysis of an underground subway station structure. Structure was modeled in ABAQUS. Ground motions were scaled such that PGV varies from 5 cm/s to 80 cm/s. Both PGA and PGV were adopted as IM in the study. Maximum storey drift angle, central column damage and energy ratio were chosen as DM. The selection of central column damage as DM was based on understanding that central column is weakest component of underground structure under earthquake excitation. The limit states were defined in terms of deformation and water proof performance of subway structure. The study concluded that PGV is better indicator than PGA. The structure investigated also proved unsafe for collapse prevention at design seismic intensity levels. The average conversion process to calculate PGV from PGA was also discussed in the paper.

Basone, Cavaleri, Trapani, & Muscolino, 2017 [26] Performed Fragility analysis using IDA on 4 structural models with different level of complexity with stationary, non-stationary evenly modulated (NSEM) and fully non stationary accelerograms (FNS). The results were compared to give insights about using stationary, NSEM and FNS accelerograms. Stationary accelerograms produced highest demand in terms of interstorey drifts for all structural configurations considered. The intensity measure (IM) was crucial in defining collapse probability which was highest for FNS accelerogram in case of Spectral acceleration as IM and highest for stationary accelerogram in case of PGA as IM. Therefore IM needs be carefully considered in case of artificial accelerograms. Also the demand in case of FNS and NSEM accelerogram was similar.

Moon, Lee, & Lee, 2018 [27] Performed fragility analysis on buildings with varying plan irregularities from 0 to 10%. Failure probability was calculated using first order reliability

methods. Material uncertainty along with ground motions was used in analysis. An integrated computational framework was established to combine reliability and structural analysis. As per findings the proposed makes it possible to use computationally expensive models easily. Ground motion records were categorized as per PGA/PGV ratio. Numerical results showed the increase of vulnerability with increase in plan irregularity. Failure probabilities using proposed method and Monte Carlo simulations were also compared which showed superiority of proposed method.

2.4 Other Literature

Inel & Ozman, 2006 [28] carried pushover analysis on 3 and 7 storey RC frame using default and user defined hinge properties in SAP2000 and studied the difference between the results. The effect of plastic hinge length and transverse reinforcement was also studied. It was concluded that plastic hinge length and transverse reinforcement have no influence on base shear capacity but considerable effect on displacement capacity of frames. Increasing the spacing of transverse steel reduces the displacement capacity. Time history analysis was also performed and the hinging pattern was studied. It was seen that plastic hinge formation in upper levels was not adequately captured by pushover analysis.

2.5 Summary of Literature Survey

Nonlinear time history analysis can more accurately predict the hinging pattern in building as compared to pushover analysis. PGA as an IM is useful in nuclear structures. However for conventional buildings as well as high rise towers, S_a brings lesser variability in EDP (Engineering Demand Parameter) than PGA. The lesser the variability in EDPs, more is the suitability of IM. The effect of epistemic uncertainty is more pronounced in near collapse regions for buildings but for other states it hardly influences seismic parameters. Fragility estimation is post processing intensive exercise and it requires sound knowledge of statistical techniques. Use of Hunt and fill

algorithm and computer programs like Opensees has significantly reduced the time of obtaining IDA curves. The IDA though majorly used for buildings also bear significant applicability in assessing risk for bridges, underground subway station and containment structure of nuclear power plant also. Most of the buildings in a region are more or less similar, hence can be grouped into categories and reference fragility curves for such region can be established which will give a crude estimation of damage occurred during an earthquake. The fragility curves derived for a building while experiencing aftershocks of an earthquake event with damage from previous events showed that building become more vulnerable in exceeding damage parameter. Scale factors used in IDA analysis is a topic that raises doubts on its legitimacy. Consequently new techniques to scale are being evolved. Scaling records by intensifying them by spectrally matching those records with conditional mean spectrum of different return periods is one of such techniques.

2.6 Gap areas

1. Significant amount of research has been carried out in fragility analysis of buildings, bridges, nuclear structures and underground structures.
2. For buildings uncertainty in modeling as well as ground motion records is mostly used. However, the variation in structural damping parameters and soil parameters are not considered together with ground motion uncertainty using IDA.
3. This gap area w.r.t consideration of uncertainty in soil, earthquake ground motion record and damping parameters is taken up in this study to derive fragility curves.

3 MODAL ANALYSIS AND NONLINEAR STATIC PUSHOVER ANALYSIS

3.1 Details of structure

For the purpose of this study, a G+3 storey single bay RCC frame building (Figure 3.1, Normal building) with a rectangular floor plan (Figure 3.2) constructed at IIT-Guwahati for experimental purposes is considered. Numerical model of the building has been created in SAP2000. The height of the building is 11.7m excluding 1.2m parapet wall. The plan dimensions are 3.3m x 4.5m (Figure 3.2). The geometrical model of the building along with dimensions is shown in Figure 3.3. The typical plan and 3D model of this building in SAP2000 is given in Figure 3.4 and Figure 3.5 respectively. The geometric data of the building is presented in Table 3.1.

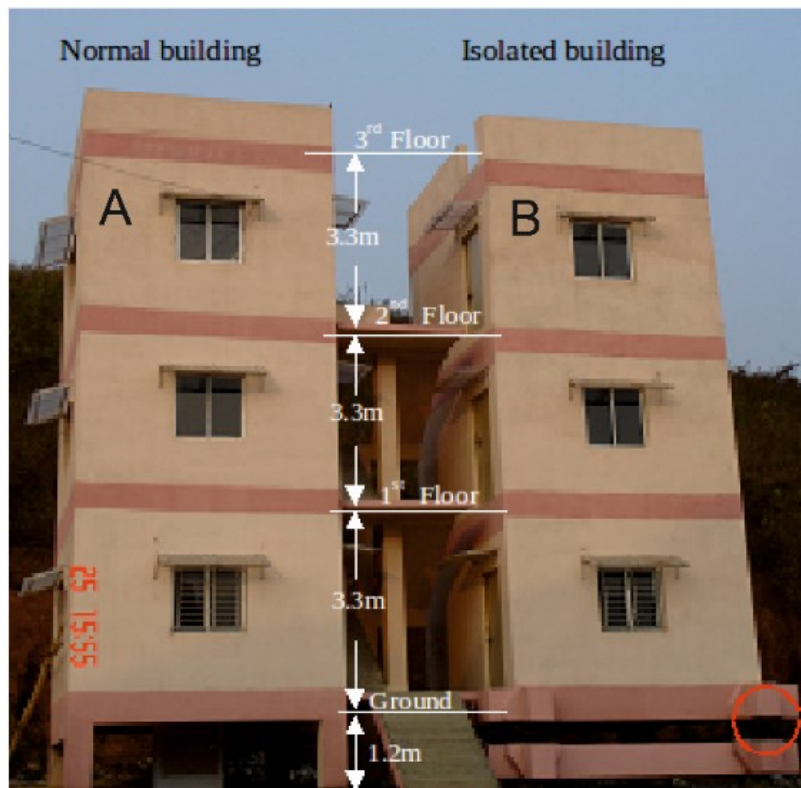


Figure 3.1: RC structure considered

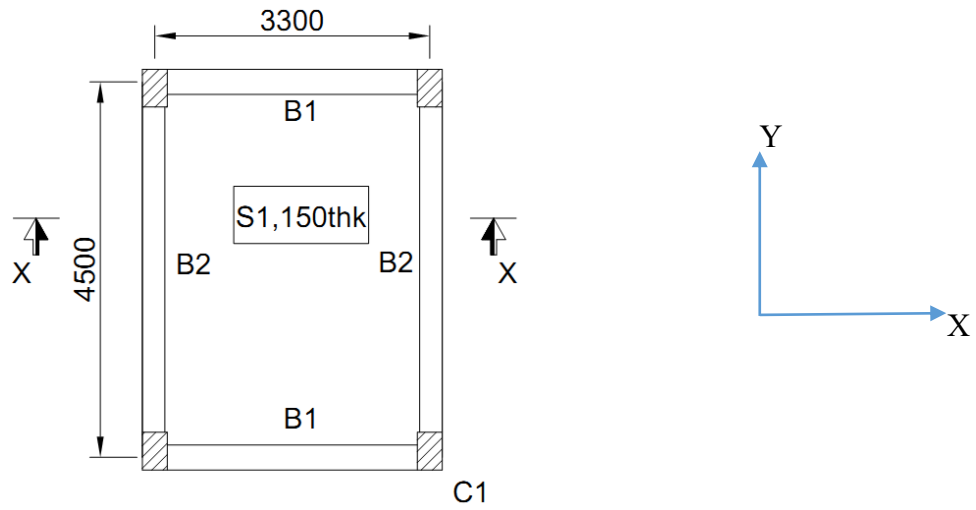


Figure 3.2: Typical floor plan of building

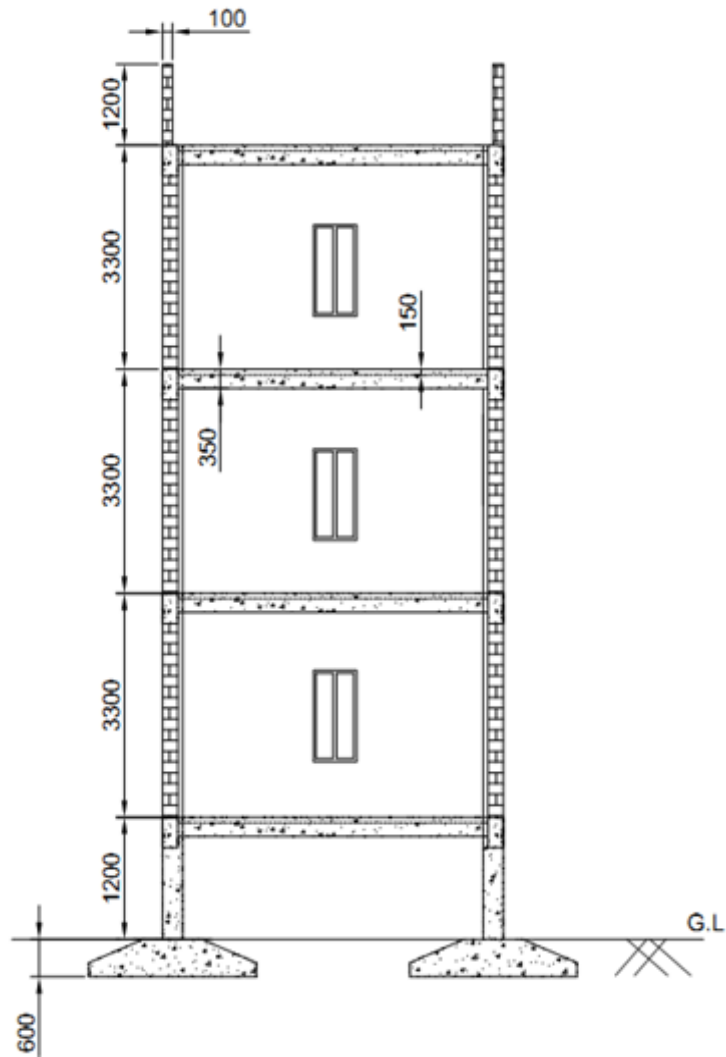


Figure 3.3: Section X-X (Refer Figure 3.2)



Figure 3.4: Typical plan of building in SAP2000

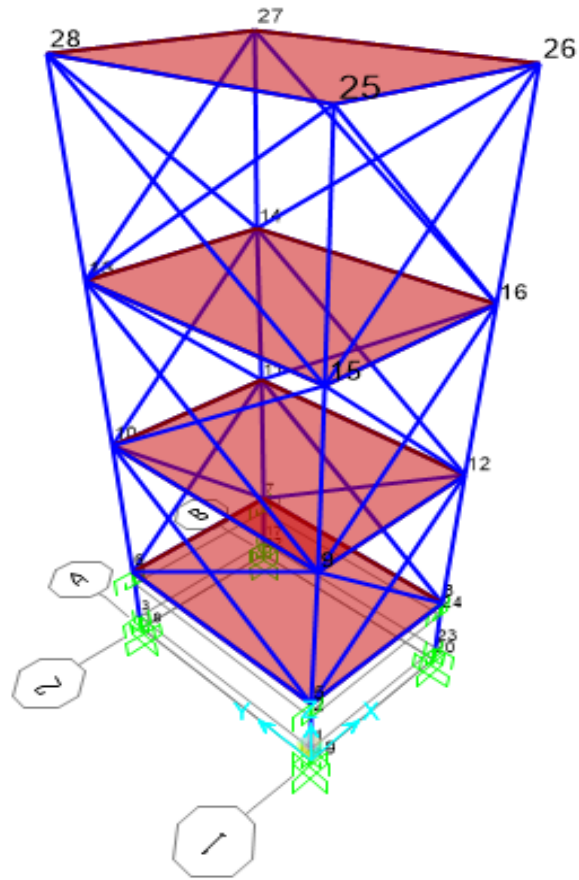
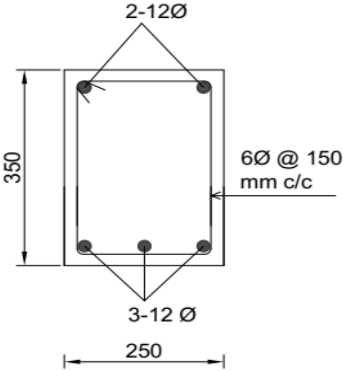
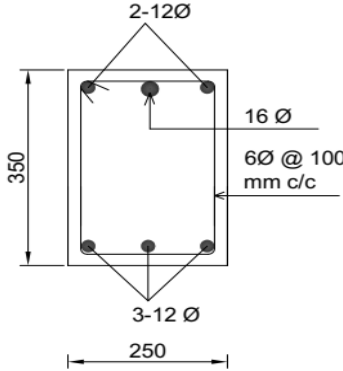


Figure 3.5: 3D view of SAP2000 model of building

Table 3.1: Geometric data of the building

No. of storeys	G+3
Total height	12.9m
Floor height	1.8m (bottom most storey) to 3.3m (Typ.)
Beams	B1 (along shorter span) and B2 (along longer span). (Refer Table 3.2) (Figure 3.2).
Column	C1 (Refer Table 3.2)
Thickness of brick walls	230mm
Equivalent X bracing rectangular section along shorter span	230mm X 340mm
Equivalent X bracing rectangular section along longer span	230mm X 400mm

Table 3.2: Cross section of frame members

Member	Width mm	Depth mm	Cross section	
			Near mid-span	Near beam-column junction
B1 beam	250	350		

Member	Width mm	Depth mm	Cross section	
			Near mid-span	Near beam-column junction
B2 Beam	250	450		
C1 Column	300	400		

3.2 Material properties

Concrete grade: M30

Reinforcement Grade: Fe 500 HYSD

Density of Brick: 20 kN/m³

Density of concrete: 25 kN/m³

3.3 Modeling of various structural and non-structural elements:

The columns and beams were modeled as frame elements with two nonlinear plastic hinges (one at each end of frame element). The reinforcement of beam and column was not explicitly modeled. The reinforcement was used in deriving force-deformation relation for hinges properties.

Floor and roof slabs were modeled using four noded quadrilateral shell elements. Automatic meshing of slab into 4 noded shell elements was used.

3.4 Modeling of hinges

The inelastic behavior of beams and columns was modeled by using concentrated plastic hinges Figure 3.6. The elastic deformation occurs in entire member length except hinges where post yield deformation occurs. In SAP2000 the option to provide default hinge properties is also available which is based on FEMA 356 recommendations. In this study, however user defined, deformation controlled and Moment M-3 hinges were used. These hinges were applied at locations 0.05 and 0.95 points of length of a particular frame element.

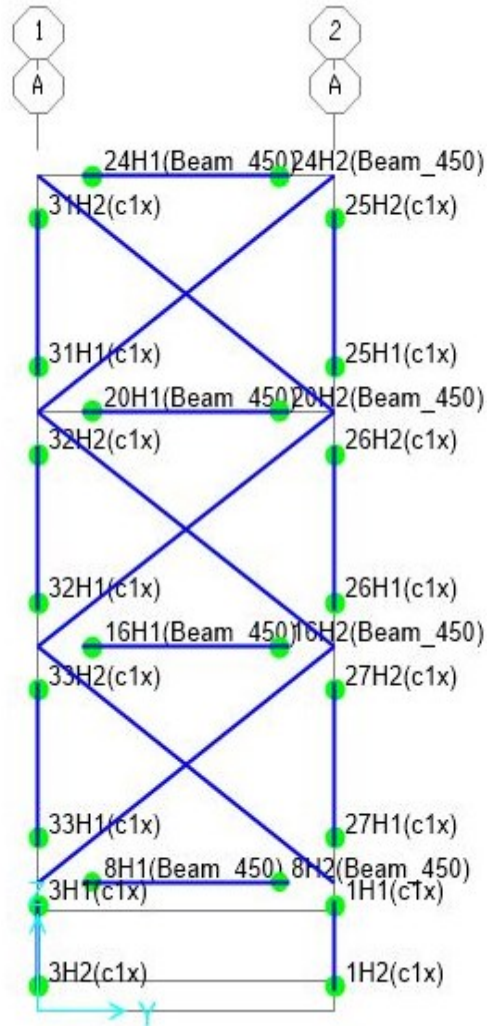


Figure 3.6: Assignment of hinges to beams and columns

Hinge properties for beams and columns are input in SAP2000 in the form of moment curvature curve or moment rotation curve as 5 points A, B, C, D and E. This format is as recommended by ATC-40, 1996 [29] given in Figure 3.7.

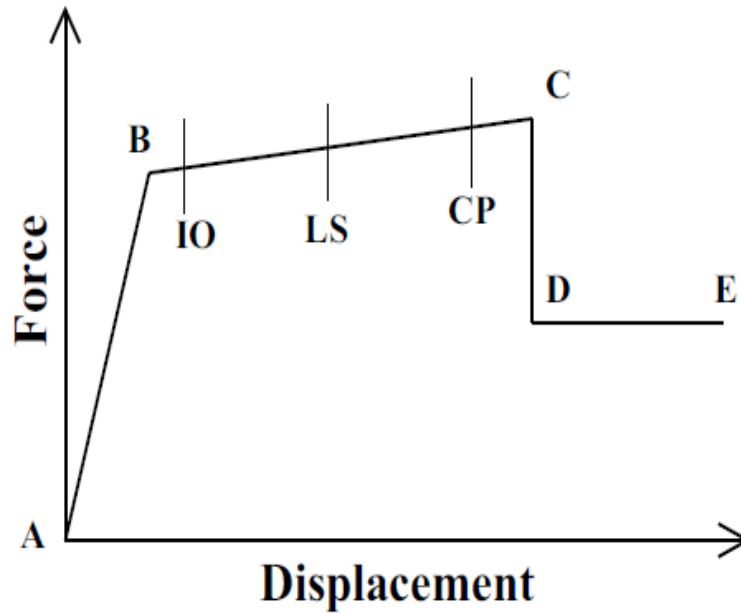


Figure 3.7: Force-displacement curve for hinge input

A represents origin, B yield point, C ultimate point, D residual strength and E rotation or displacement capacity. The force deformation curve shown in the Figure 3.7 is represented in the present work by means of moment curvature relationship Figure 3.7. The performance states IO (Immediate occupancy), LS (Life safety) and CP (Collapse prevention) are also input in hinge properties. These indicators are useful in evaluating performance of structure.

The format (Figure 3.7) recommended by ATC 40, 1996 [29] assumes stiffness of concrete to remain constant up to yield. However, stiffness of concrete gets changed after 1st cracking. Also concrete undergoes strength degradation which ATC-40, 1996 [29] format fails to capture. Hence another format as shown below was used which overcome above limitations by accounting post crack stiffness and post peak load strength degradation [30].

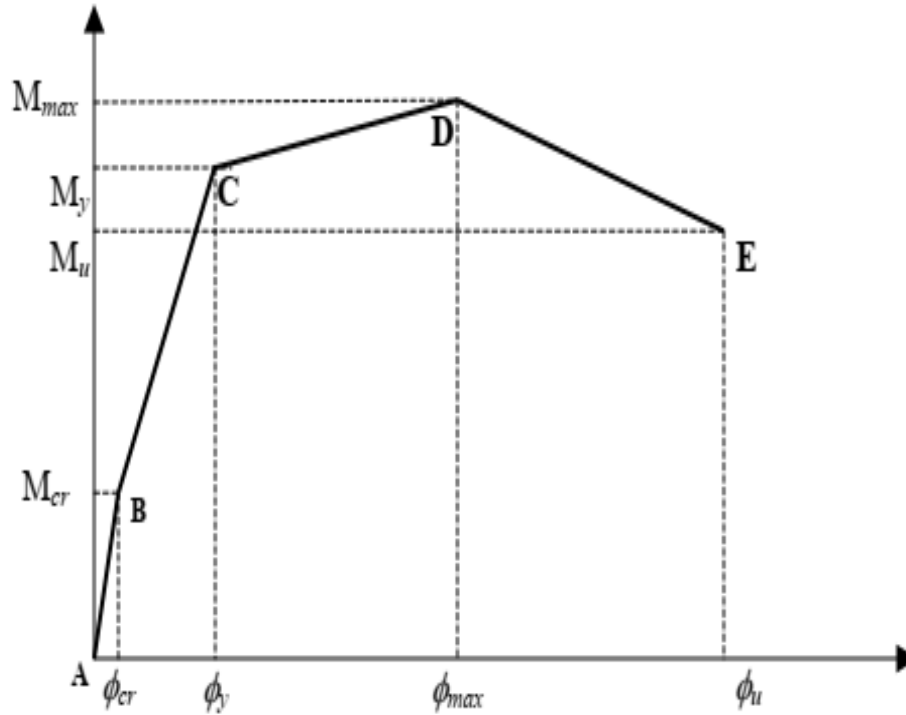


Figure 3.8: Moment curvature curve

3.5 Moment-curvature relationship

The moment curvature relation which is used in user defined Hinge properties is derived by using Kent and Park model (Figure 3.9) for concrete and IS 456:2000 [31] curve for steel (Figure 3.10). The stress strain curve adopted by IS 456:2000 [31] do not consider degradation of concrete due to increase in strain. The value of stress after reaching strain of 0.0020 is kept constant in IS 456:2000 [31] curve as f_{ck} (characteristic strength of concrete) which in this case is 30N/mm^2 . But Kent and Park model considers strength degradation also and seems more realistic particularly for large value of strains. Hence Kent and Park model [32] is used in this study.

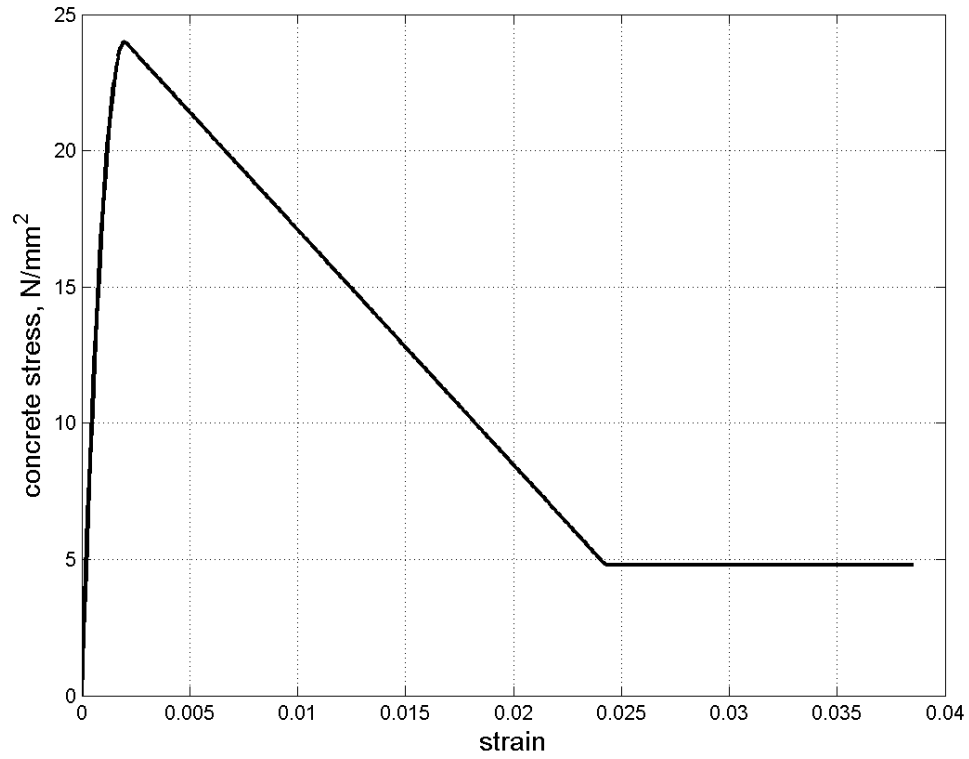


Figure 3.9: Kent and Park model for concrete [32]

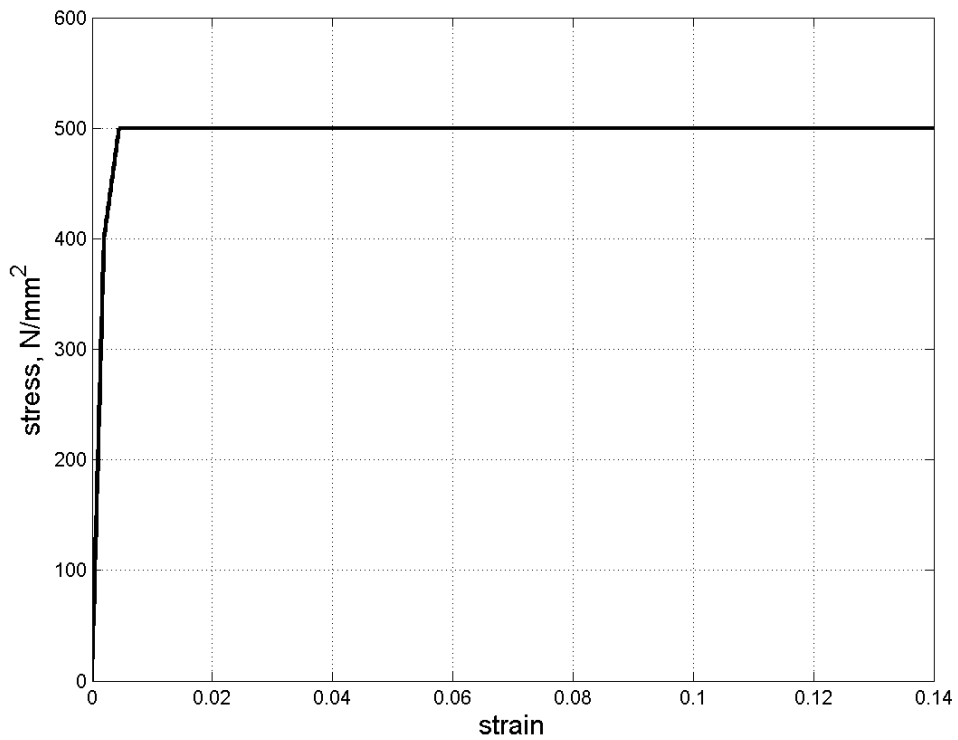


Figure 3.10 Stress-strain curve for HYSD Fe500 steel (IS 456:2000 [31])

The moment-curvature relationship for reinforced concrete beams and columns are derived on basis of following assumptions:

- Plane sections before bending remain plane after bending.
- Stress-strain curves for both concrete and steel are known.
- Tension carrying capacity of concrete is neglected.

A program is made in excel to obtain moment curvature characteristics of column and beam sections. The extreme compressive strain in concrete is restricted to 0.02 to avoid buckling of longitudinal reinforcement bars in between two successive shear stirrups. Spalling of concrete cover is also modeled in case the strain outside the confined core exceeds ultimate compressive strain of unconfined concrete (0.005). For columns moment curvature characteristics are derived considering axial load. The cross sections near the supports are only used (Refer Table 3.2).

The derived moment-curvature ($M-\phi$) curve for Beam B1 and B2 using hogging moments (i.e. tension at top) for their sections is shown in Figure 3.11. The points of improved force displacement curve are obtained from the curve and then input into SAP2000. The $M-\phi$ curve of beam B1 and B2 which are used in hinge properties in SAP2000 is shown in Figure 3.12. The curves are more or less following the shape of moment curvature curve shown in Figure 3.8. The gradual drop occurring in moment capacities signifies the transition from entire section to confined section between the links. After drop confined section (between links) is only active in resisting. The cover portion has undergone cracking and is rendered useless. The $M-\phi$ curves for column in X and Y direction for different floors taking into account axial loads is given respectively in Figure 3.13 and Figure 3.14. It can be observed that for ground floor column due to high axial load the moment capacity is larger but ultimate curvature or ductility is reduced.

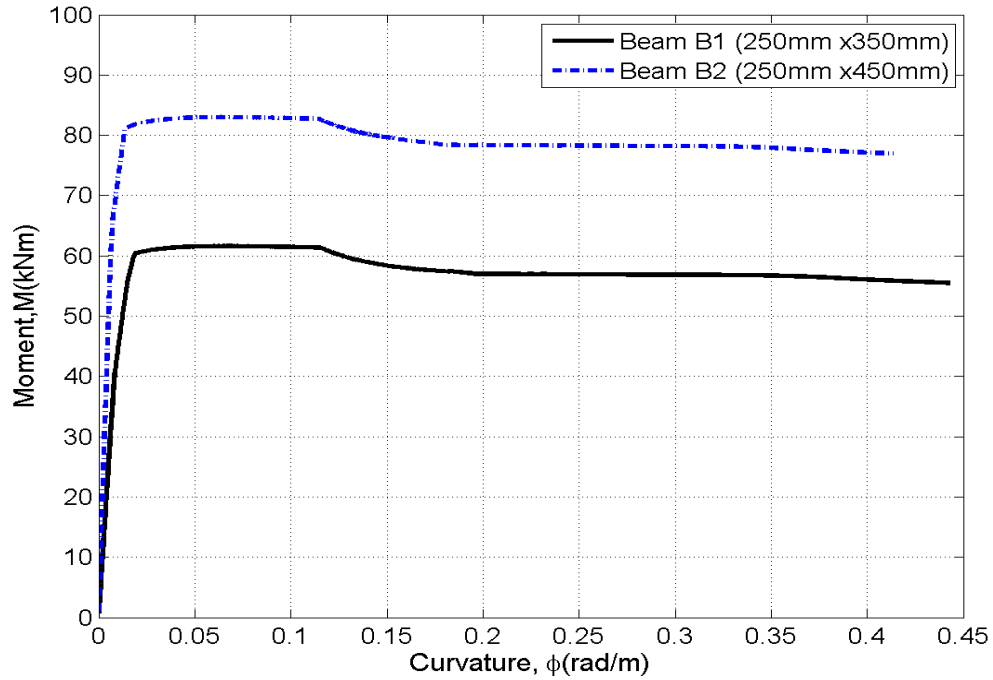


Figure 3.11: M- ϕ curve for beam sections of RC frame under 'hogging' bending moment

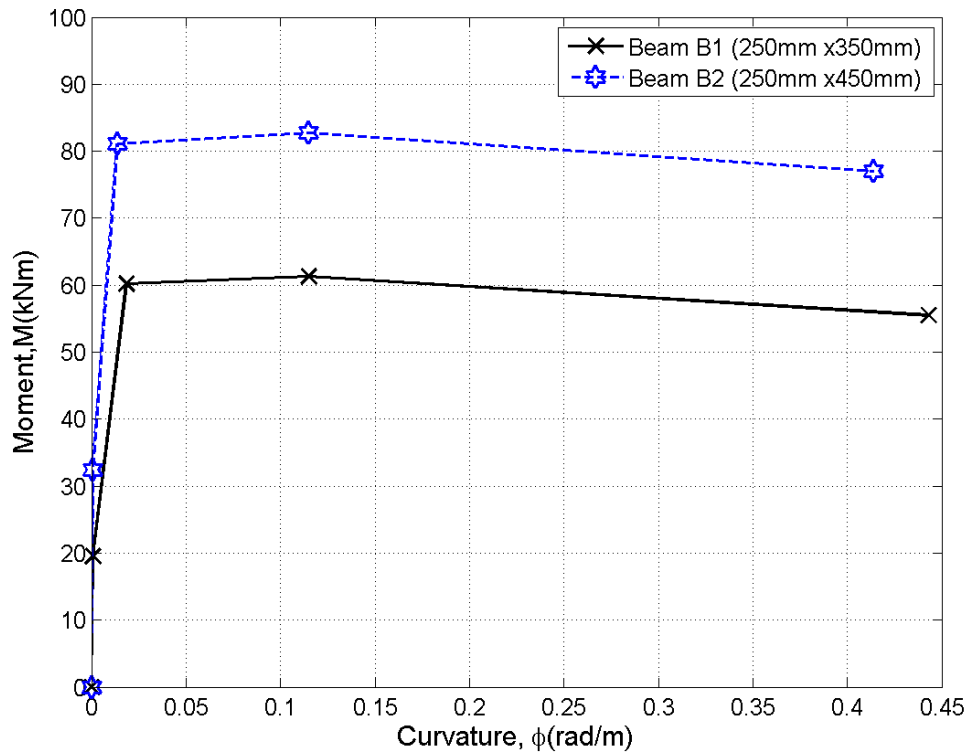


Figure 3.12 Hinge property of beams B1 and B2 (as input to SAP2000)

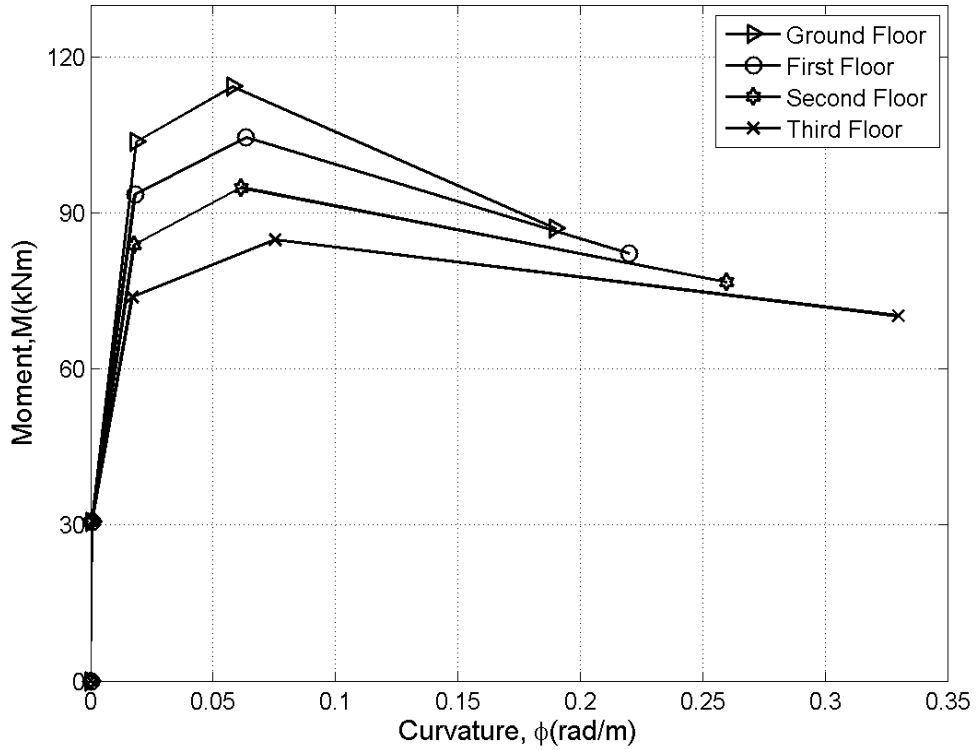


Figure 3.13: M- ϕ curve for column C1 acting in Y direction for different floor heights as input to SAP2000

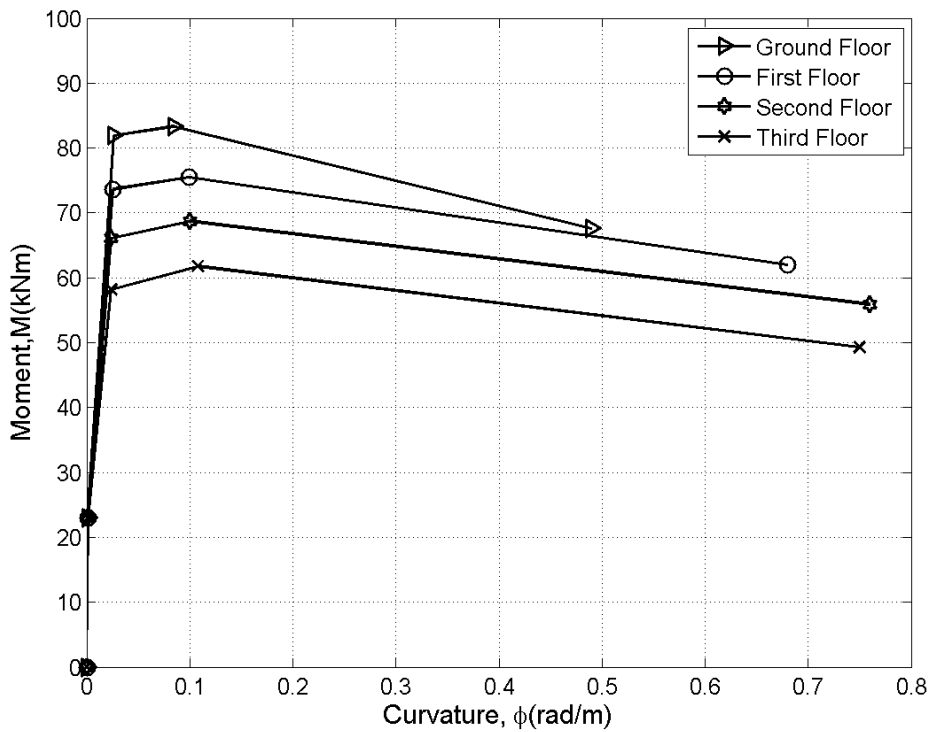


Figure 3.14: M- ϕ curve for column C1 acting in X direction for different floor heights as input to SAP2000

3.6 Modeling of masonry infill

Infill walls are the nonstructural components during normal state. However, during Earthquake motions these are helpful to reduce the response of structure. There are two approaches for modeling infill wall. One is macro model approach (strut model) and other is micro model approach (finite element). In this study, masonry infill walls were modeled as equivalent struts using the IS: 1893 (Part 1): 2016 [33] recommendations. Infill wall modeled as equivalent strut increases the stiffness of the structure. This increase is directly reflected in frequency of the structure which shows an increase after inclusion of strut elements. This increase for X and Y direction is shown in Table 3.5. The width of equivalent diagonal strut is calculated [33] as:

$$w_{ds} = 0.175\alpha_h^{-0.4}L_{ds} \quad (3.1)$$

Where

L_{ds} = Diagonal length of masonry infill wall (Figure 3.15)

$$\alpha_h = h \left(\sqrt[4]{\frac{E_m t \sin 2\theta}{4E_f I_c h}} \right) \quad (3.2)$$

I_c , moment of Inertia of adjoining column

t , thickness of infill wall = 230mm

E_m and E_f , moduli of elasticity of infill material and RC MRF (Moment resisting frame) respectively.

θ , angle of diagonal strut with horizontal.

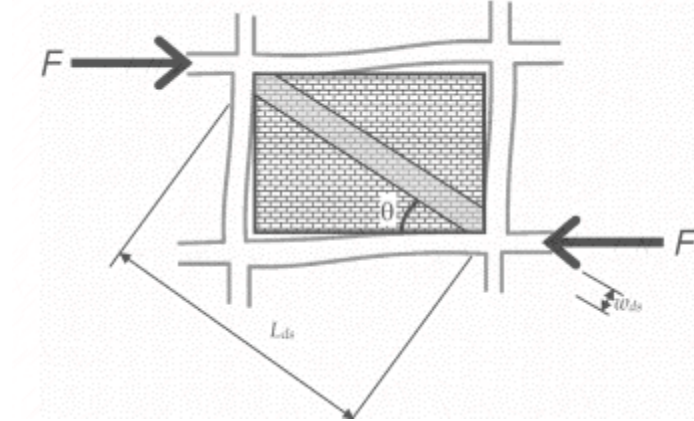


Figure 3.15: Equivalent strut representation for infill wall

For shorter direction (X axis) and longer direction (Y axis), the width is obtained as 550mm and 650mm respectively.

Normally infill walls in buildings are provided with openings. The presence of openings in infill walls reduces the strength and stiffness of infilled frames. According to [34] the stiffness contribution of infill can be ignored if opening area of infill wall is greater than 40% of area of infill. Also, the openings can be ignored if the area occupied is less than 5% of area of infill panel. For 5% to 40% area, the proposed equation for reduction factors to be used on width of equivalent strut is given in [34] as:

$$\rho_{\omega} = 1.05 - 2.56\alpha_{co} \quad (3.3)$$

Where

$$\alpha_{co} = \frac{\text{Area of opening}}{\text{Area of infill}} \quad (3.4)$$

Here, for 3300mm span, $\alpha_{co} = \frac{\text{Area of opening}}{\text{Area of infill}} = \frac{1500 \times 1000}{3000 \times 3000} = 0.167, \rho_{\omega} = 0.622$

For 4500mm span, $\alpha_{co} = \frac{\text{Area of opening}}{\text{Area of infill}} = \frac{2000 \times 1000}{3900 \times 3000} = 0.171, \rho_{\omega} = 0.61$

These reduction factors are applied on calculated equivalent strut width. The final equivalent strut width is 340mm and 400mm for X and Y direction respectively.

3.7 Modal analysis

Modal analysis was performed to evaluate the free vibration mode shapes of structure. Mode shapes describe the configuration into which a structure will naturally displaced. A structure with n degrees of freedom has n modal shapes. For the structure considered for the study the frequency of 1st seven modes along with mass participation (derived from output table of SAP2000) is presented in Table 3.3. The total mass of the building with brick walls is 110 tonnes. The support conditions at bottom have been varied from fixed support to 0.5G, 1.0G and 2.0G (G is shear modulus of soil) using soil springs. The frequencies for various support cases are given in Table 3.4. The deformed shape of the building for major modes in X, Y and Z direction for fixed supports is shown in Figure 3.16, Figure 3.17 and Figure 3.18 respectively.

Table 3.3 Frequency and mass participation in different modes for fixed support

Mode No.	Frequency	UX	UY	UZ	Σ UX	Σ UY	Σ UZ
-	Hertz	-	-	-	-	-	-
1	3.986589	9.00E-01	0.00E+00	0.00E+00	9.00E-01	0.00E+00	0.00E+00
2	5.005356	0.00E+00	9.00E-01	1.06E-20	9.00E-01	9.00E-01	1.06E-20

Mode No.	Frequency	UX	UY	UZ	Σ UX	Σ UY	Σ UZ
3	5.637392	0.00E+00	0.00E+00	0.00E+00	9.00E-01	9.00E-01	1.11E-20
4	11.65216	8.74E-02	9.71E-19	4.91E-17	9.90E-01	9.00E-01	4.91E-17
5	14.50726	0.00E+00	8.45E-02	9.82E-18	9.90E-01	9.90E-01	5.90E-17
6	19.39526	0.00E+00	6.50E-17	1.16E-16	9.90E-01	9.90E-01	1.75E-16
7	20.95250	0.00E+00	1.73E-17	6.10E-01	9.90E-01	9.90E-01	6.10E-01

In Table 3.3 UX, UY and UZ denote the ratio of mass participated wrt total mass in X, Y and Z direction respectively.

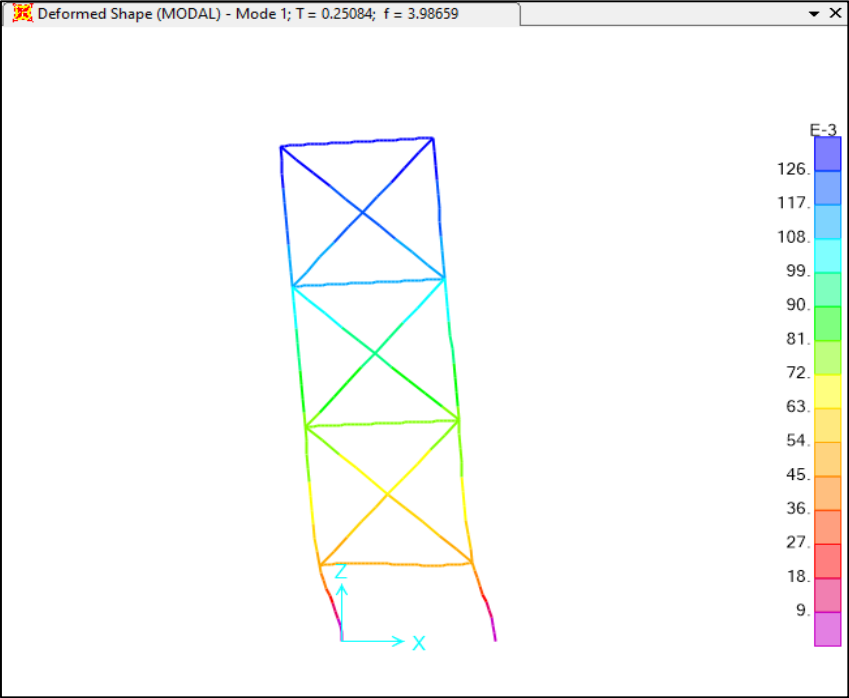


Figure 3.16 Deformed shape of building for mode no. 1 (first mode X-direction)

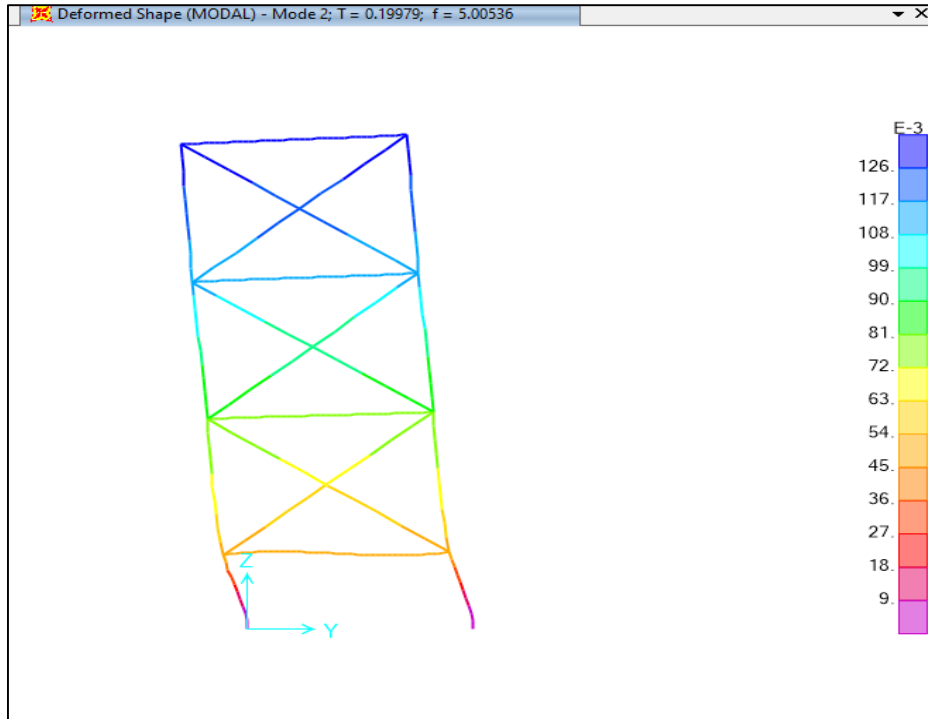


Figure 3.17 Deformed shape of building for mode no. 2 (Y direction)

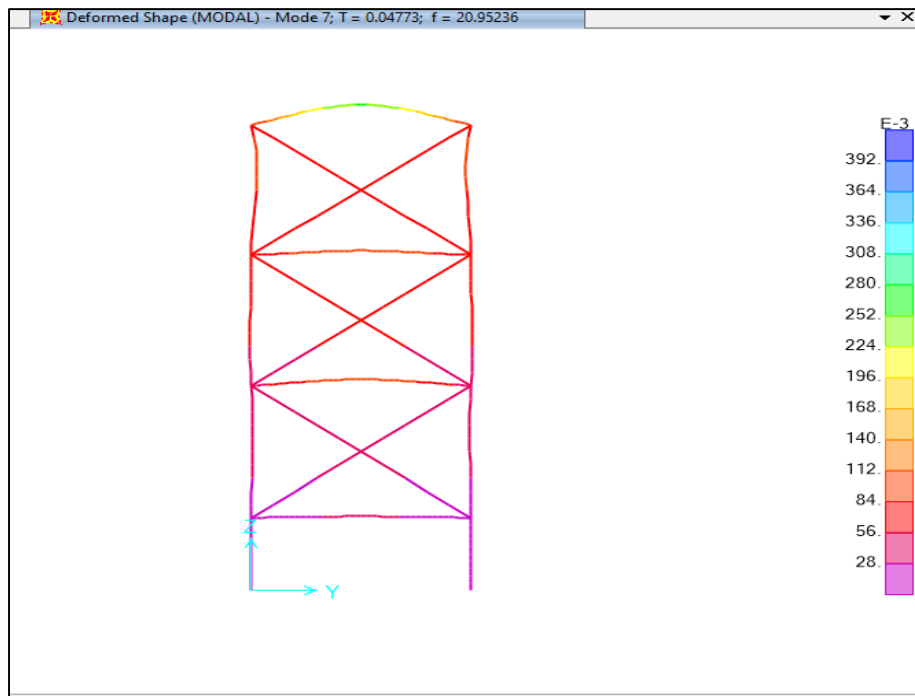


Figure 3.18 Deformed shape of building for mode no. 7 (Z direction)

Table 3.4: Frequency for various support cases

Direction	Frequency, Hz	Support Conditions			
		Fixed	Soil Springs		
			(2.0G)	(1.0G)	(0.50G)
X Direction	1 st Mode	3.99	3.85	3.50	2.68
	2 nd Mode	11.65	11.42	10.85	9.56
Y Direction	1 st Mode	5.00	4.83	4.42	3.43
	2 nd Mode	14.5	14.17	13.35	11.36

The infill wall is modelled as equivalent strut as per IS 1893:2016 [33] recommendations. Table 3.5 brings the comparison between frequencies of structure with and without equivalent strut modeling. It is found that frequency of structure on account of equivalent strut is almost 80% higher than frequency of structure without equivalent strut.

Table 3.5: Comparison of fundamental modes frequencies for structure with fixed support with and without modeling infill wall as equivalent strut

Direction	Structure with Infill wall as Equivalent strut	Normal Structure without Equivalent strut	Ratio of increase in frequency with infill as strut
	Frequency(Hz)	Frequency(Hz)	-
X	3.98918	2.227171	1.79
Y	5.03436	2.739726	1.84

3.8 Non-linear static pushover analysis

Pushover analysis defined as per ATC-40, 1996 [29] is an incremental static analysis used to determine the force-displacement relationship, or the capacity curve, for a structural element. The analysis involves application of horizontal loads, in a prescribed pattern, to a computer model of the structure, incrementally i.e. “pushing” the structure in steps; and plotting the total applied shear force and associated lateral displacement at each increment, until the structure reaches a limit state of collapse condition. This analysis produces pushover curve that gives relation between base shear and roof displacement.

This curve is constructed to represent the first mode response of the structure based on the assumption that fundamental mode of vibration is the predominant mode. This is generally valid for buildings with period up to 1 second. Pushover analysis was performed separately for X and Y directions to study performance of building in both directions. The analysis is performed using displacement controlled load application, where the structure is subjected to incremental static lateral load pattern until roof displacement reached a target value. This analysis was performed to get an accurate picture of all the weak points of building and how the forces are redistributing during progressive yielding. Procedure for Pushover analysis as performed in SAP2000:

1. Model the structure.
2. Derive moment curvature characteristics for all beams and column sections.
3. Define deformation controlled moment M- ϕ hinges for beams and columns and substitute moment-curvature relations obtained in step 2.

4. Define pushover load case with load application as displacement controlled. Monitor displacement U1 (for X direction analysis) and U2 (in case of analysis in Y direction) at topmost joint.
5. Run analysis and obtain pushover curve.

The deformed shape of structure for X and Y directions are given below in Fig. 3.18 and 3.19 respectively:

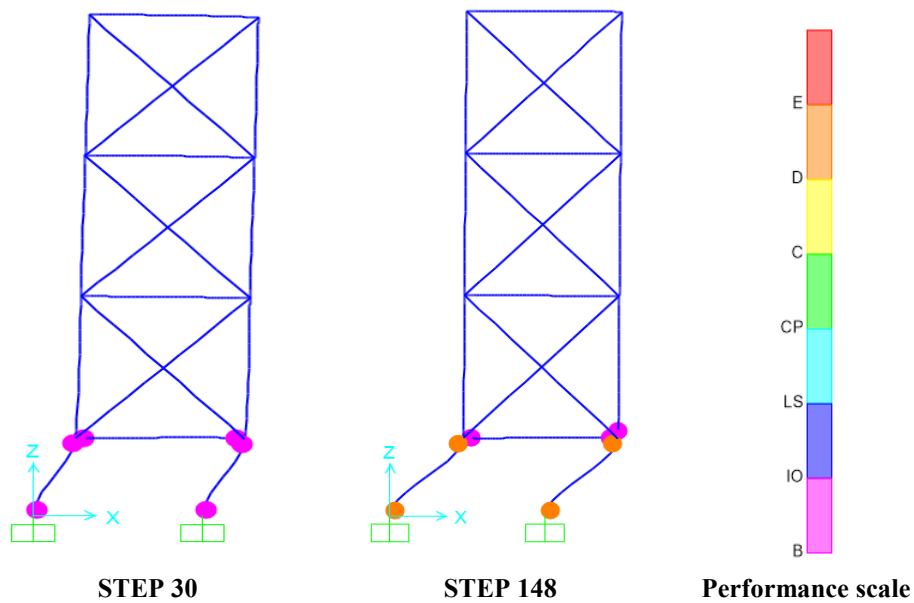


Figure 3.19: Deformed shape of the frame for analysis in X-direction

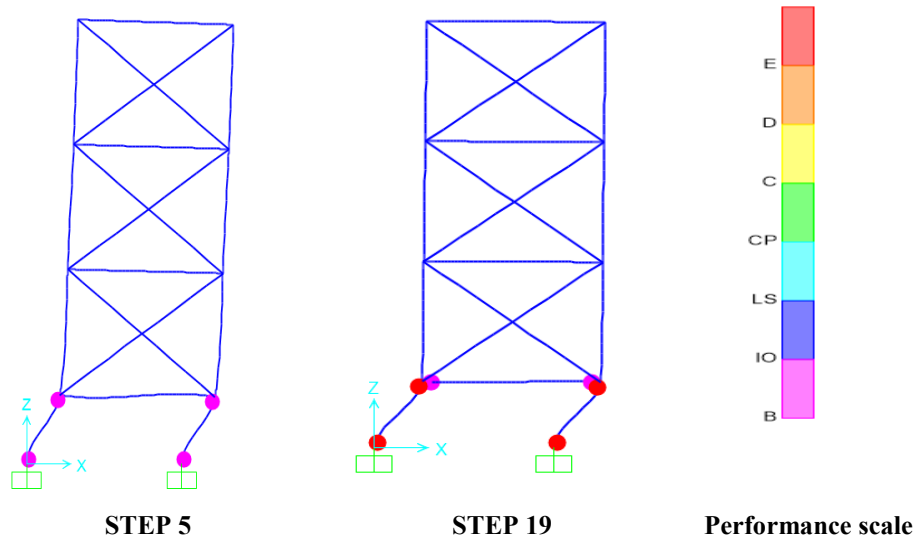


Figure 3.20: Deformed shape of the frame for analysis in Y-direction

3.9 Discussion on obtained pushover curves

The hinges in bottom most storey columns as shown in Figure 3.19 and Figure 3.20 experiences full deterioration in the last steps of pushover analysis i.e. these hinges capacity in terms of moment is completely utilized. These are completely passing through entire region of moment-curvature curve. The reason for hinges to form only at bottom storey is because the structure considered has an irregularity in the form of soft storey. The bottom most floor has significantly lower stiffness than the other storeys because of absence of masonry walls in bottom storey.

The Pushover curve for X and Y directions for fixed support and 1.0G support are given in Figure 3.21 and Figure 3.22 respectively. It can be clearly observed that pushover curve in Y direction has higher capacity but lower ductility than in X direction. This is due to moment curvature curves for column in X and Y directions which also bear similar characteristics. It is also observed that peak ultimate load of the model with fixed support is higher than that of the model with soil structure interaction considering 1.0G soil shear modulus. Pushover curves for all support cases is given respectively for X and Y direction in Figure 3.23 and Figure 3.24. It can be noticed that fixed

supported model has considerably higher capacity and higher initial stiffness than all soil spring supported model cases. Also, the initial stiffness before cracking and stiffness after cracking and before yielding is least in 0.5G soil shear modulus case. The peak ultimate load for all the cases with soil structure interaction is approximately same in both X and Y directions. The support cases 1.0G and 2.0G are more or less showing a similar behavior. The peak load taken by structure in X direction is varying from 378 kN to 410 kN for all support cases. But for Y direction peak load is varying from 510 kN to 550 kN. On an average the peak load in Y direction is approximately 35% higher than X direction's peak load.

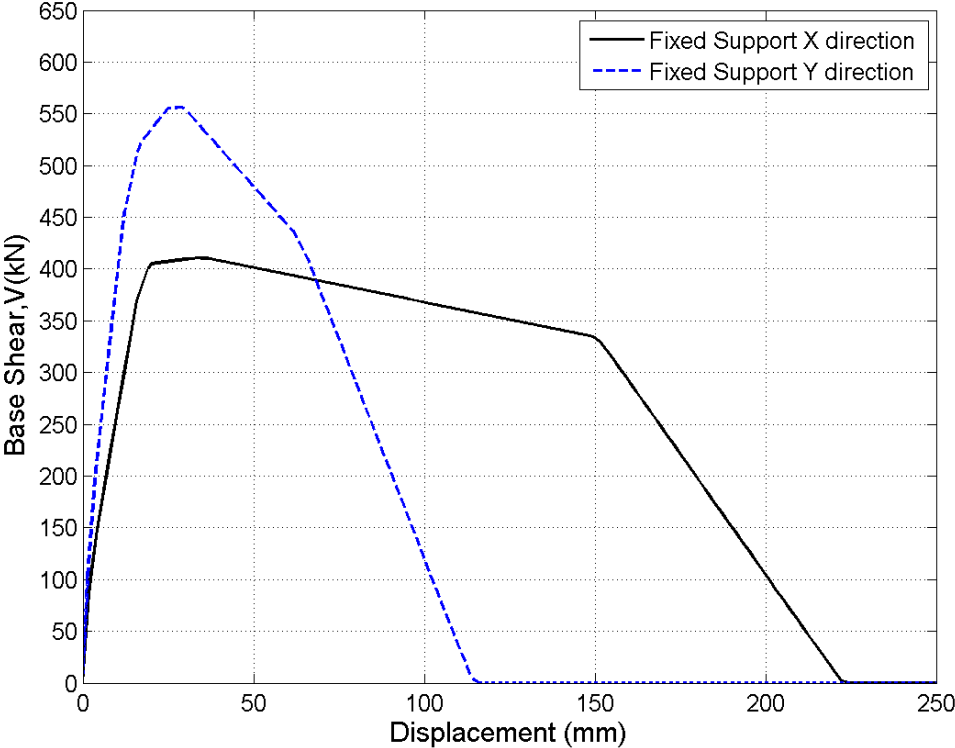


Figure 3.21: Pushover curves for fixed support

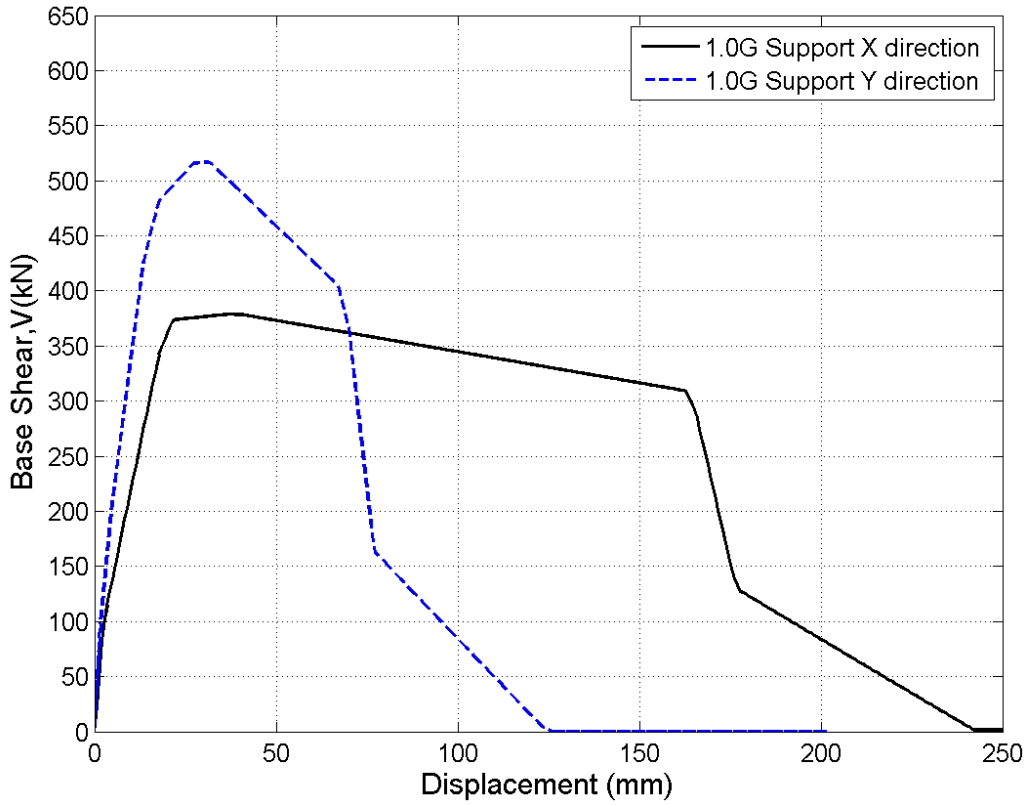


Figure 3.22: Pushover curves for 1.0G support

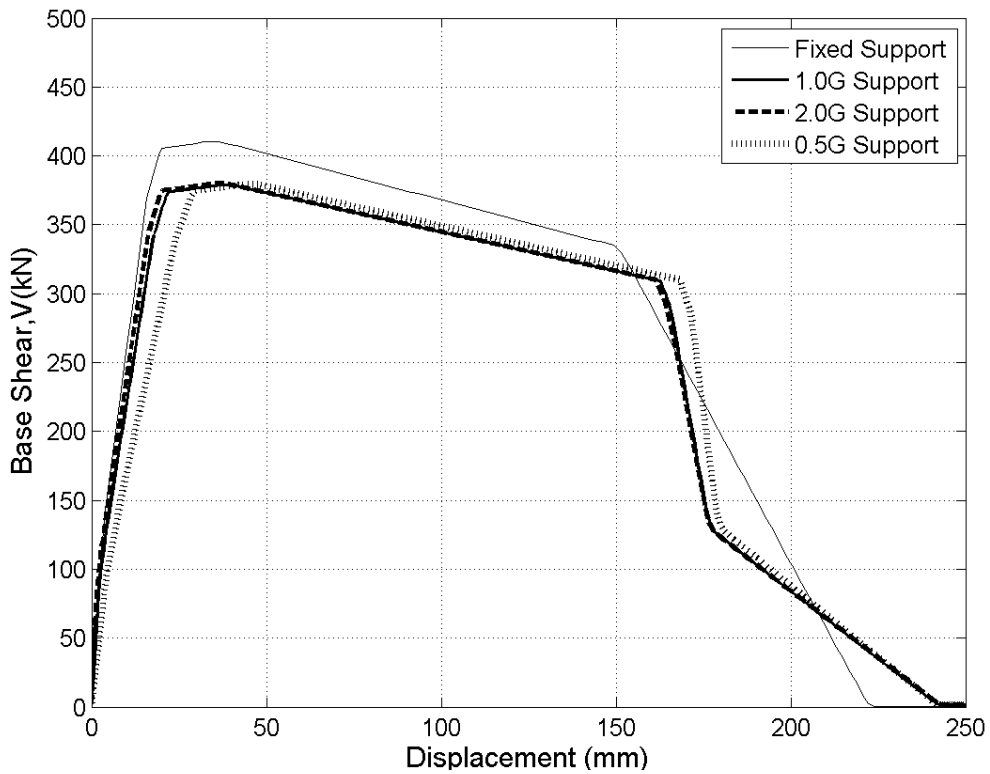


Figure 3.23: Pushover curves for X direction

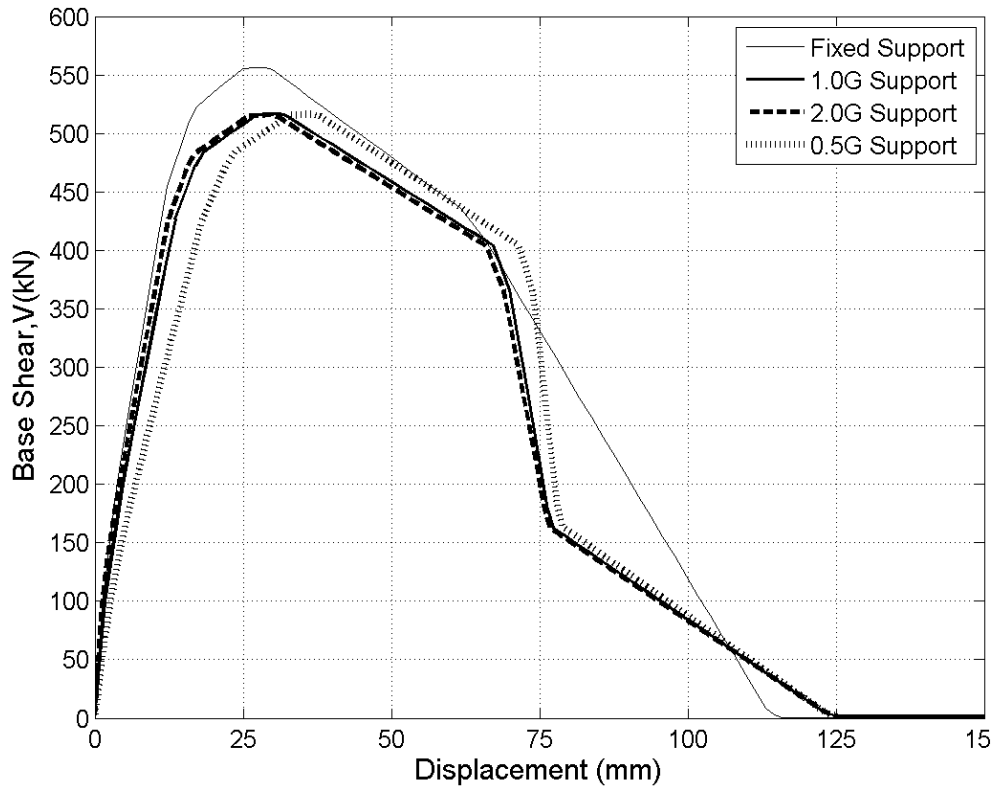


Figure 3.24: Pushover curves for Y direction

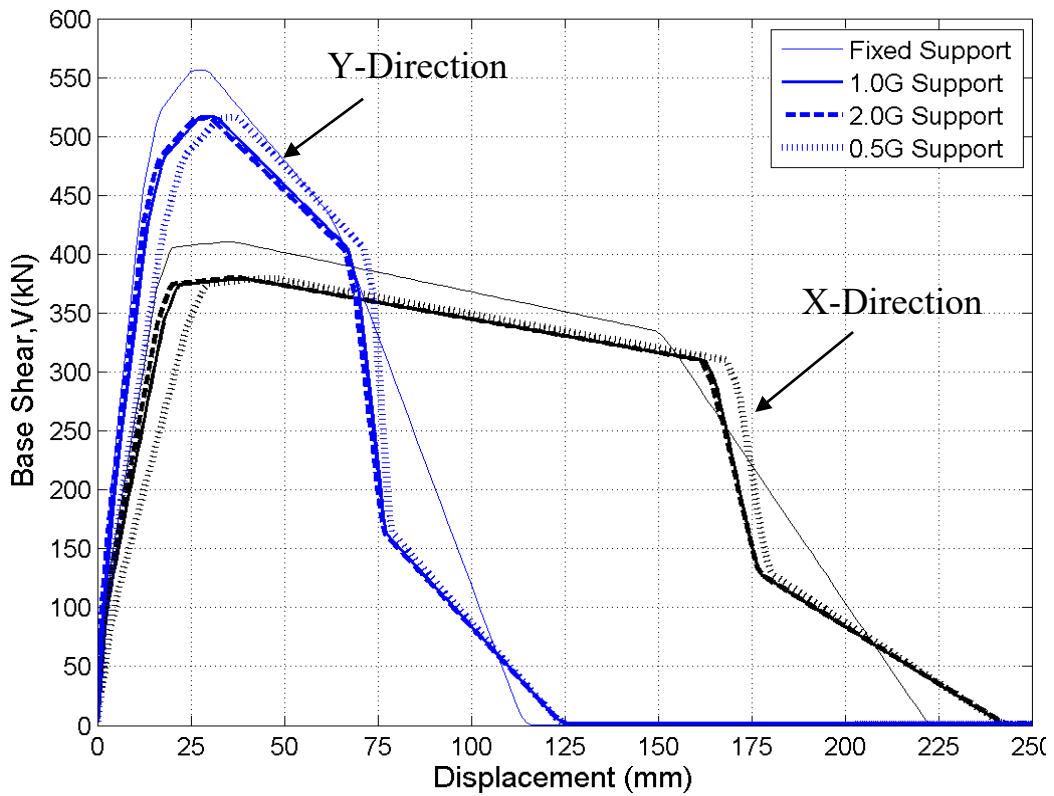


Figure 3.25: Pushover curves for X and Y direction for all support cases

3.10 Displacement ductility calculations

Displacement ductility of a structure is calculated as the ratio of failure displacement to yield displacement.

$$\text{Displacement ductility } (\mu) = \frac{\text{maximum displacement at failure } (d_m)}{\text{Yield displacement } (d_y)} \quad (3.5)$$

The pushover curve obtained from SAP2000 analysis is operated by FEMA 356 [10] procedure to obtain displacements (failure and yield). This procedure adopts an iterative graphical technique to convert capacity curve into a bilinear curve. Bilinear curve points are selected such that area of pushover curve lying above and below this bilinear curve is approximately same. The 2nd and last points of bilinear curve are respectively used as yield and maximum displacement at failure. However, FEMA 356 [10] also suggests that base shear at target failure displacement shall not be less than 80% of effective yield strength of structure. Therefore, if base shear at last point of bilinear idealization is less than 80% of effective yield strength then failure displacement is simply taken as the displacement at 80% of effective yield strength. This condition also implies that failure displacement can be selected corresponding to point where base shear is equal to 80% of effective yield strength. To be on conservative side we have considered this failure displacement criterion at 85% of yield strength.

This idealization into bilinear is mainly used to obtain effective lateral stiffness (K_e), effective yield strength (V_y) and post yield slope (α) for structure. The bilinear idealization of pushover curve in X and Y direction for fixed supported model is graphically shown in Figure 3.26 and Figure 3.28 being superimposed on respective pushover curves. And after applying FEMA 356 [10] condition the bilinear curves are presented in Figure 3.27 and Figure 3.29. Effective yield strength (V_y) and displacement points, d_m and d_y corresponding to maximum and yield displacement are indicated in respective figures.

3.10.1 For X direction (Fixed support):

Yield displacement (d_y) = 15.52 mm

Yield strength = $V_y = 410.09$ kN, 85% of yield strength = $0.85 * V_y = 348.58$ kN

Maximum displacement (d_m) = 43.95 mm, Corresponding base shear = 405.50 kN ($> 0.85 * V_y$)

Therefore d_m is chosen corresponding to 348.58 kN and is 128.6 mm.

$$\text{Displacement ductility } (\mu) = \frac{d_m}{d_y} = \frac{128.6}{15.52} = 8.28$$

Effective lateral stiffness of building in X-direction (K_e) = 26.438×10^6 N/m and

Post yield stiffness of building in X-direction (α) = -0.169×10^6 N/m

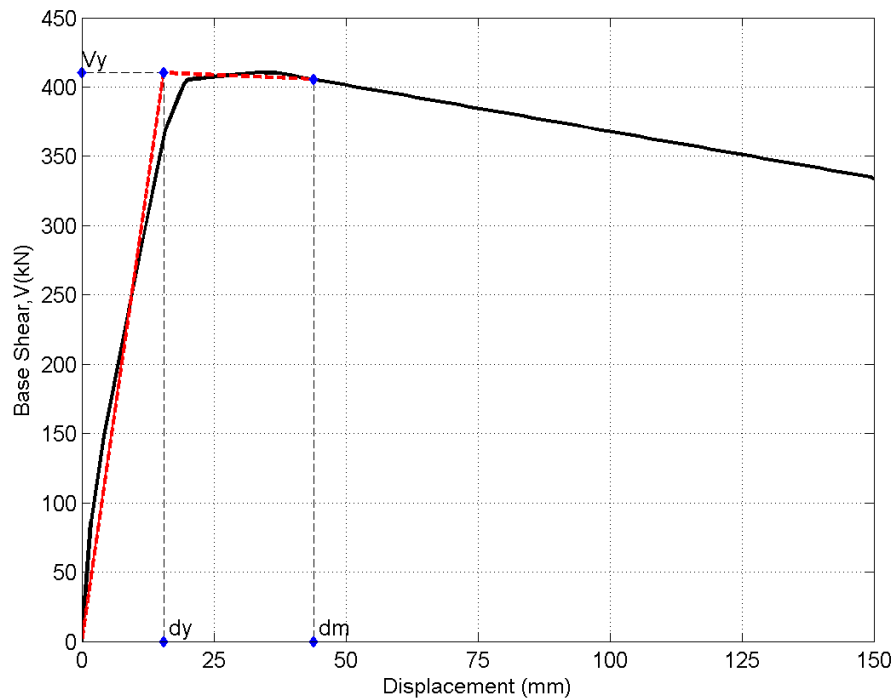


Figure 3.26 Bilinear idealization of pushover curve-X direction for fixed support

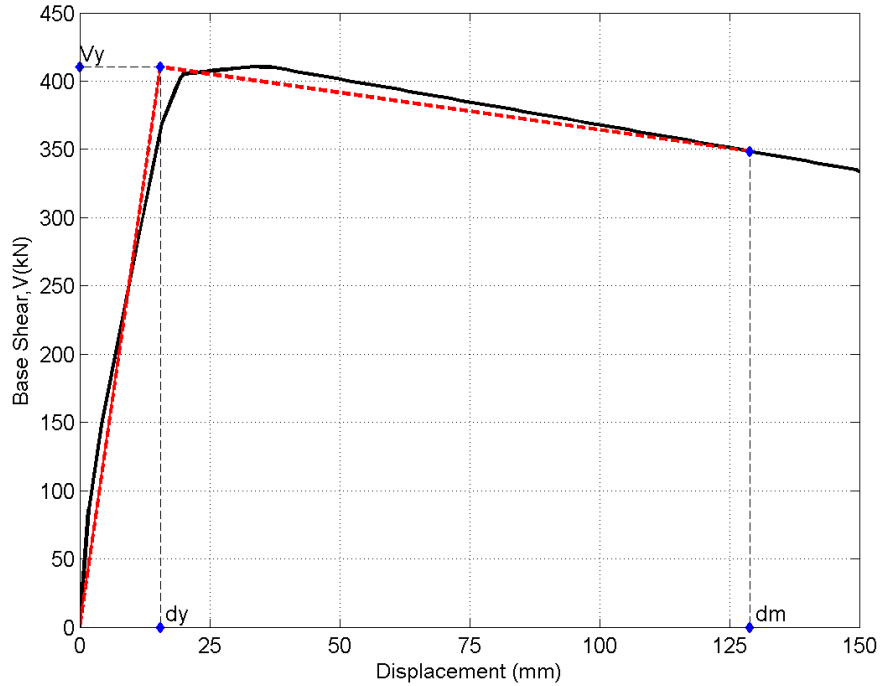


Figure 3.27 Bilinear idealization of pushover curve-X direction for fixed support(FEMA 356 -85% criteria)

3.10.2 For Y direction (Fixed support):

Yield displacement (d_y) = 13.476 mm

Yield strength = V_y = 556.080 kN, 85% of yield strength = 472.67 kN

Maximum displacement (d_m) (from bilinear curve) = 38.40 mm, Corresponding base shear = 522.58 kN (>472.67 kN)

Therefore d_m = 51.93mm (corresponding to 472.67 kN)

$$\text{Displacement ductility } (\mu) = \frac{d_m}{d_y} = \frac{51.93}{13.476} = 3.853$$

Effective lateral stiffness of building in Y-direction (K_e) = 41.265×10^6 N/m and

Post yield stiffness of building in Y-direction (α) = -1.344×10^6 N/m

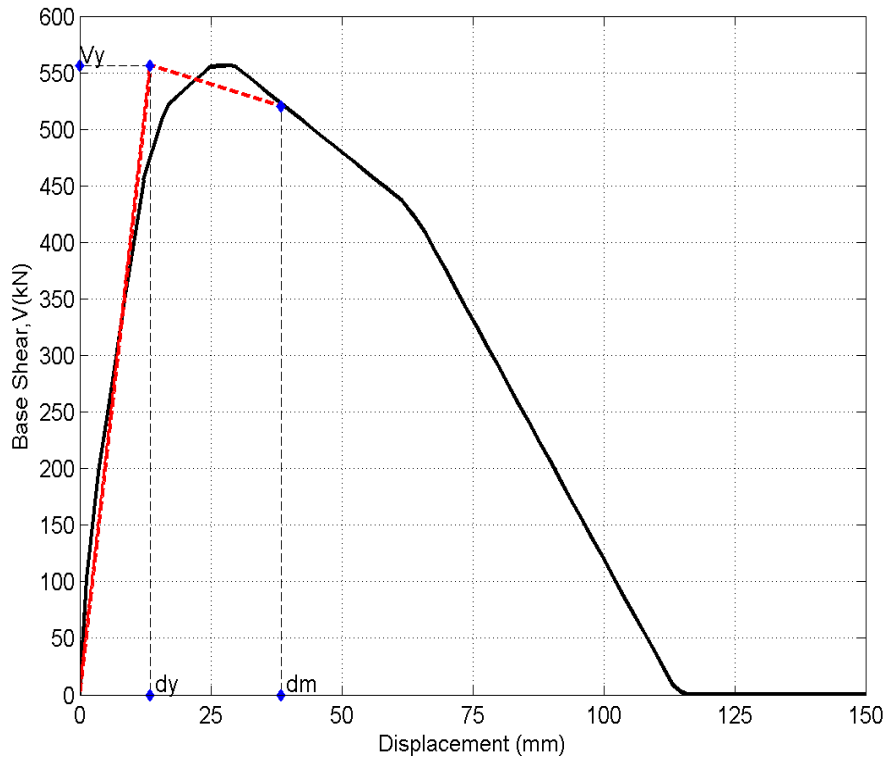


Figure 3.28: Bilinear idealization of pushover curve-Y direction for fixed support

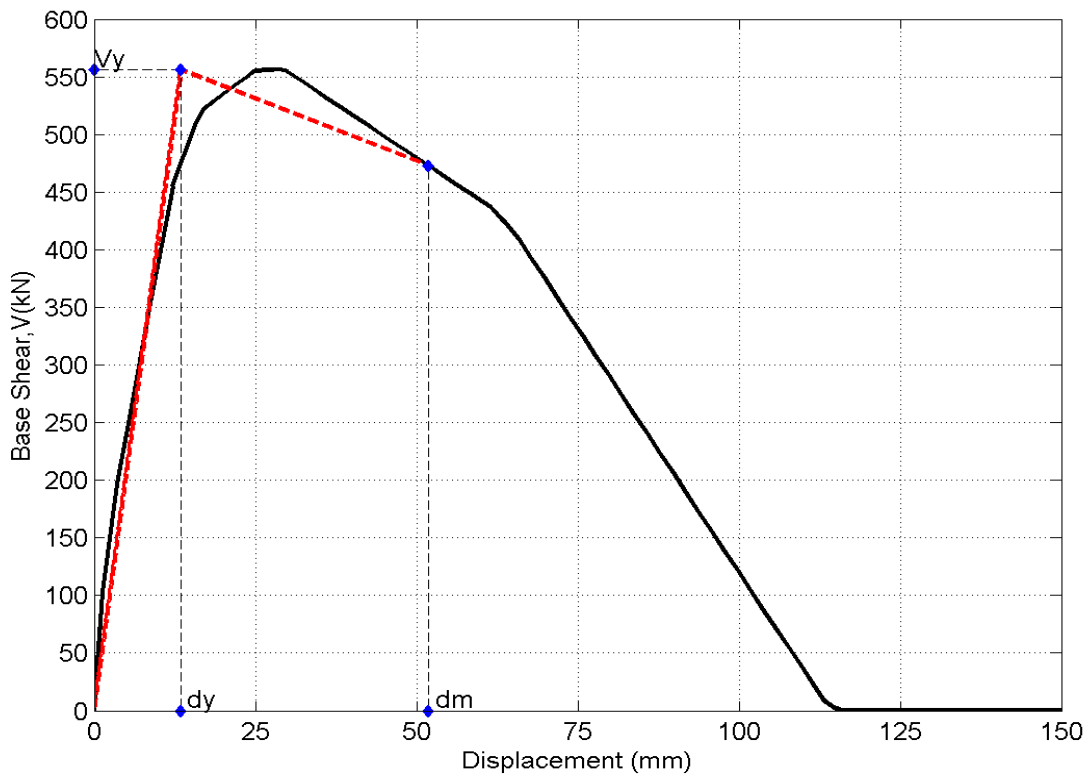


Figure 3.29: Bilinear idealization of pushover curve-Y direction for fixed support (FEMA 356, 85% criteria)

Similarly the procedure is adopted for different support conditions for X and Y directions. The summary of the parameters of bilinear curve for all 4 support conditions is given in Table 3.6 and Table 3.7 given below:

Table 3.6: Bilinear curve comparison for 4 support conditions for X direction

			Fixed	2.0 G	1.0 G	0.5 G
Yield Displacement	d_y	mm	15.52	15.6	17.29	24.5567
Yield Strength	V_y	kN	410.2	379.1305	378.1832	378.7356
Displacement Ductility	μ	-	8.311856	8.99359	8.143436	6.108313
Effective lateral Stiffness	K_e	kN/mm	26.43041	24.30324	21.87294	15.4229
Post Yield Stiffness	α	N/m	-0.54221	-0.45605	-0.45929	-0.45288

Table 3.7: Bilinear curve comparison for 4 support conditions for Y direction

			Fixed	2.0 G	1.0 G	0.5 G
Yield Displacement	d_y	mm	13.476	18.448	14.097	18.448
Yield Strength	V_y	kN	556.08	513.676	512.91	513.676
Displacement Ductility	μ	-	3.853517	4.397356	4.054054	3.341826
Effective lateral Stiffness	K_e	kN/mm	41.26447	39.61275	36.38434	27.84454
Post Yield Stiffness	α	N/m	-2.16914	-1.74898	-1.78702	-1.78351

3.10.3 Importance of bilinear idealization:

As we load the structure to increasing intensities of ground motions, the structure undergoes degradation of stiffness which leads to decrease of frequency of structure. The mass participation as seen in Table 3.3 of modal analysis for the first mode is obtained as approximately 90%. This means that structure can be idealized as single degree of freedom to calculate new frequency of structure using relation:

$$f = 2 * \pi * \sqrt{\frac{k}{M}} \quad (3.6)$$

Where k =stiffness and M = mass of structure

Calculation of frequency corresponding to a particular intensity of time history requires values of stiffness and mass. The stiffness is assumed as secant stiffness on bilinear curve for a particular roof displacement calculated from NLTHA. The reduced frequency is then used to find spectral acceleration which is final response of structure used to plot IDA (Incremental Dynamic Analysis) curves. However, in the present work we have not used bilinear idealization of the structure and actual structure with link elements at the base is considered for the NLTHA and incremental dynamic analysis.

3.11 Concluding remarks

1. The fundamental frequencies of the structure in X and Y direction are obtained as 3.99Hz and 5.00Hz respectively for fixed supports. With variation in support conditions using soil properties as 0.5G, 1.0G and 2.0G, the frequency of the structure for X direction is decreased by 30%, 11% and 3% respectively.
2. The structure without modelling infill wall as equivalent strut and with modelling infill as equivalent structure is also compared w.r.t frequency. It is found that without modelling

infill as equivalent strut reduces the frequency for both X and Y direction by 45% approximately.

3. From results of pushover curves it is found initial stiffness of the structure decreases when support boundary condition are varied from fixed support boundary condition to the support with springs having stiffness corresponding to 2.0G, 1.0G and 0.50G shear modulus. Compared to fixed support, the 2.0G, 1.0G and 0.5G support case has 92%, 82.7% and 58.3% initial stiffness value. There is not an appreciable difference in initial stiffness and peak capacities for supports with stiffness corresponding to shear modulus of 1.0G and 2.0G support condition.
4. From Table 3.6 and Table 3.7 it is observed that displacement ductility for X direction is varying from 6.1 kN/mm to 8.99 kN/mm with lowest value for 0.5G soil spring support condition. While for Y direction the values of displacement ductilities are varying from 3.34 kN/mm to 4.38 kN/mm with 0.5G soil spring support condition bearing lowest value.

4 INCREMENTAL DYNAMIC ANALYSIS

4.1 General information on analysis procedures

There is a hierarchy of four levels of structural analysis appropriate for the evaluation of existing buildings (FEMA 273). As we adopt higher level procedure, the accuracy of the model is enhanced but at the cost of greater computational efforts. The two basic procedures, the Linear Static Procedure (LSP) and the Linear Dynamic Procedure (LDP), are mainly used for buildings which respond primarily in the elastic range. The Nonlinear Static Procedure (NSP) can evaluate buildings loaded beyond the elastic range but does not fully capture the dynamics of response, especially higher mode effects. The Nonlinear Dynamic Procedure (NDP) is the most complete form of analysis, modeling both dynamic effects and inelastic response. However, it is sensitive to modeling and ground motion assumptions. The NDP procedure is based on a step by step integration of the equations of motion with the stiffness matrix updated as the member state changes [35]. NDP is affected by damping, earthquake loads and soil-structure interaction. These concepts are discussed below.

4.2 Modeling of damping

After a structure is put into free vibration the amplitude of displacement will decay with time. This process is referred to as damping. Not only free vibration, damping realizes its presence in forced vibration response also for e.g. seismic effects. Inherent damping is basically energy dissipation which is not explicitly accounted. The energy dissipation due to inelastic regions of structure is commonly accounted explicitly and hence this is not included in inherent damping. The principal

sources for damping are internal friction in materials (material damping) and sliding contact among common surfaces (interfacial damping). Material damping is dependent upon type of material and comes from complex molecular interaction within the material while interfacial damping is basically Coulomb friction among members and connections of a structural system and non-structural components like partitions, facades etc. These damping sources are commonly referred as inherent damping sources.

Experiments have shown that most of the energy dissipation mechanisms through the structure are dependent on displacement amplitude rather than frequency of the structure. Hence the most suitable form of formulating damping in structures may be friction damping. The mathematical model for Coulomb (friction) damping is given as

$$f_d = \mu \frac{\dot{u}}{|\dot{u}|} = \mu \text{sgn}(\dot{u}) \quad (4.1)$$

In which μ is the friction coefficient of contacting surfaces, \dot{u} is the first derivative of displacement and $\text{sgn}(\bullet)$ is the mathematical sign function. This modelling approach demands nonlinear analysis which may require large amount of computational resources. This is the reason viscous damping models are used in typical engineering practice for the sake of simplicity as they lead to the linear analysis of equations of motion. The mathematical model for viscous damping is

$$f_d = c\dot{u} \quad (4.2)$$

In which c is viscous damping constant and \dot{u} is the first derivative of displacement. One can understand that the viscous damping is velocity dependent and not displacement dependent. Since viscous damping is used to linearly model the structural behavior, any source of nonlinearity is relatively unknown and consequences of using this model are ignored. Consider the equation of motion for a linear elastic MDOF system with linear viscous damping as below:

$$M\ddot{u}(t) + C\dot{u}(t) + Ku(t) = 0 \quad (4.3)$$

In which M , C and K are mass, damping and stiffness matrices and $u(t)$ is the displacement vector $\dot{u}(t)$ and $\ddot{u}(t)$ and represent the first and second order derivatives of time at different degrees of freedom respectively. The damping of structure is assumed to be viscous and frequency dependent for the sake of convenience in analysis. One of the methods is to solve the equation of motion using the modal analysis; in this case damping values are directly assigned to the modes. Damping ratios can be calculated using the Rayleigh damping which is a special case of Caughey series (Caughey and O'Kelly, 1965) [36].

4.2.1 Caughey damping

Caughey expressed the damping matrix as:

$$C = M \sum_j a_j [M^{-1}K]^j \quad (4.4)$$

Where M is the mass matrix, K is the stiffness matrix, and a_j are coefficients computed from solving the following system of equations:

$$\zeta_n = \frac{1}{2} \sum_j a_j w^{2j-1} \quad (4.5)$$

In Eq. 4.5, a and w are the viscous damping ratios and the associated vibration frequencies. There is no requirement that the frequencies be actual modal frequencies of the system. In Eq. 4.4 and 4.5 the index j can take any integer value, and there can be gaps in the sequence. The only restriction is that the number of terms in the summation is equal to the number of frequencies for which associated damping ratios are set. It is common to limit the range of j from 0 to $N-1$, where N is less than or equal to the number of modes in the system (in which case n ranges from 1 to N). It is important to note that when using Eq. 4.4 and 4.5 the damping at a given frequency will be zero only if it is set to zero for that frequency.

There are three main problems with Caughey damping. First, any damping matrix based on j other than 0 and 1 will have a bandwidth greater than that of stiffness matrix. Second, inverse of M has to be formed. But the problem is that M is usually singular. Third, the extraction of damping ratio has numerical difficulties when j is large.

One common approach to solve the above problem is to restrict j to 0 and 1. Resulting damping matrix becomes

$$C = a_0M + a_1K \quad (4.6)$$

The above damping is commonly referred to as Rayleigh damping also known as proportional damping or classical damping model.

In equation 4.6, a_0 and a_1 are real scalars with 1/sec and sec units respectively.

This damping can also be expressed as function of mass and stiffness matrices under the assumption of linear viscous damping in structures for m^{th} mode of system as:

$$\zeta_m = \frac{a_0}{2w_m} + \frac{w_m a_1}{2} \quad (4.7)$$

The coefficients a_0 and a_1 can be determined from specified damping ratios ζ_i and ζ_j for the i^{th} and j^{th} modes, respectively (Chopra, 2007) [37]

$$\begin{Bmatrix} \zeta_i \\ \zeta_j \end{Bmatrix} = \frac{1}{2} \begin{bmatrix} 1/w_i & w_i \\ 1/w_j & w_j \end{bmatrix} \begin{Bmatrix} a_0 \\ a_1 \end{Bmatrix} \quad (4.8)$$

Table 4.1 and Table 4.2 gives the Rayleigh coefficients used in this project for X and Y direction respectively. a_0 and a_1 are obtained using Eq. 4.8 and substituting the values of 1st and 2nd mode frequencies of the structure as ω_i and ω_j for respective damping ratio values for i^{th} mode equal to that of j^{th} mode.

Table 4.1 : Rayleigh coefficients for X direction

		Fixed	Soil Springs (2.0G)	Soil Springs (1.0G)	Soil Springs (0.50G)
Frequency	1 st Mode	3.99	3.85	3.5	2.68
	2 nd Mode	11.65	11.42	10.85	9.56
4% Damping	a ₀	1.4939	1.447	1.330	1.052
	a ₁	0.000814	0.000834	0.000887	0.00104
5% Damping	a ₀	1.867	1.809	1.662	1.315
	a ₁	0.001018	0.001042	0.001109	0.0013
7% Damping	a ₀	2.614	2.532	2.327	1.841
	a ₁	0.001425	0.001459	0.00155	0.00182

Table 4.2: Rayleigh coefficients for Y direction

		Fixed	Soil Springs (2.0G)	Soil Springs (1.0G)	Soil Springs (0.50G)
Frequency	1 st Mode	5.00	4.83	4.42	3.43
	2 nd Mode	14.50	14.17	13.35	11.36
4% Damping	a ₀	1.8688	1.8106	1.6691	1.3242
	a ₁	0.000653	0.00067	0.000717	0.000861
5% Damping	a ₀	2.336056	2.263306	2.086392	1.655328
	a ₁	0.000816	0.000838	0.000896	0.001076
7% Damping	a ₀	3.270479	3.168628	2.920949	2.31746
	a ₁	0.001143	0.001173	0.001254	0.001507

4.3 Soil structure interaction

SSI is a phenomenon in which the response of the soil influences the motion of structure and response of structure influences motion of the soil.

To model SSI effects accurately the soil and structure are modeled together. But this approach is however costly and time consuming. With the aim of making a simplified dynamic soil-structure interaction analysis, instead of a complete computationally cumbersome numerical modeling, it is possible to model the soil by springs which have equivalent characteristics.

In this project discrete spring element of SAP2000 has been adopted to model soil. Spring is provided at each support. The stiffness values for the spring in 6 directions, 3 rotational and 3 translational is calculated from Table 5.2 of ASCE 4-16 [1] which gives equivalent spring constant for lumped representation of structure foundation interaction at surface for rectangular base.

Table 4.3: Soil Spring constants

Motion	Equivalent Spring constant
Horizontal	$k_x = 2(1 + \nu)G\beta_x\sqrt{BL}$
Rocking	$k_\phi = \frac{G}{1 - \nu}\beta_\phi BL^2$
Vertical	$k_z = \frac{G}{1 - \nu}\beta_z\sqrt{BL}$
Torsion	$k_t = \frac{16GR^3}{3}$ <p>where R is</p> $R = 4\sqrt{BL(B^2 + L^2)}/6\pi$

where ν is Poisson's ratio of foundation medium, G = shear modulus of foundation medium, B is width of basemat/foundation perpendicular to direction of horizontal excitation, L is length of the basemat in the direction of horizontal excitation and $\beta_x, \beta_y, \beta_z$ = constants that are functions of the dimensional ratio, L/B which are adopted from ASCE 4-16 [1].

The soil supporting the structure is layered with data up to 10m depth known. Table 4.4 gives the properties of the foundation soil like Poisson's ratio, density and shear wave velocity

Table 4.4: Foundation Soil Properties

Layer	Depth (m)	Poisson's ratio	Density (kg/m ³)	E (KN/m ²)	Shear wave velocity(m/sec)
1	3	0.3	1700	299250	260
2	3	0.3	1700	450920	315
3	4	0.3	1700	586530	364

The weighted average shear velocity is
$$= \frac{\sum h}{\sum \frac{h}{v}} = \frac{3+3+4}{\frac{3}{260} + \frac{3}{315} + \frac{4}{364}} = 312\text{m/s}$$

This shear velocity will be used in evaluating spring stiffness for discrete springs.

Other properties are summed up below:

Bulk Density = 1700kg/m³. Plan dimensions of footing are 2500mm X 1500mm.

For X direction:

L=2500mm and B=1500mm.

L/B= 1.67,

From Fig. 5.1 of ASCE4-2016 [1], Constants $\beta_x, \beta_y, \beta_z = 0.98, 0.55$ and 2.14 respectively.

For Y Direction:

L=1500mm and B=2500mm. L/B= 0.60,

From Fig. 5.1 of ASCE4-2016 [1], Constants $\beta_x, \beta_y, \beta_z = 1.0, 0.48$ and 2.10 respectively.

The spring stiffness values for X and Y direction is given in Table 4.5.

Table 4.5: Spring stiffness values

		Units	2.0G	1.0G	0.50G
Horizontal	k_x	N/mm	3266127.68	816531.92	204132.98
Horizontal	k_y	N/mm	3332783.347	833195.8368	208298.9592
Rocking	$k_{\psi x}$	N.mm	4.87589E+12	1.21897E+12	3.04743E+11
Rocking	$k_{\psi y}$	N.mm	2.55319E+12	6.38299E+11	1.59575E+11
Vertical	k_z	N/mm	3918767.232	979691.8081	244922.952
Torsion	k_t	N.mm	4.96844E+23	1.24211E+23	3.10528E+22

4.4 Ground motion selection

Selection and scaling of earthquake ground motions are an important aspect in seismic load definition that will act on structure during structural analysis. The seismic resistance design codes normally suggest using at least three or seven ground motion records, for the time-history analysis purposes, which shall be compatible to the design spectrum. For example Section 16.1.3 of ASCE/SEI 7-05 [38] recommends that minimum of three appropriate ground motions must be used for analysis. It is also well known that spectral matching modify the frequency content of

ground motion record so as to match response spectrum to target spectrum. To preserve the original non stationary content of record, intensity based scaling method has been used which modifies amplitude only [39]. Since in our project incremental scale factors on ground motions are to be used, we have used intensity based scaling. A total of 12 no. of ground motion records have been used for both horizontal directions in which 11 are real earthquake accelerograms and 12th is the design basis ground motion of an NPP site. The ground motion records along with their PGA is given in Table 4.6. The normalized response spectra (RS) for all 12 ground records are presented in Figure 4.1, Figure 4.2 and Figure 4.3 for 4%, 5% and 7% damping.

Table 4.6: Ground motion records

S.No.	Record	PGA (g)
1	Chi chi	0.182
2	Kobe	0.820
3	Parkfield	0.357
4	Northridge-2	0.098
5	Coyote	0.124
6	Imperial Valley	0.169
7	Loma Gilroy2	0.357
8	Mammoth Lake	0.429
9	Nahaani	0.148
10	Whittier Narrows	0.186
11	Tarapur (Design Basis Earthquake)	0.200
12	El Centro	0.318

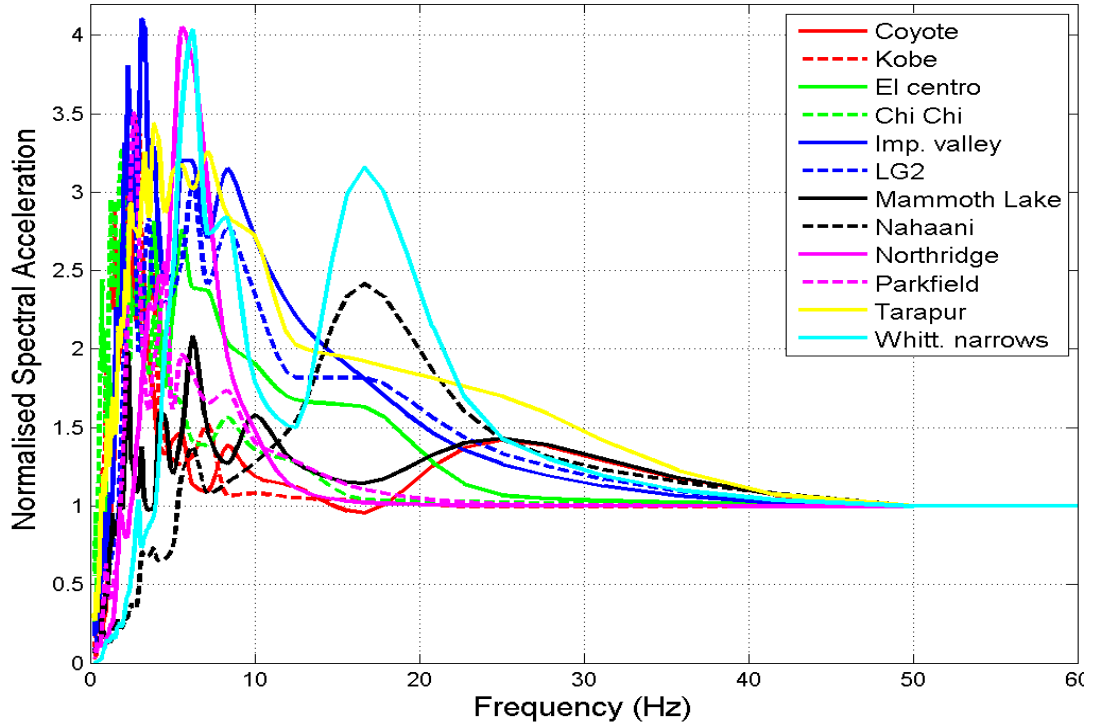


Figure 4.1: Normalized response spectra for 12 time histories for 4% damping

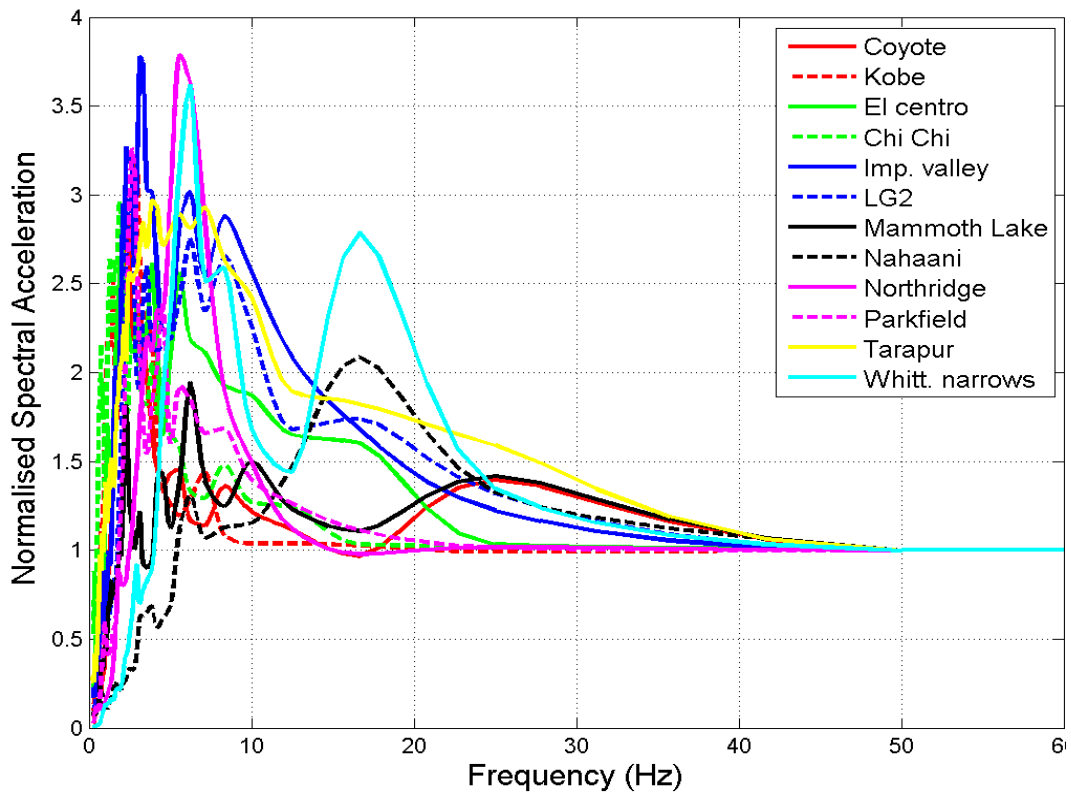


Figure 4.2: Normalized response spectra for 12 time histories for 5% damping

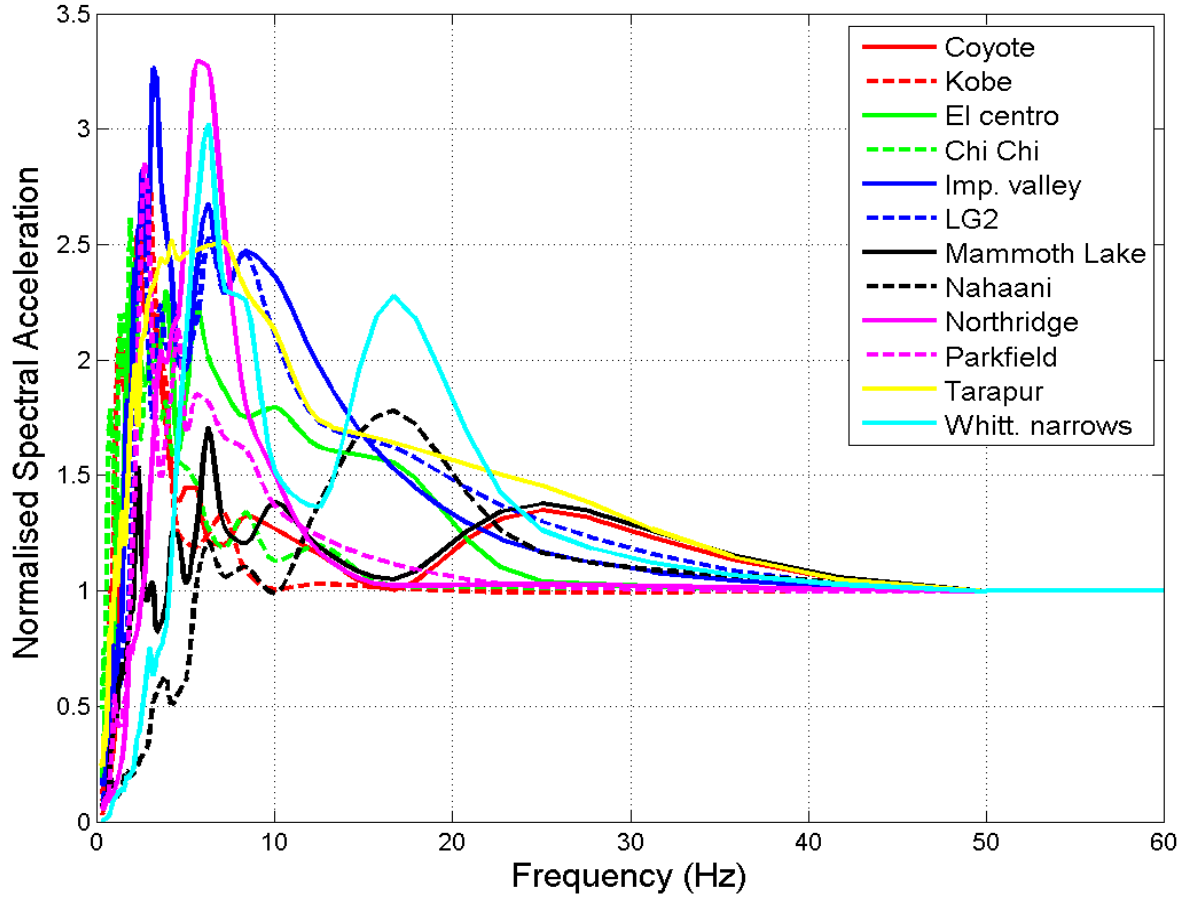


Figure 4.3: Normalized response spectra for 12 time histories for 7% damping

4.5 Nonlinear time history analysis

Dynamic analysis for various time histories was performed using direct integration method. This method involves numerically solving the equation of motion of structure.

$$[M]\{\ddot{x}(t)\} + [C]\{\dot{x}(t)\} + [K]\{x(t)\} = \{F(t)\} \quad (4.9)$$

Where,

$[M]$ is the mass matrix of the structure

$[C]$ is the damping matrix of the structure

$[K]$ is the stiffness matrix of the structure

$\{\ddot{x}(t)\}$ is the acceleration vector as a function of time, t

$\{\dot{x}(t)\}$ is the velocity vector as a function of time, t

$\{x(t)\}$ is the displacement vector as a function of time, t

$\{F(t)\}$ is the force vector as a function of time, t

To carry out non-linear dynamic analysis we need to impose non linearity into above equation of motion by defining stiffness matrix from elastic to inelastic range. Earthquake loads are reversing in nature. The loads change their directions continuously. This reversing nature of the loads demands a hysteresis model [40].

4.5.1 Pivot hysteresis model

A lot of research has been carried out in defining hysteretic rules. Initially elasto-plastic rules were used to model nonlinear behavior of all elements. This elasto-plastic behavior seems reasonable for steel members, but for reinforced concrete this model is not suitable because of stiffness degradation of RC members. The Takeda model was the first model purely for modeling behavior of RC members. This model demonstrated that constantly changing stiffness of reinforced concrete, producing less damping per cycle than an elasto-plastic response must be explicitly accounted for in hysteresis rules to produce realistic non-linear dynamic results. However Takeda models suffer from various limitations like inability to consider variable column axial loads, unsymmetrical sections, biaxial bending effects and sudden strength degradation in non-ductile members. The most accurate models are fiber models in which member cross section is divided into many longitudinal fibers representing reinforcement, confined and unconfined concrete. Cyclic stress strain rules are defined for all fibers which provide estimation of moment curvature hysteretic response. But fiber models require huge computational cost and storage requirement which limit these models only for experimental purposes only.

Pivot model, which is based on 3 simple geometrical rules only, easily capture the dominant nonlinear characteristics of complicated members and demonstrate close similarity in results with highly accurate fiber model. The model is based on the observations made on several experimental data on reinforced concrete columns. These observations show that the unloading, back to zero force from any displacement level is generally guided towards a single point in the force-displacement plane, on the idealized stiffness line [41]. Further, it was observed that all force displacement paths tend to cross the elastic loading line at approximately the same point. The first point was named as “primary pivot point” and the second point was named as “pinching pivot point”. Thus, the model basically needs to define only two parameters, namely, α parameter characterise the so-called primary pivot point and controls the unloading stiffness of the member and β parameter gives the pinching pivot point and controls the pinching behavior of the member.

4.5.2 Assumptions of Pivot hysteresis model

The Pivot hysteresis model utilizes the following two observations made from experimental hysteretic results of reinforced concrete members [41]:

- (1) Unloading stiffness decreases as displacement ductility increases, and
- (2) Following an inelastic excursion in one direction, upon load reversal, the force displacement path crosses the idealized initial stiffness line prior to reaching the idealized yield force (unlike elasto-plastic response).

4.5.3 Parameters for hysteretic response:

Parameters, ' α_1 ' and ' β_1 ' control the response in one loading direction and the parameters ' α_2 ' and ' β_2 ' control the response in the other loading direction. The primary pivot points P1 through

P4 in Figure 4.4, control the amount of softening expected with increasing displacement, and the pinching pivot points PP2 and PP4 fix the degree of pinching following a load reversal. Once, the deformation exceed yield limit in either direction, a subsequent strength envelope gets developed. The modified strength envelope, acting as upper bound for future cyclic loading, is defined by lines joining point PP4 to s1 and point PP2 to s2 (Figure 4.4). The point s1 and s2 move along the strength envelope and are defined by the previous maximum displacements.

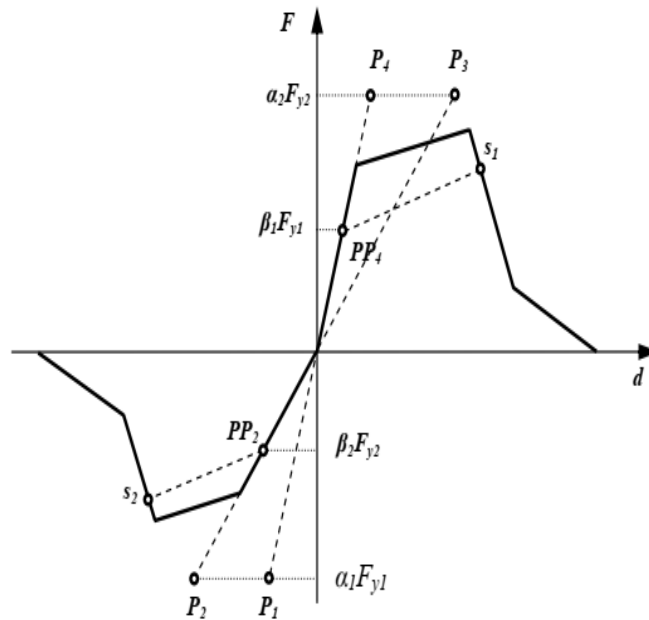


Figure 4.4: Pivot point designations

Dowell et al (1998) provided the contours for ' α ' and ' β ' as a function of axial load ratio and longitudinal reinforcement ratio. The contours were developed using the fiber element analysis of various circular column RC columns and were validated with the experimental results. Since, the model was originally developed for circular bridge columns, the axial load ratio was considered only up to 20% of the axial load capacity of the column.

Difficulty in applying original Dowell parameters to RC frames:

- i. Sections are normally circular.
- ii. Axial load can reach higher than 20% of axial load capacity of columns.
- iii. Transverse reinforcement also contributes in beams and columns which were not considered in Dowell models.

To derive the Pivot model parameters for rectangular columns, expressions developed by Sharma et al. [42] were used. These expressions were developed by analyzing the database of results of experiments on columns and beam-column joints subjected to cyclic loads. Two new parameters were given namely k_α and k_β , which could consider the effect of longitudinal and transverse reinforcement as well as the axial load on the columns were proposed. The parameters are defined as

$$k_\alpha = pt/ALR \quad (4.10)$$

$$k_\beta = (ALR)^{0.25} \times (psh)^{0.20} \quad (4.11)$$

where,

pt = percentage longitudinal reinforcement,

psh = percentage volumetric shear reinforcement

$$ALR = \text{Axial load ratio} = \frac{\text{total applied axial load on the column}}{\text{ultimate axial load capacity of the column}}$$

The equation relating ' α ' and ' k_α ' is given as (Sharma et al, 2013, [42])

$$\alpha = 0.170 k_\alpha + 0.415 \quad (4.12)$$

Similarly, the equation relating β and k_β is given as

$$\beta = 0.485 k_{\beta} + 0.115 \quad (4.13)$$

For the considered RC frame structure as seen in Figure 3.19, hinges are forming only at bottom storey columns, so hysteresis model is required only for bottom storey columns only. The values of α and β parameters as calculated are given in Table 4.7.

The force-deformation characteristics for link elements are provided in SAP2000 in form of moment-rotation curve. The curve was generated by converting moment-curvature curves derived for bottom storey columns into moment-rotation. Unlike hinges definition in SAP2000, the link definition in SAP allows more than 5 points to be inserted into force-deformation property which gives more freedom to accurately define profile of the respective curve. The moment rotation curves for link element for X and Y direction for the bottom column are presented in Figure 4.5 and Figure 4.6 .

The force deformation curves (or moment-rotation curves) generated after analyzing model for 2 different intensities 0.4g PGA and 1.8g PGA for ‘Coyote earthquake ’ ground motion record with 7% structural damping using NLTHA is given in Figure 4.7 and Figure 4.8 and that of 0.4g earthquake intensity for ‘Coyote earthquake’ in Y direction is given in Figure 4.9

Table 4.7: Parameters for Pivot model

Parameter	value
k_{α}	5.552656
k_{β}	0.73565
α	1.358951
β	0.47179

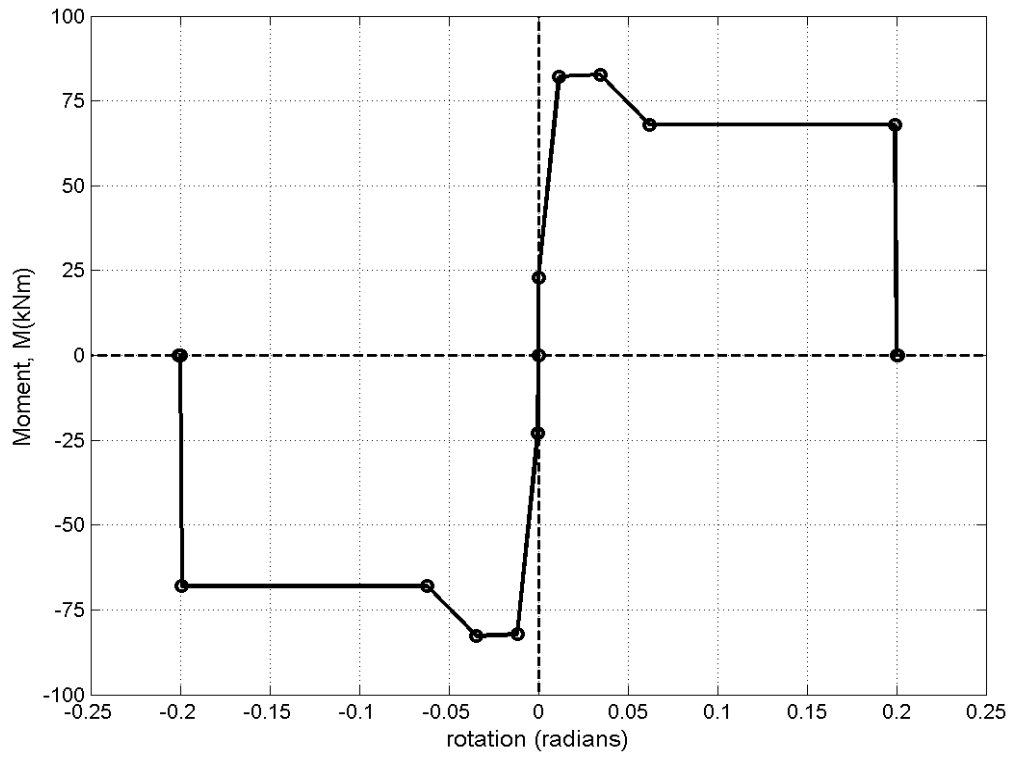


Figure 4.5: Moment-rotation curve for link X direction

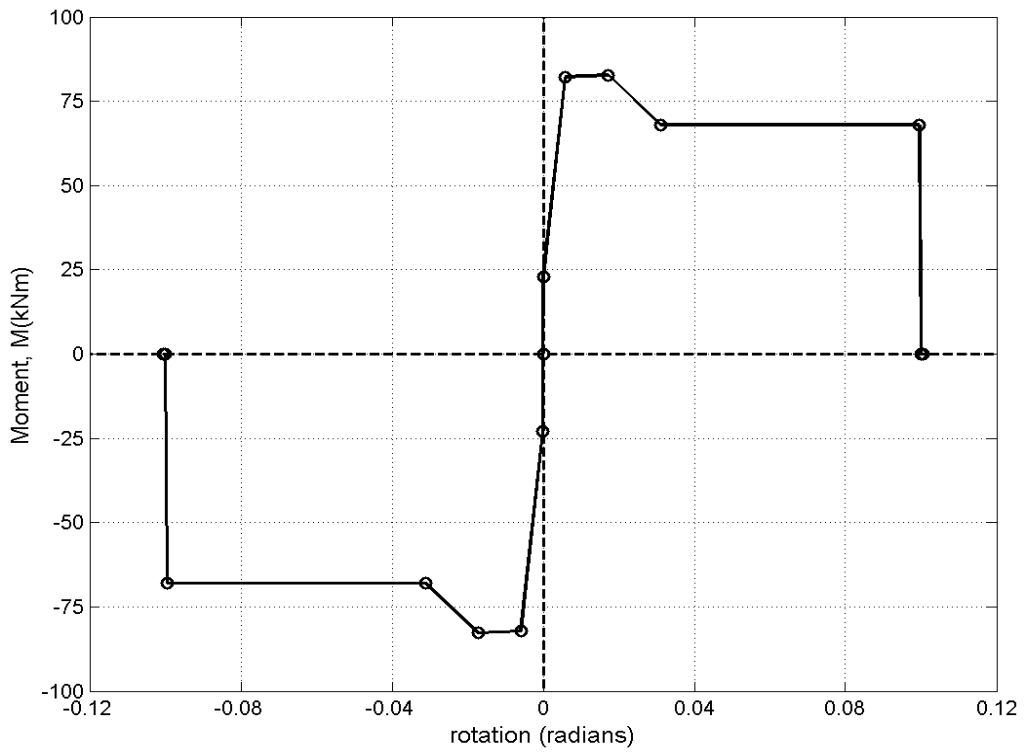


Figure 4.6: Moment-rotation curve for link Y direction

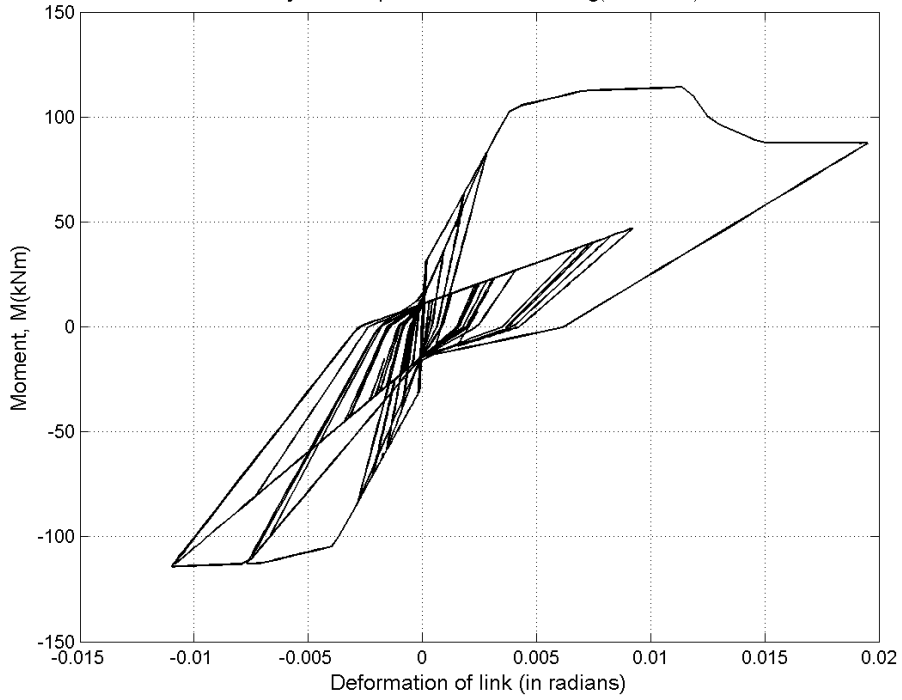


Figure 4.7 Force deformation curve for link element for 0.4g scale factor and 7% damping, X direction

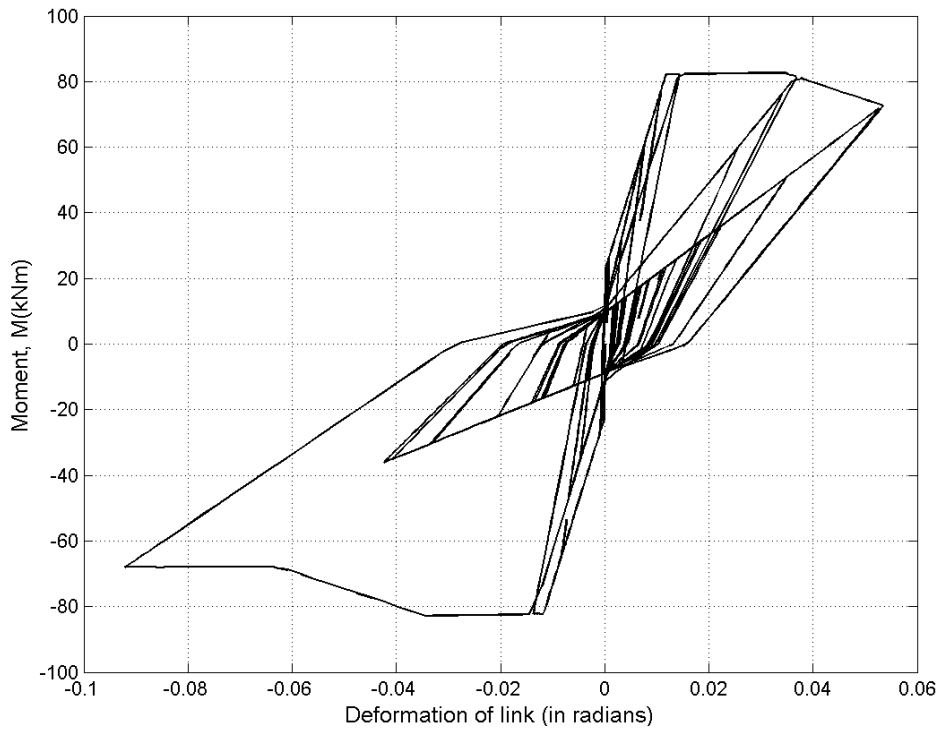


Figure 4.8: Force deformation curve for link element for 1.8g scale factor and 7% damping, X direction

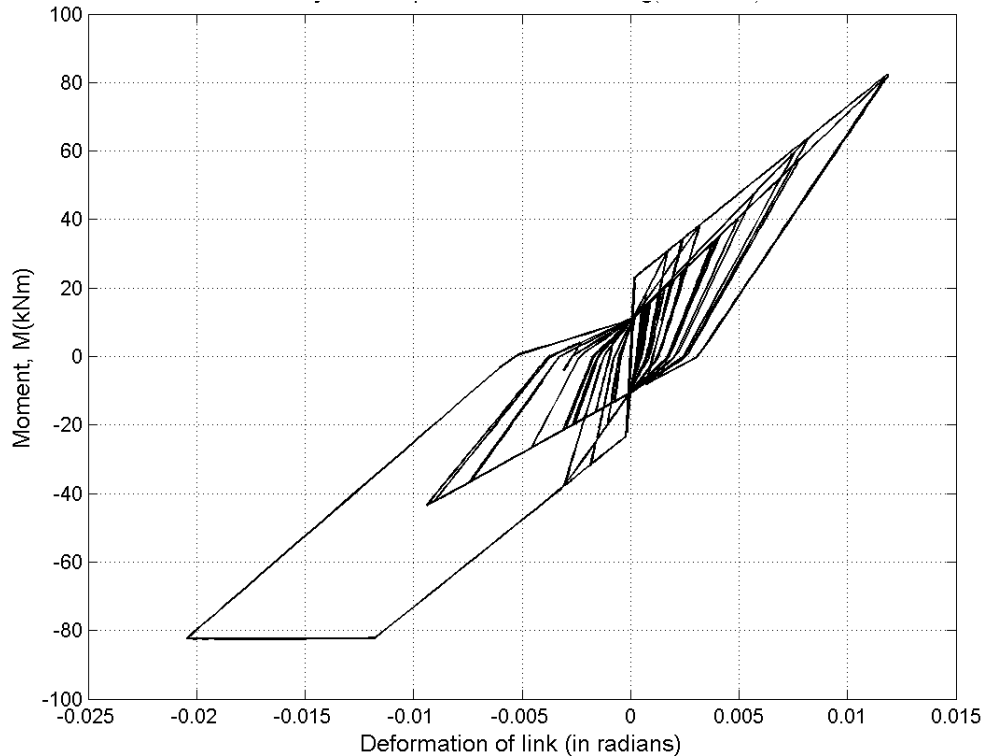


Figure 4.9: Force deformation curve for link element for 0.4g scale factor PGA and 7% damping, Y direction

4.6 Incremental dynamic analysis (IDA)

In order to derive fragility curves, we need to obtain the probability of exceeding a specified damage state. Various methods can be employed to find this probability out of which Incremental dynamic analysis is quite promising. The complete methodology of performing IDA is well presented in Vamvatsikos & Cornell, 2002 [2].

Specifically, IDA involves subjecting a structural model to one (or more) ground motion record(s), each scaled to multiple levels of intensity. The result is a curve that shows the Engineering Demand Parameter (EDP) plotted against the Intensity Measure (IM) used to control the increment of the ground motion [22].

IDA basically revolves around 3 parameters: scale factor, Intensity measure and damage measure otherwise known as Engineering demand parameter.

Scale factor

Scale factor is employed to scale the ground motion record in such a way that structure goes all from elastic to yielding to collapse stage. To achieve this, a single ground motion record is scaled up and down on an average 9 times in this study. Consequently, a total of 144 x 9 (12 time histories, 4 support conditions, 3 damping cases and 9 scale factors) time history analysis are performed for each horizontal direction.

Intensity measure (IM)

In the present age of high end computation abilities, non linear dynamic analysis is widely gaining popularity, it is increasingly important to understand which characteristics of a recorded ground motion records are most strongly related to the response caused in the structure. Consequently, a value should be defined to quantify the effect of a record on a structure that is IM. As per Vamvatsikos & Cornell(2002) [2] pre-requisite for selection of IM is that it should be scalable and monotonically increasing with scale factor. Though many quantities e.g. Moment Magnitude, Duration, or Modified Mercalli Intensity etc can characterise the intensity of a ground motion record, but whether these quantities can be scaled or not also contributes to their choice as IM. The quantities like Moment Magnitude, Duration, or Modified Mercalli Intensity are non scalable and hence not used as IM. Common examples of scalable IMs are the Peak Ground Acceleration (PGA), Peak Ground Velocity and Spectral Acceleration at the structure's first-mode period S_a (T_1). PGA is site specific and does not contain information about structure characteristics. On the other hand S_a (T_1) is more structure specific and more efficient than PGA (Shome et al.1998) [43]. Consequently, S_a is selected as IM for this study.

Damage measure (DM)

In IDA, IM is input and DM is output. DM is an observable quantity that is part of, or can be deduced from output of corresponding nonlinear dynamic analysis. The output of this analysis give us choices like maximum base shear, node rotations, peak storey ductilities, global drift ratio and interstorey drift ratio etc to be used as DM.

Choice of DM also depends on application of IDA. If the damage to nonstructural contents in a multi-storey frame needs to be assessed, the peak floor accelerations are the obvious choice. On the other hand, for structural damage of frame buildings, interstorey drift relates well to joint rotations and both global and local storey collapse, thus becoming a strong DM candidate.

For tall, long-period buildings, the higher modes typically contribute significantly to the seismic response (at least in the elastic range). Thus, global drift ratio is less effective for tall, long-period buildings than it is for a shorter building whose response is dominated by the fundamental mode.

Since structure considered in study is experiencing deterioration of hinges only for bottom storey, interstorey drift ratio has been selected as DM.

4.6.1 Characteristics of IDA curves

The characteristics of IDA curves are explained in this section. The Figure 4.10 gives IDA curve for single record of El Centro and Northridge ground motions for fixed support. Since IDA curves are dependent on accelerograms, different ground records will produce different curves. All curves have a typical linear region initially where the structure behaves elastically. This behavior terminates when the 1st non linearity comes into play. The initial slope for a given IM and DM can be called its elastic stiffness. After initial elastic portion the curves slightly softens where local slope or stiffness decreases with higher IM and then undergo hardening region and again softening.

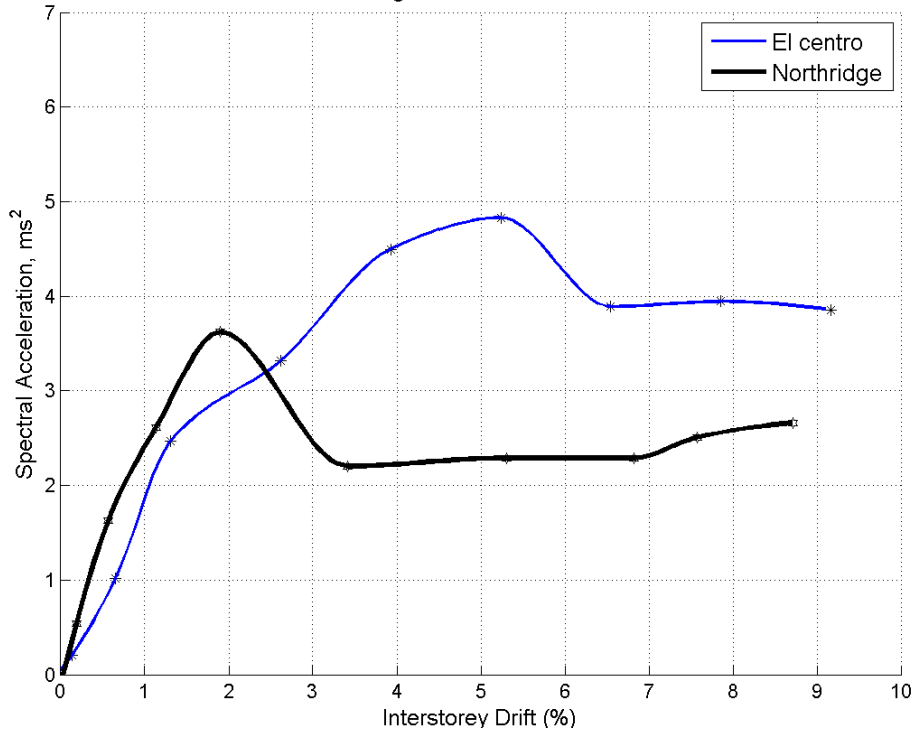


Figure 4.10: IDA curves for 2 ground motion records for fixed support for 7% damping

Eventually the structure enters instability region indicated by increasing DM while IM decreases continuously. Both curves in Figure 4.10 are terminating at different levels of IM. ‘El Centro’ curve seems to weave around initial elastic stiffness line. Both curves have shown softening and hardening behavior mildly. The hardening behavior is amplified in Northridge record at around 7% DM after showing regions of softening and almost constant S_a .

Termination of IDA curve

IDA curve should be terminated at a point where global dynamic instability occurs. This point also known as capacity point can be set by using FEMA-350 20% IM based rule. According to which the point on the curve where the tangent slope becomes 20% of its elastic slope is defined to be capacity point. The flattening of the curve is taken as an indicator of dynamic instability. But while applying this rule care should be taken regarding hardening behavior of curve also. Sometimes the

structure undergoes stages of flattening and then hardening. In those situations, we should discourage terminating at the very 1st point where 20% IM rule satisfies.

We can also use 10% DM based rule (assuming DM as inter storey drift). As per this rule the point where curve achieves 10% of DM is the capacity point of structure.

In this study we have chosen capacity point using both rules. If such point occurs after 10% DM then the point corresponding to 10% DM is selected as capacity point.

The same IDA curves of Figure 4.10 after termination are given in Figure 4.11.

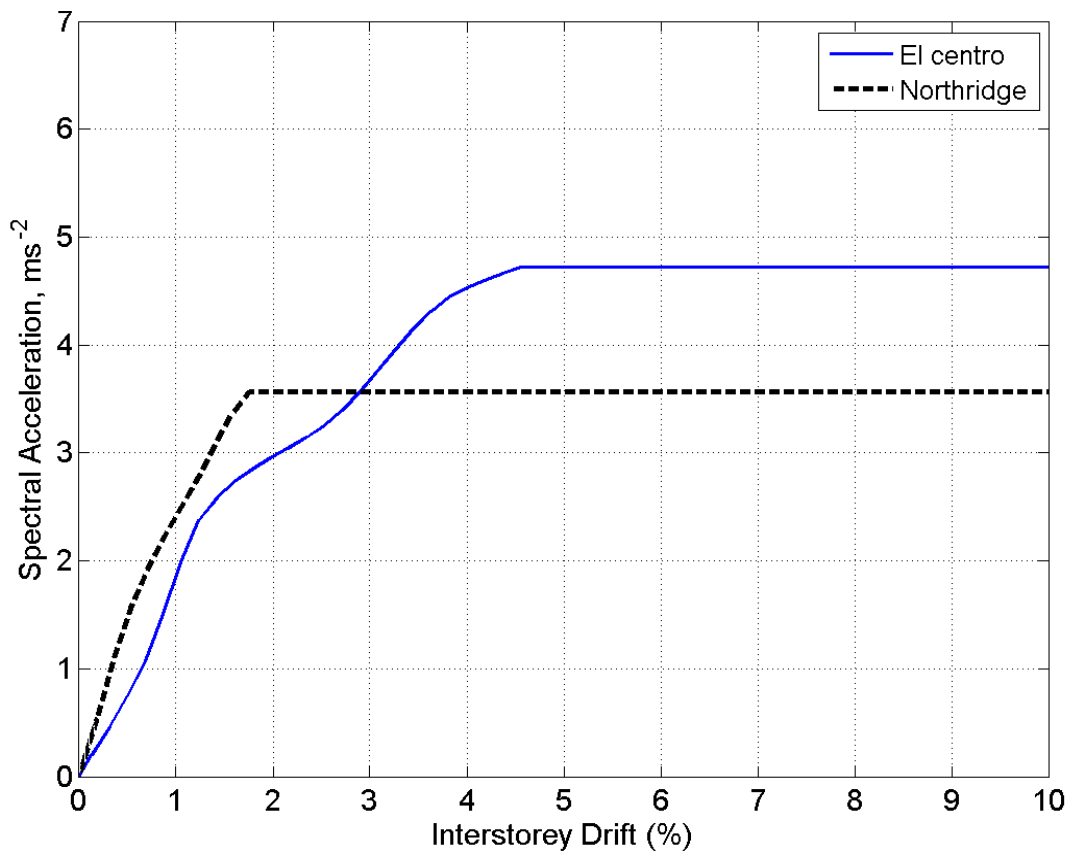


Figure 4.11: Flattened IDA curves for 2 time histories

IDA curves for Whittier narrows time history for fixed support for different damping values is shown in Figure 4.12. It is observed that the demand of S_a is least in case of 7% damping followed by 5% and then 4% damping value. This trend is similar to response spectrum where higher the

damping lesser the value of S_a is observed. Similar comparison is made in Figure 4.13, where the different damping curves are more or less overlapping each other. There are regions where demand for 5% damping is coming lesser than 7% damping. This is due to limitation of lesser number of analysis points (9 analysis points or scale factors are only used for each time history). It is because, hysteretic energy dissipation is different for different damping curves at higher acceleration. At 4% damping if the hysteretic energy dissipated is slightly more than that at 7% damping the Spectral acceleration attracted at 4% damping will be lesser than that at 7% damping.

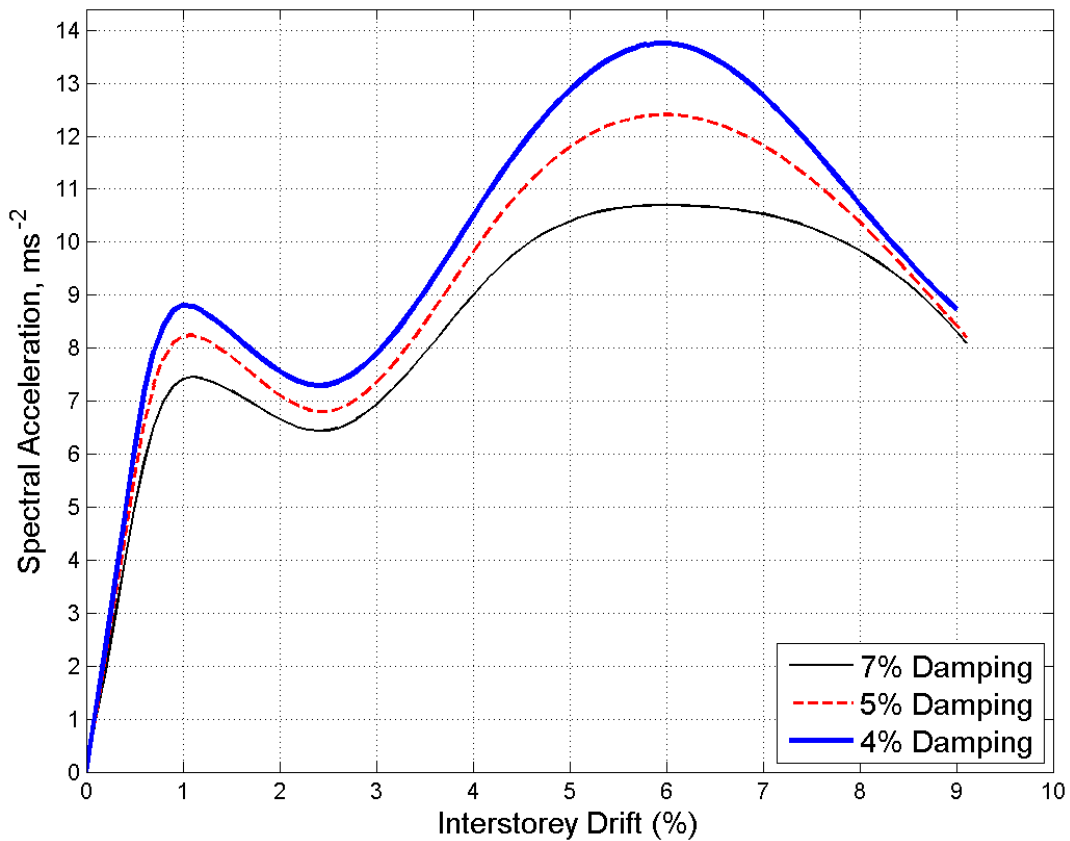


Figure 4.12: IDA curve for Whittier Narrows TH with different Damping for fixed support

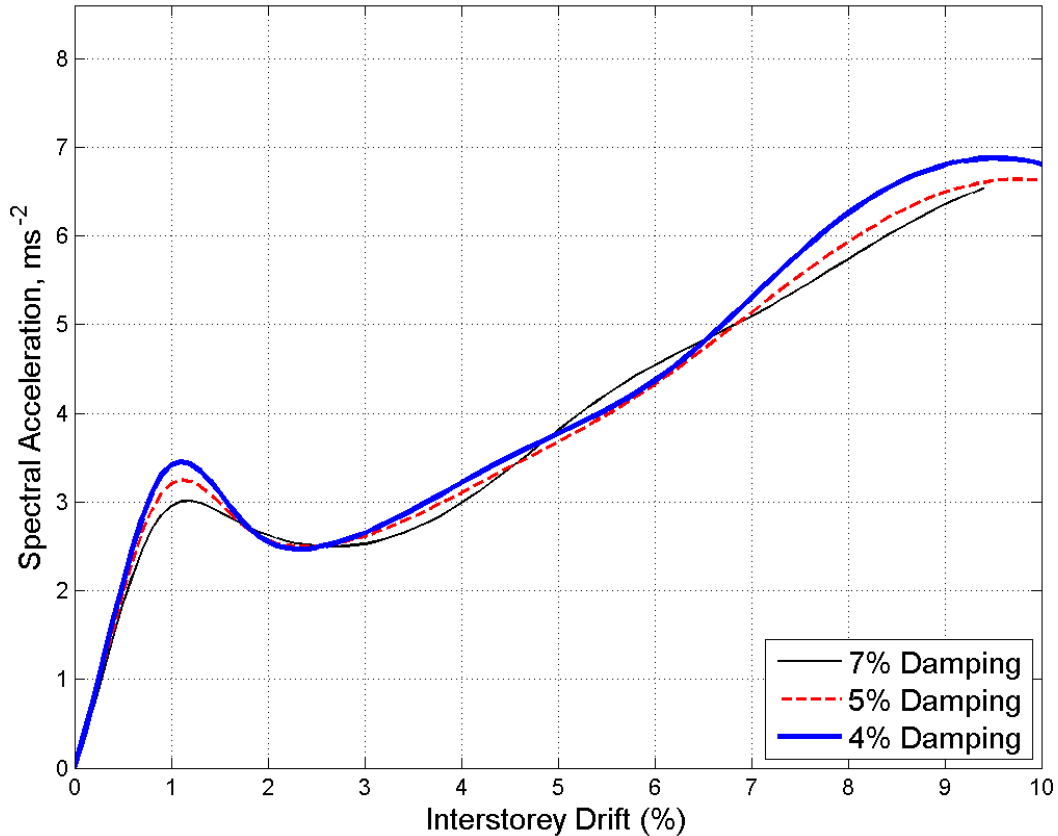


Figure 4.13: IDA curve for Loma Gilroy2 TH with different damping cases

The flattening of curves is accomplished considering both IM and DM criteria. The IDA curves for all 12 time histories are briefly explained below:

Coyote TH (Figure 4.14): Dynamic instability occurs at around 2% DM for all cases. This instability is marked by flat lines arrived using termination criteria. The curves for different cases are not showing significant variation from each other. The maximum demand for all the cases vary from 7.6m/s^2 to 9m/s^2 . Demand for 7% damping cases is observed to be minimum for all 4 support conditions. None of the curves have shown hardening after achieving their peak.

Kobe TH (Figure 4.15): The maximum demand of S_a is varying from 12m/s^2 to 9m/s^2 . Some of the curves have shown hardening after reaching 1st peak and subsequent softening. In

initial elastic region all the curves are overlapping each other. Deviation starts after DM of 1%. The demand is observed as maximum for fixed base and 7% damping case. Also it is observed that 7% damping cases have no significant hardening. However most of 4% and 5% damping cases are undergoing hardening.

El Centro TH (Figure 4.16): For this TH most almost all the curves are undergoing hardening after initial softening. The demand is varying from 3.9m/s^2 to 5.1m/s^2 . The curves for fixed base case are lying higher as compared to soil spring supported base.

Chi Chi TH (Figure 4.17): The curves are not marked by flat lines. Here the curves are terminated using 10% criteria only. All curves are undergoing appreciable hardening after 1st softening. Curves for fixed supports are lying higher than 0.5G soil spring supports case. The curves of 1.0G and 2.0G soil spring cases are lying approximately between fixed and 0.5G cases. The maximum demand is varying from 6.8m/s^2 to 8.2m/s^2 .

Imperial Valley TH (Figure 4.18): The curves are undergoing hardening after initial softening. The maximum demand is varying from 6m/s^2 to 7.9m/s^2 . The maximum demand is observed for fixed support case with 4% damping.

Loma Gilroy2 TH (Figure 4.19): The curves are undergoing hardening after initial softening. The maximum demand is varying from 3.4m/s^2 to 6.2m/s^2 . The curves of 2.0G soil spring support and 4% damping along with fixed support case and 4% damping are attracting maximum demand. The cases of soil support with 1.0G and 0.5G springs have minimum demand.

Mammoth Lake TH (Figure 4.20): The curves are showing appreciable variation from each other. The maximum demand is varying from 4.0 m/s^2 to 8.0 m/s^2 . Fixed support case with 4

% damping is attracting maximum demand. The cases of soil support 1.0G and 0.5G soil springs have minimum demand

Nahaani TH (Figure 4.21): The curves are undergoing continuous hardening. The maximum demand is varying from 4.6 m/s^2 to 5.4 m/s^2 . Fixed support case with 4 % damping is attracting maximum demand.

Northridge TH (Figure 4.22): The curves are not undergoing hardening for this case. The maximum demand is varying from 2.5 m/s^2 to 3.8 m/s^2 . Fixed support case with 7 % damping is attracting maximum demand.

Parkfield TH (Figure 4.23): The 0.5G soil spring support case is attracting least demand and is showing significant variation from other curves. The maximum demand is varying from 5.5 m/s^2 to 10.4 m/s^2 . The fixed support case with 4% damping and 5% damping are the cases attracting maximum demand.

Tarapur DBE (Figure 4.24): This earthquake record is attracting least S_a demand out of all 12 cases. The curves are very near to each other. The maximum demand is varying from 1.7 m/s^2 to 2.1 m/s^2 . The cases of fixed support with 4% damping and 0.5G support with 7% damping are attracting maximum demand.

Whittier Narrows TH (Figure 4.25): The curves are undergoing hardening after initial softening. The maximum demand is varying from 8.8 m/s^2 to 13.1 m/s^2 . The case of 0.5G soil spring support with 4% damping is attracting maximum demand.

The combined 144 curves for all support cases and damping types for X direction is presented in Figure 4.26 with drift limits of 2%, 4% and 6% highlighted on all curves.

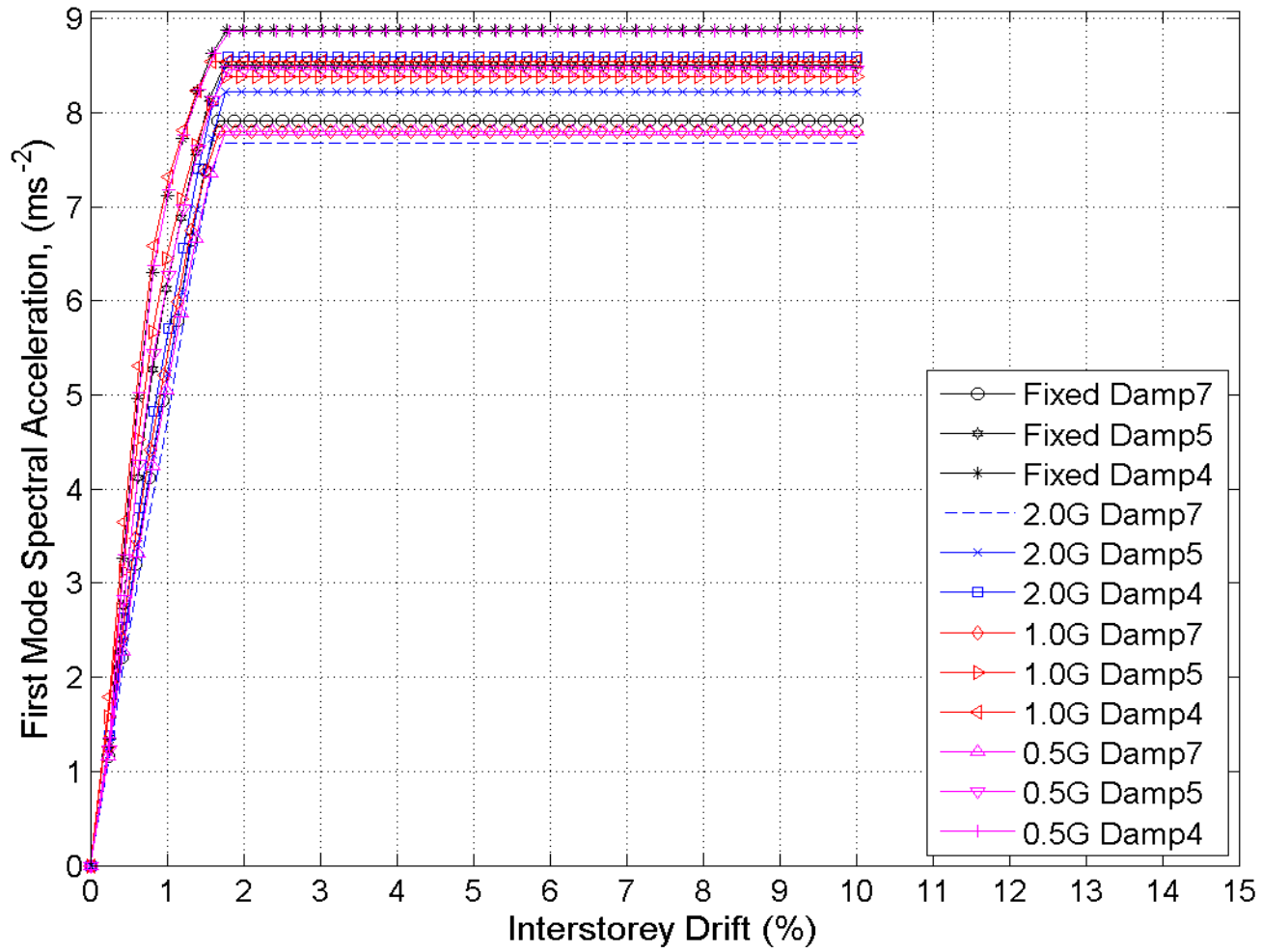


Figure 4.14: IDA curve for TH-Coyote for all 12 cases (X direction)

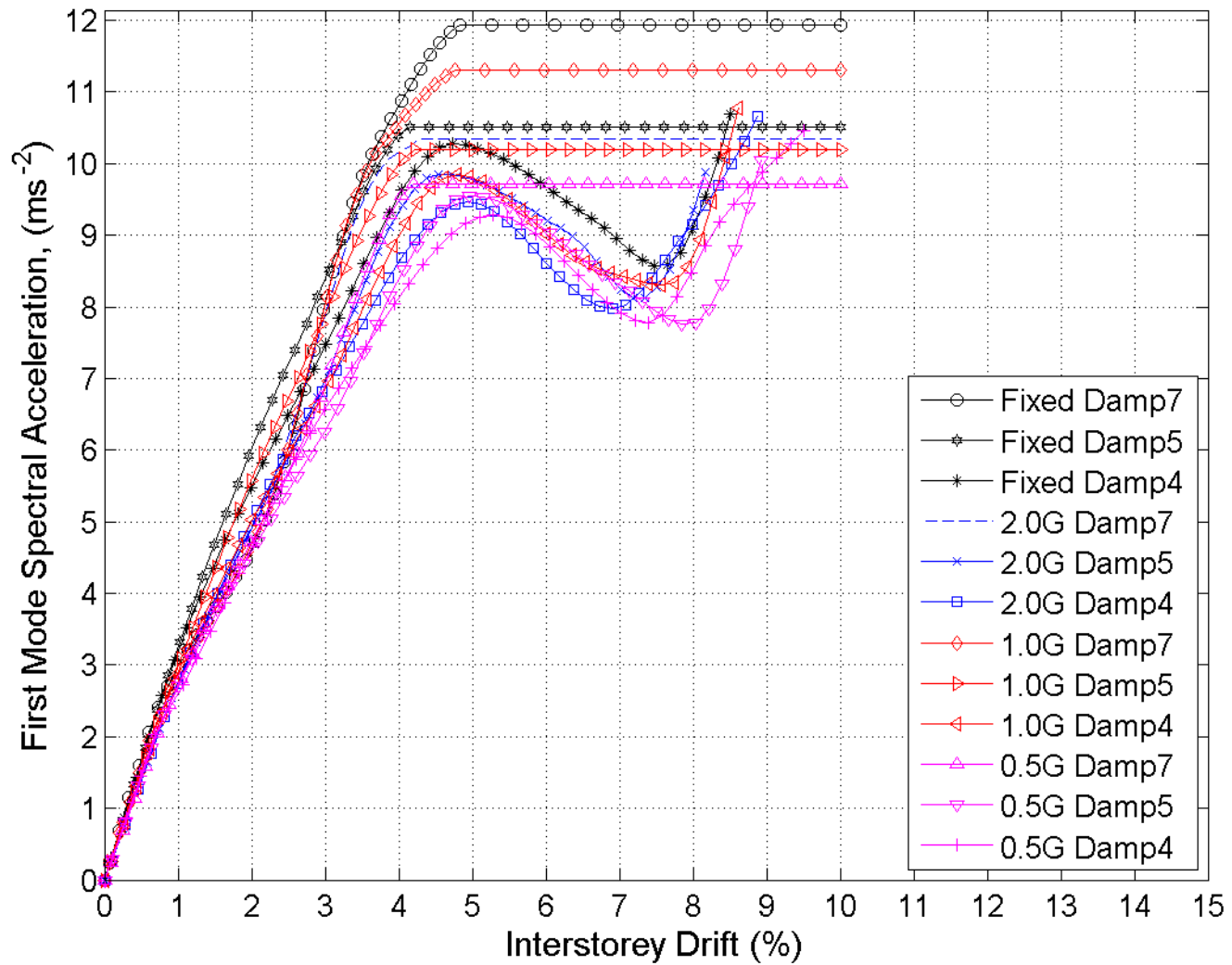


Figure 4.15: IDA curve for TH-Kobe for all 12 cases (X direction)

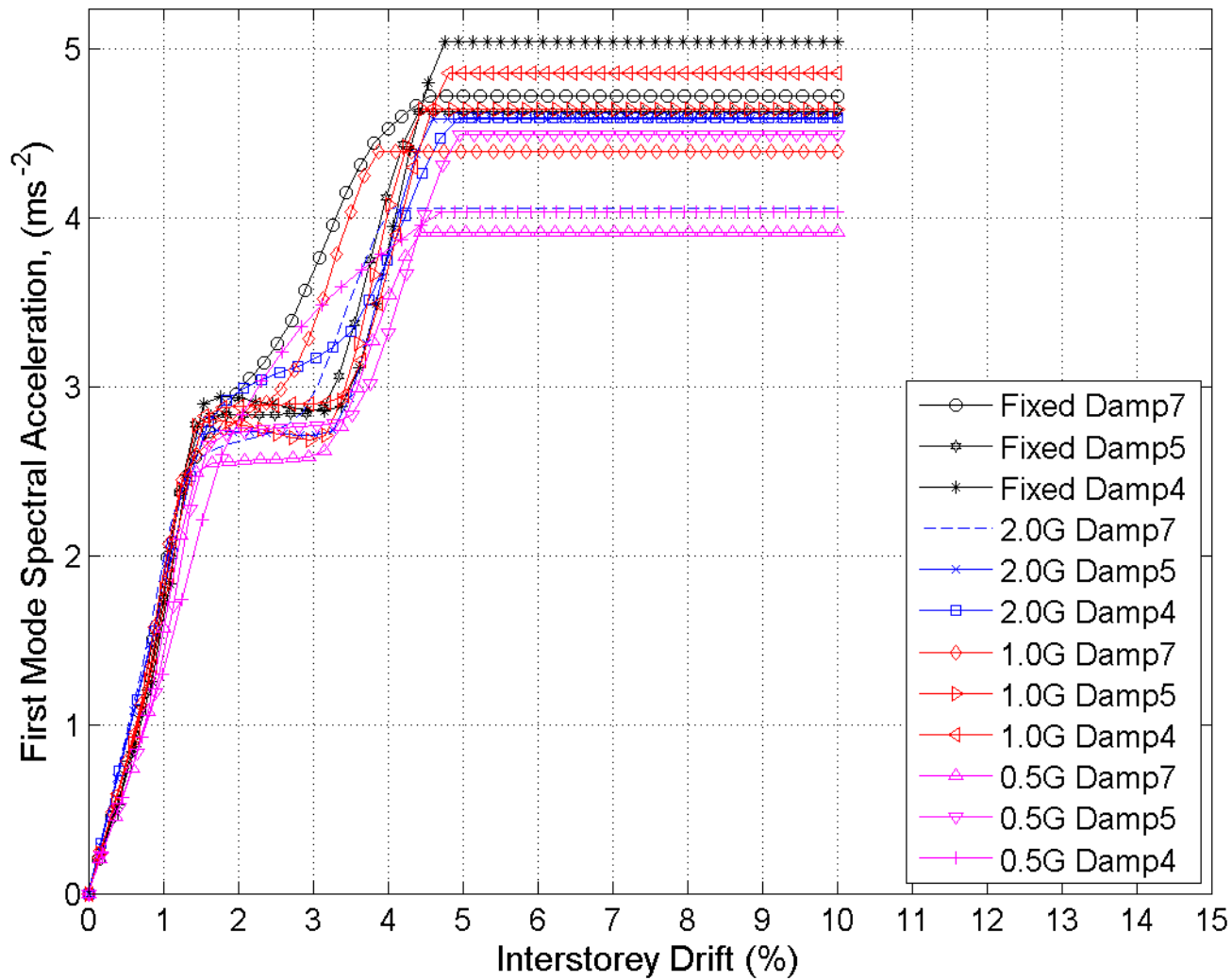


Figure 4.16: IDA curve for TH-EI Centro for all 12 cases (X direction)

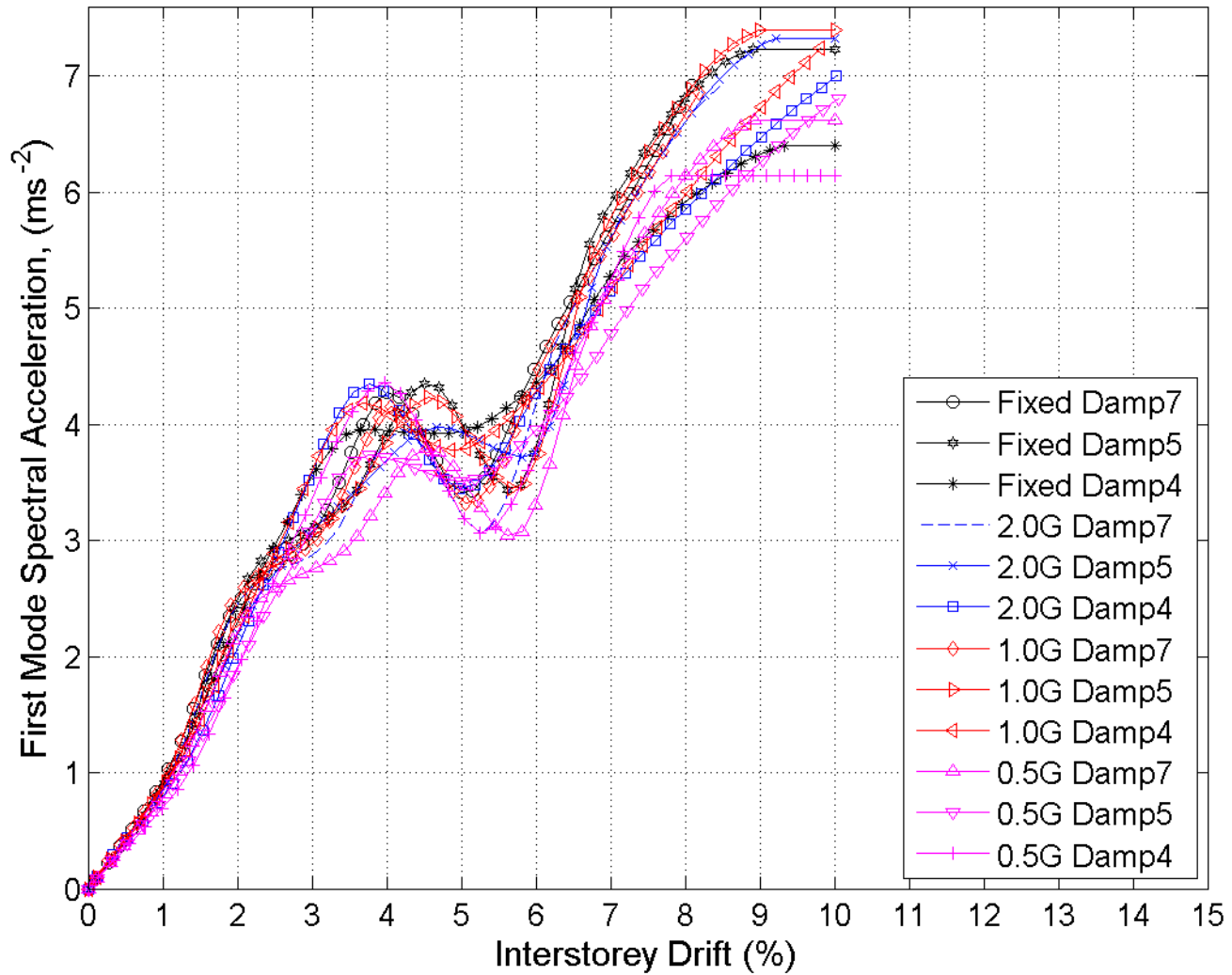


Figure 4.17: IDA curve for TH Chi-chi for all 12 cases (X direction)

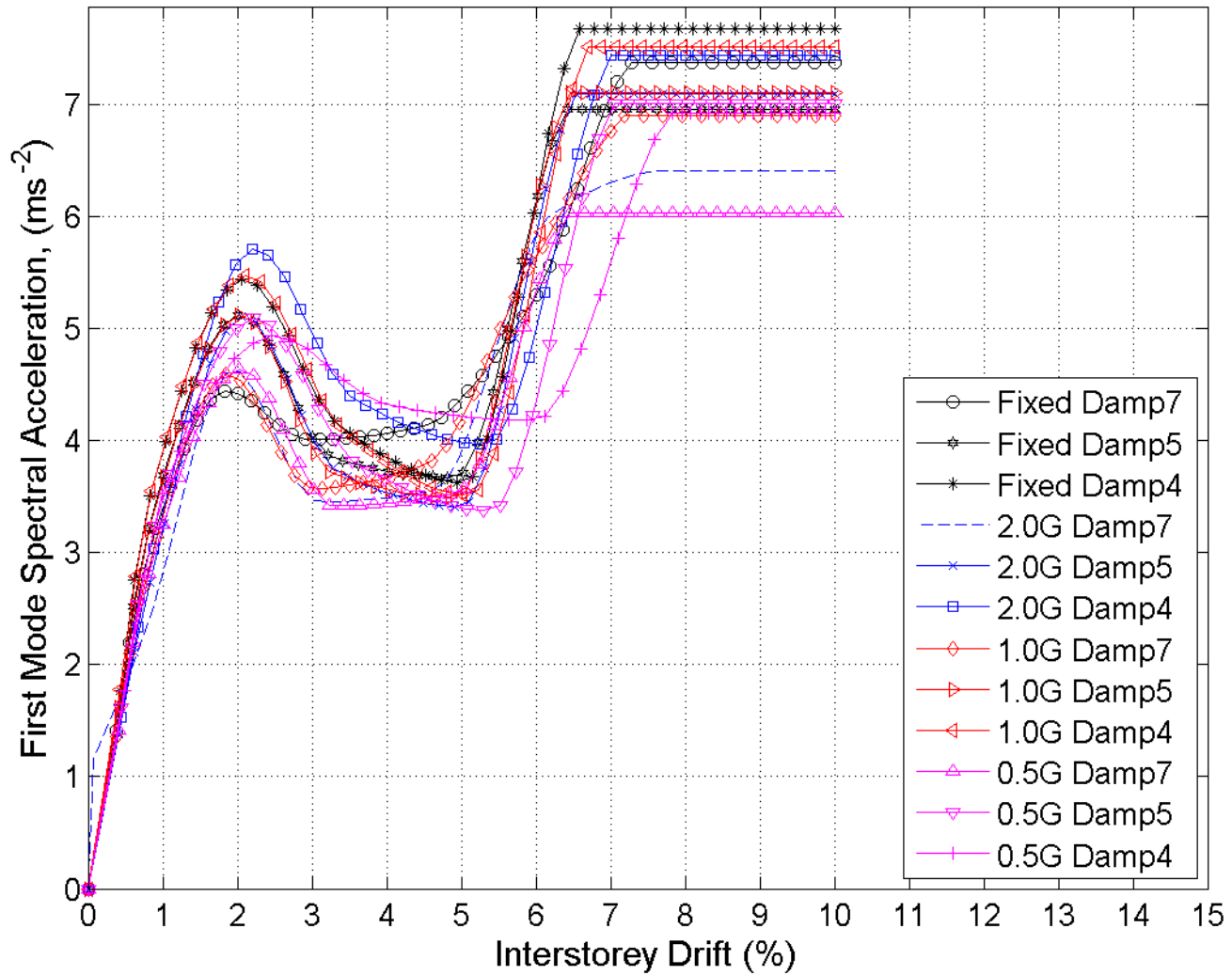


Figure 4.18: IDA curve for TH-Imperial Valley for all 12 cases (X direction)

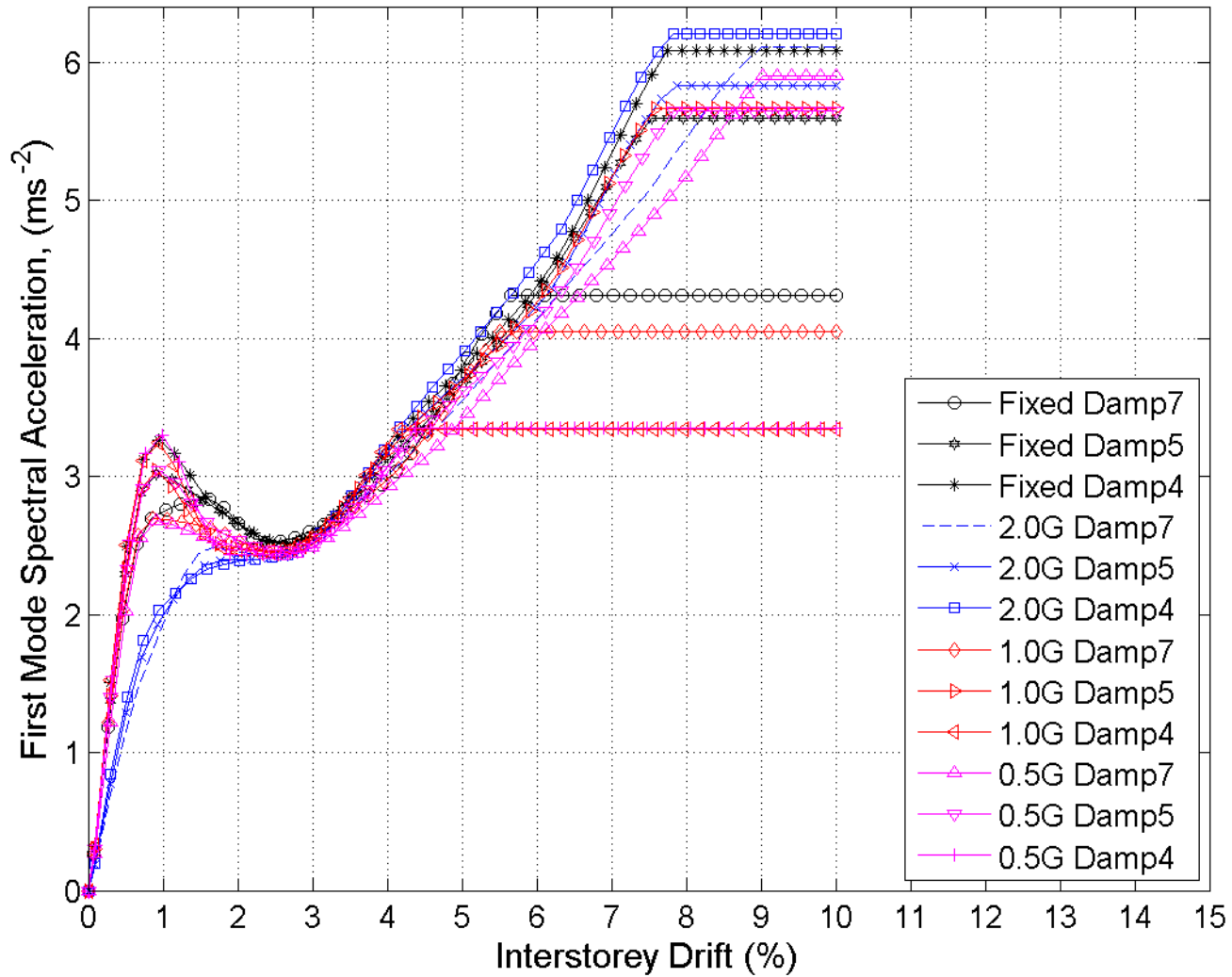


Figure 4.19: IDA curve for TH-Loma Gilroy2 for all 12 cases (X direction)

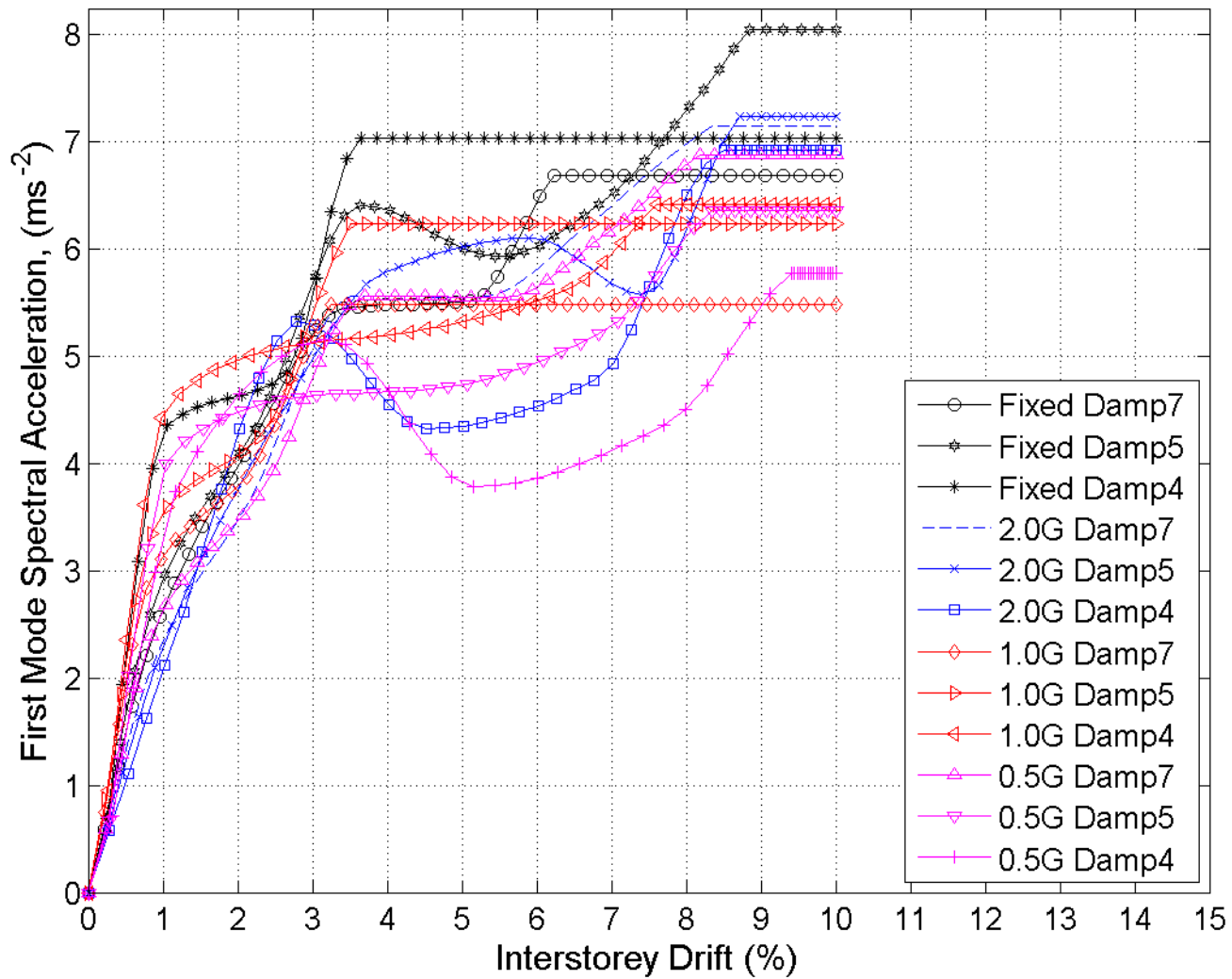


Figure 4.20: IDA curve for TH-Mammoth Lake for all 12 cases (X direction)

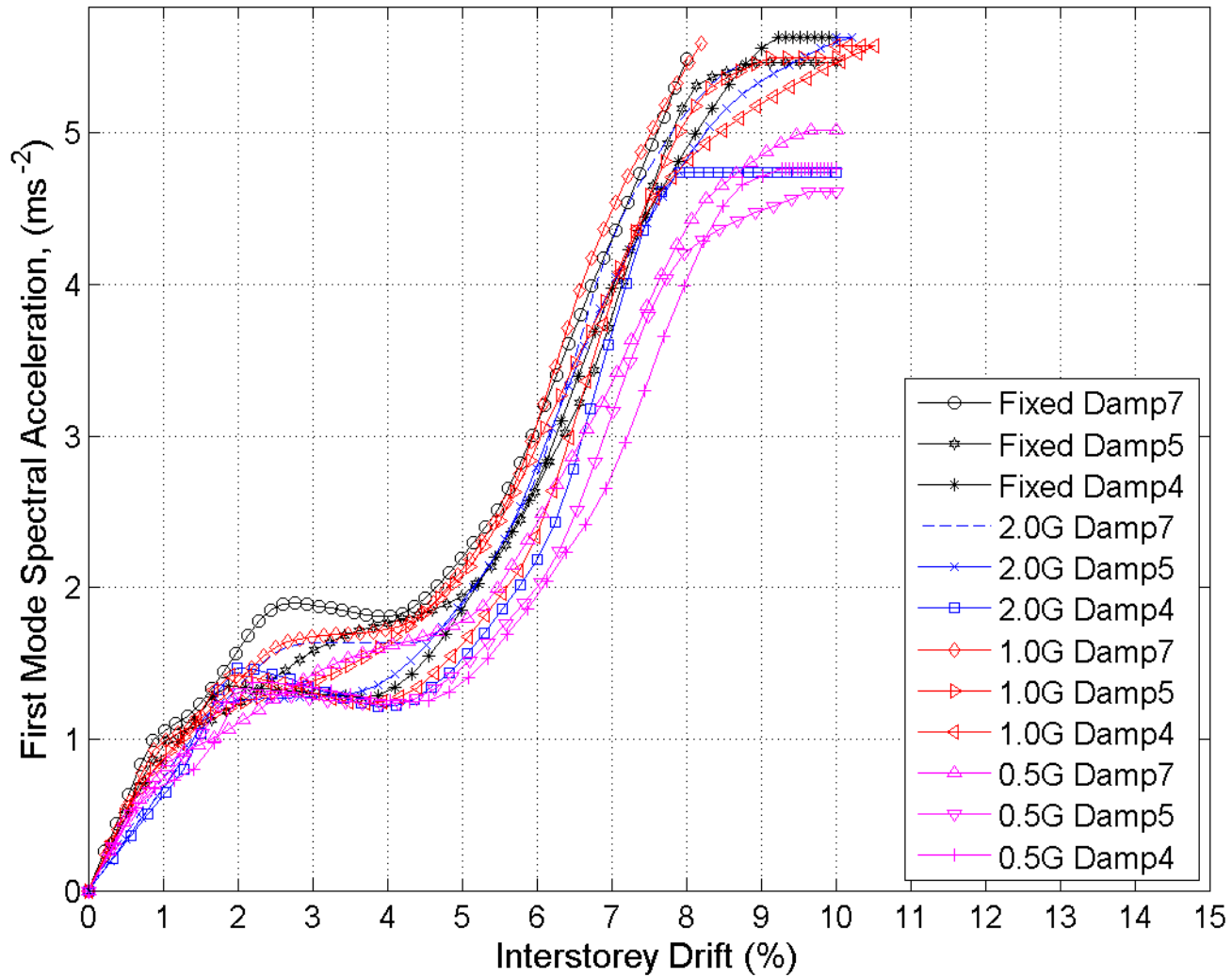


Figure 4.21: IDA curve for TH-Nahaani for all 12 cases (X direction)

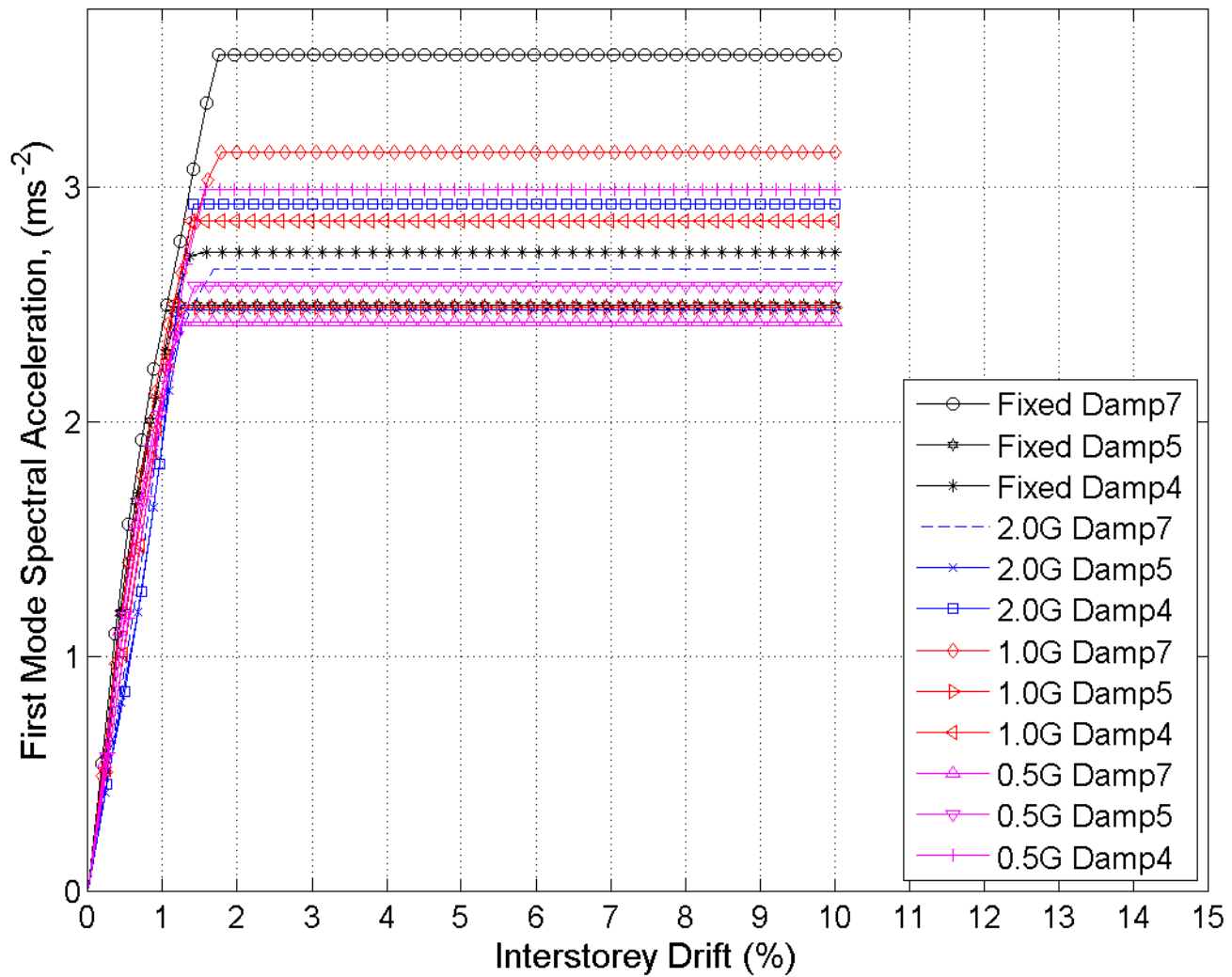


Figure 4.22: IDA curve for TH-Northridge for all 12 cases (X direction)

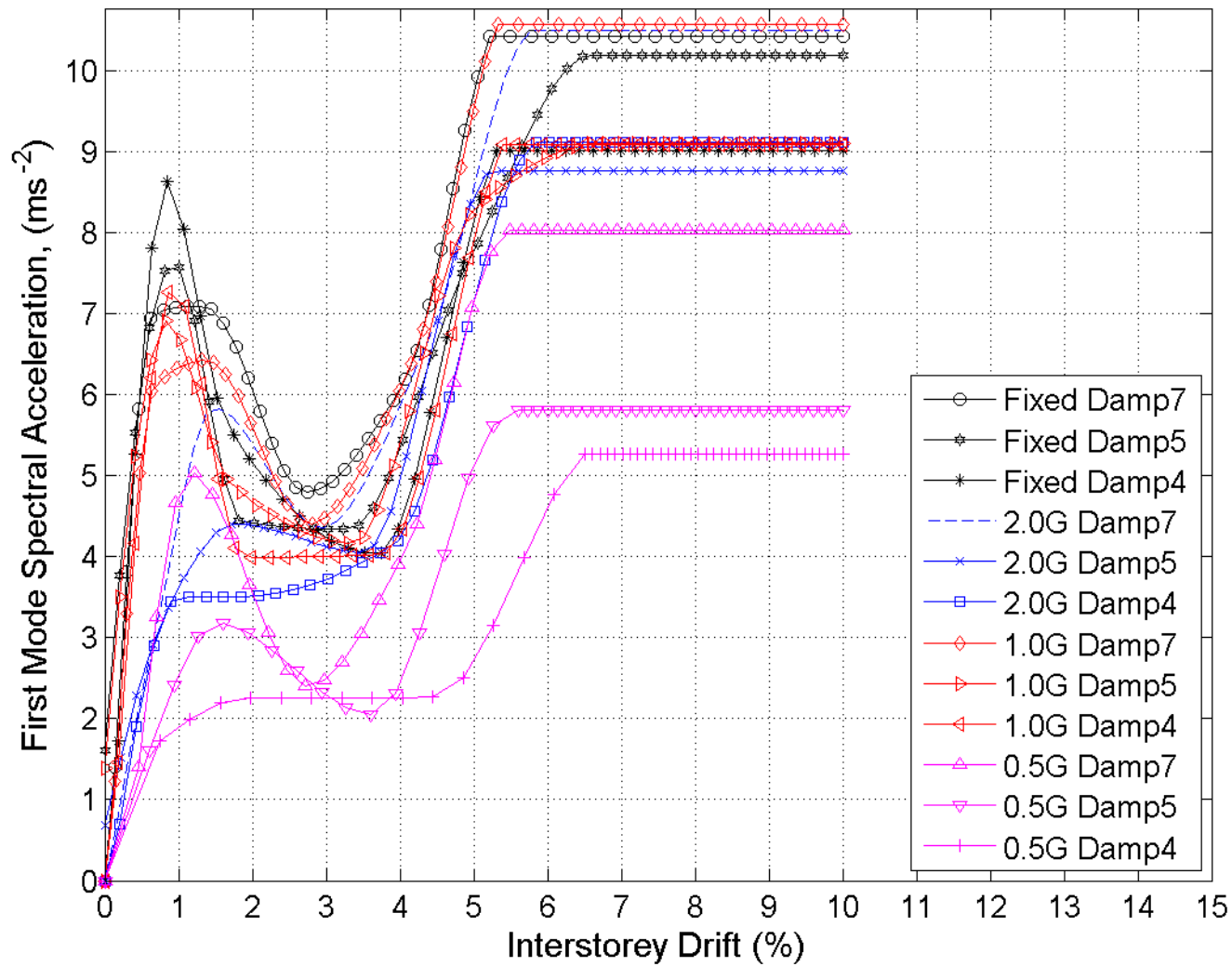


Figure 4.23: IDA curve for TH-Parkfield for all 12 cases (X direction)

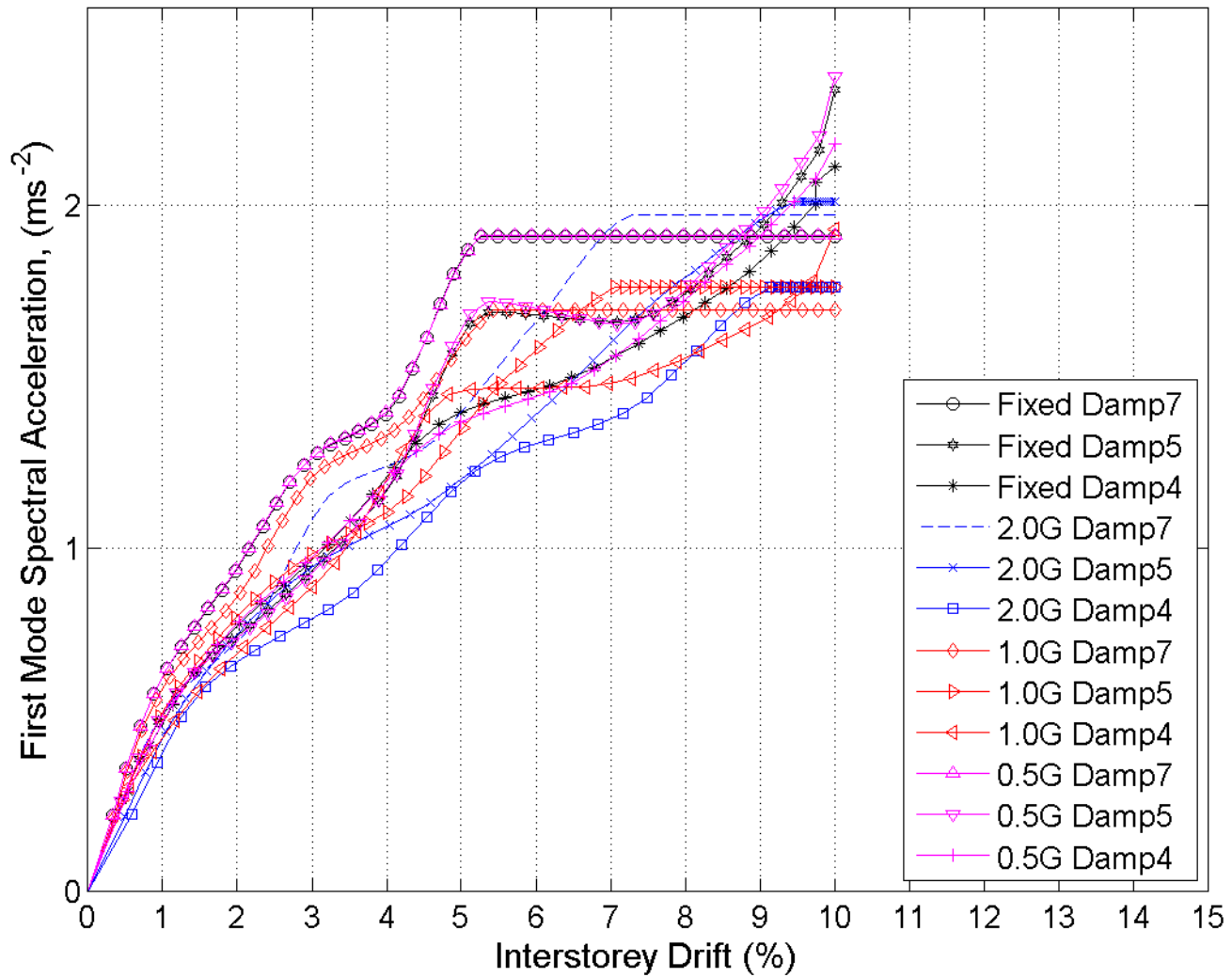


Figure 4.24: IDA curve for TH-Tarapur DBE for all 12 cases (X direction)

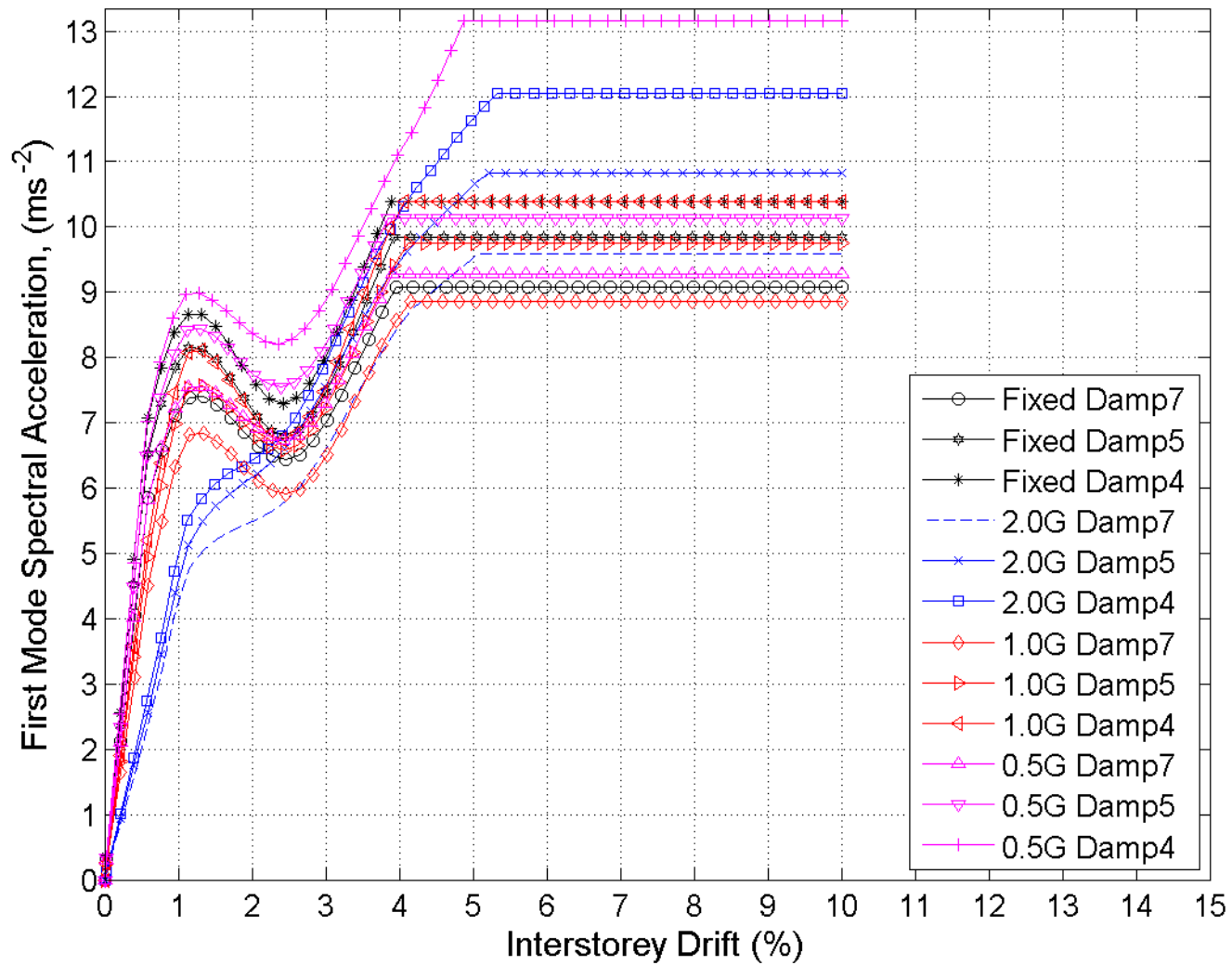


Figure 4.25: IDA curve for TH-Whittier Narrows for all 12 cases (X direction)

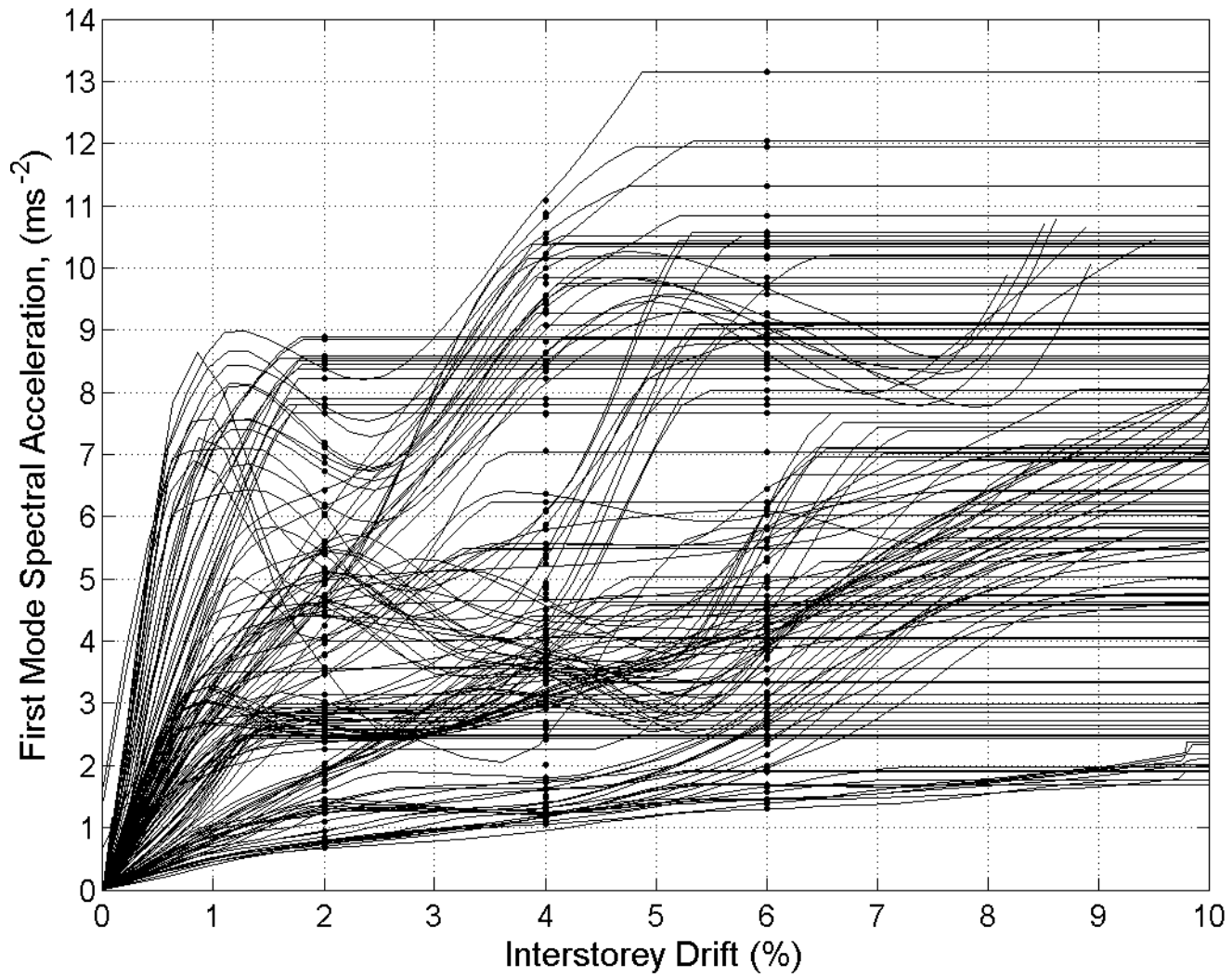


Figure 4.26: IDA curves for all cases for X direction

4.7 Concluding remarks

NLTHA has been performed on structure for 12 ground motion records using intensity based scaling approach. From the IDA curves it can be concluded that higher the damping lesser is the demand on structure. However, there are some cases where higher damping is also producing more demand than lower damping. This can be due to difference in hysteretic energy dissipation at different damping and also due to limited number of analysis points.

The variation in support conditions have not followed a particular trend. Though it is seen that for most of cases maximum demand is seen in case of fixed base conditions while minimum demand is seen in case of 0.5G soil base condition. IDA curves for each earthquake show distinct peculiarities and characteristics as per the ground motion frequency content.

5 FRAGILITY RELATIONSHIPS

5.1 Introduction

Fragility theory, a part of structural reliability, helps to determine the vulnerability of a structure when subjected to some extreme load or hazard of known intensity. For seismic hazards, fragility analysis studies the probability that a structure exceeds certain damage state for a given ground motion parameter. Fragility is usually defined as the probability that demand on structure exceeds its capacity conditional on specified hazard intensity. Therefore, seismic fragility is normally expressed as:

$$\text{Fragility} = \Pr[D \geq C | IM] = \Pr[C - D \leq 0.0 | IM] \quad (5.1)$$

Where D = seismic demand; C = seismic capacity; IM = ground motion intensity parameter.

In general, a fragility curve [44] is generated by fitting a statistical model to data on building damage level at different values of the IM. In order to obtain analytical fragility curves, structural response is initially obtained through the analysis of structures subjected to earthquake excitation of increasing intensity. Here, incremental dynamic analysis approach is used. The structural response obtained is expressed in terms of engineering demand parameters (EDPs), which are then compared to properly calibrated thresholds levels for particular damage state or limit states. In the present work, the number of structural analyses required to construct the fragility curve is large as both variability in the structural model/capacity (i.e., modelling uncertainty) and ground motion characteristics are included in the generation of fragility curves.

5.2 Briefing on limit states

Definitions of limit states have a direct effect on the fragility curves. The limit states used in this study are based on interstorey drift ratio for performance levels of Immediate Occupancy (IO), Life Safety (LS) and Collapse Prevention (CP). As per FEMA-356, IO is defined as post-earthquake damage state that remains safe to occupy, essentially retains pre-earthquake design strength and stiffness of structure. LS is defined as post-earthquake damage state that includes damage to structural components but retains a margin against onset of partial or total collapse. CP is defined as post-earthquake damage state that includes damage to structural components such that structure continues to support gravity loads but retains no margin against collapse. The different damage states (FEMA -356) [10] are shown in Table 5.1:

Table 5.1: Drift limits

Damage State	Interstorey Drift Ratio (%)
Immediate Occupancy	2%
Life Safety	4%
Collapse Prevention	6%

5.3 Test for distribution of data

The values of spectral acceleration are generally log-normally distributed. This assumption is checked using histogram and Q-Q plots. From the multi-record IDA curves given in previous chapter, values of Spectral acceleration have been calculated for each damage state for each

direction. The distribution of logarithm of first mode spectral acceleration for limit states of 6% interstorey drift for Y direction analysis is presented in form of histogram below.

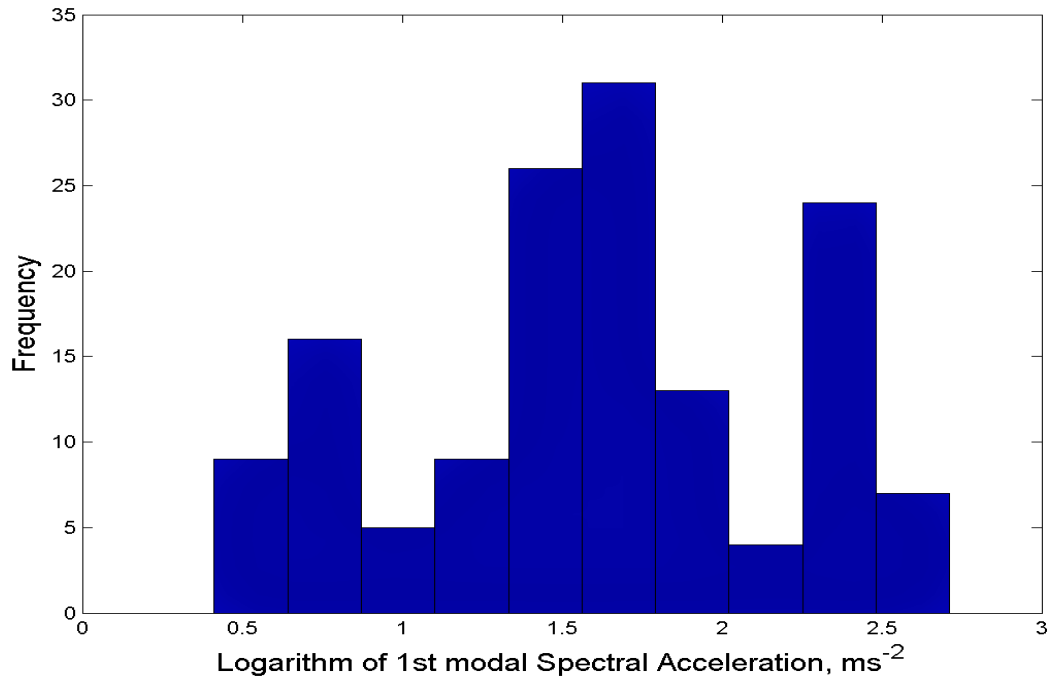


Figure 5.1: Histogram for data distribution of spectral acceleration values

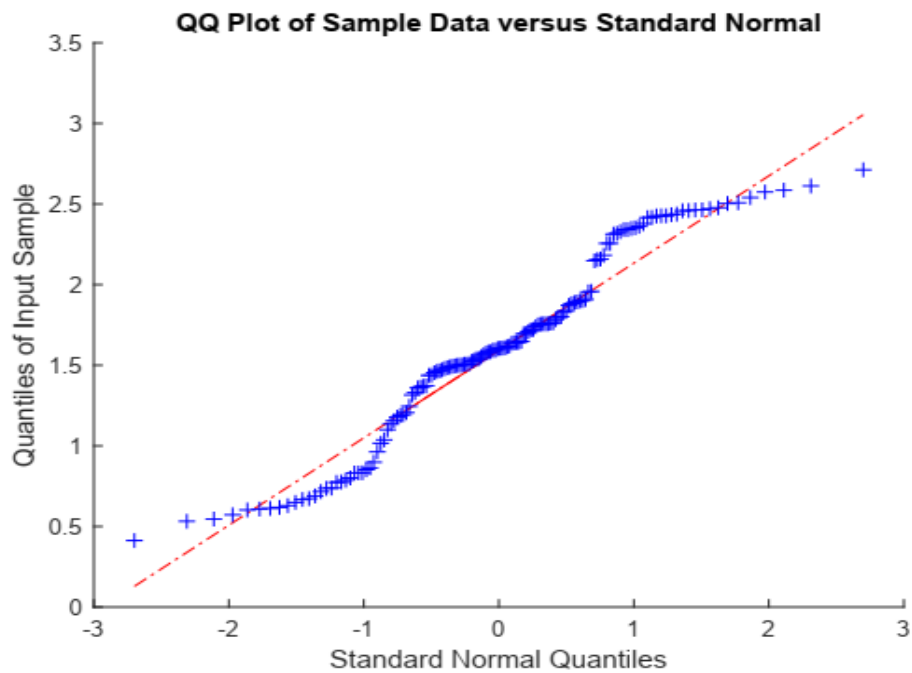


Figure 5.2: Q-Q plot for logarithm of first mode spectral acceleration values

From histogram in Figure 5.1 it is seen that distribution of log values is not perfectly following normal distribution. This may be due to limitation on quantity of data. Only 144 values have been used. Although histograms are good way to predict the distribution of data but the bin size affects their shape. This necessitates using other methods to check whether the log normality assumption is justifiable. Here graphical method known as Q-Q plot was used. In Q-Q plot given in Figure 5.2, the straight line represents standard normal distribution and the other line is representing data of spectral acceleration. It is seen that the sample data distribution is deviating from standard normal distribution near ends. Therefore, the distribution of logarithmic values of spectral acceleration as normal is considered with limited amount of data.

Statistical tests like Kolmogorov–Smirnov distribution tests can also be used.

5.4 Development of fragility curves

Now as per the procedure given in EPRI's report [44], the fragility curves for each damage state for confidence interval of 5%, 50% and 95% is obtained as discussed below:

1. Let $A = \{a_1, a_2, a_3, \dots, a_n\}$ be the set of spectral acceleration values for a particular damage state. Here n is total no. of spectral acceleration values. In this study n is equal to 144.
2. Since the data A is assumed to be log normally distributed, it means that the logarithmic values of data A (say data B) i.e. $B = \log(A) = \{\log(a_1), \log(a_2), \dots, \log(a_n)\}$ will be normally distributed.
3. Let μ be mean and β be standard deviation of data B .
4. Therefore, the median is given by $a = \exp(\mu)$.
5. We can characterize the fragility curve by symbol $LN(a, \beta)$ which means the fragility curve is lognormal with median 'a' and logarithmic standard deviation β .

6. The probability of failure $P_f(a)$ at a particular acceleration a is given by:

$$P_f(a) = \Phi(u), \text{ where } u = \ln(a/a)/\beta \quad (5.2)$$

The variable u is the transformation of lognormal parameters to standardized normal variable and is required so as to use standardized normal distribution $\Phi(u)$ tables given in textbooks and easily available in computer programs like MS-excel.

7. There are two kinds of uncertainty in fragility analysis, one is reducible which is called as uncertainty and other which is not reducible is known as randomness. Now as median capacity is uncertain we account this uncertainty by using different confidence intervals for medians by assuming that median values are also log-normally distributed. Hence sort of double log-normal is used. Here the 5% confidence interval median value is the value above which only 5% of median values lies. Similarly that median value above which 95% of median values exist is called 95% confidence median value. The 50% confidence median value is taken as median calculated from actual data. Therefore,

$$a(50\%) = a \quad (5.3)$$

$$a(5\%) = a \cdot e^{(+1.65\beta)} \quad (5.4)$$

$$a(95\%) = a \cdot e^{(-1.65\beta)} \quad (5.5)$$

Median and standard deviation values for the model along both directions are given in Table 5.2.

8. Then using equation 5.2, normal variable is calculated for each acceleration value and probability of failure value is calculated from standard distribution charts. The plot of probability of failure against first mode spectral acceleration values is known as fragility curve (Figure 5.3).

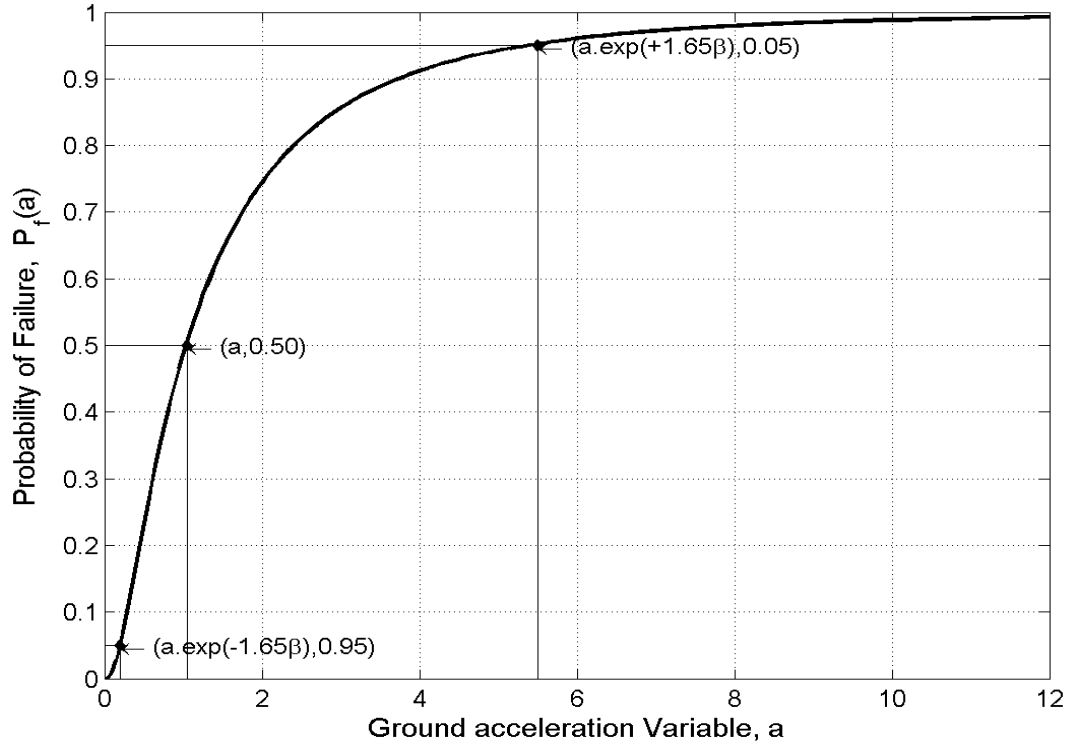


Figure 5.3: Sample fragility curve [44]

Table 5.2: Median and standard deviation for X and Y direction

Direction	Damage State	Mean, μ	Logarithmic Standard Deviation, β	Median for different confidence %		
				a (95%)	a (50%)	a (5%)
X	IO	1.144693	0.667576	1.04414	3.141478	9.451689
	LS	1.436577	0.654512	1.428509	4.206271	12.38545
	CP	1.575513	0.576584	1.866658	4.833218	12.51435
Y	IO	1.408914	0.686457	1.318191	4.091508	12.69956
	LS	1.58231	0.637214	1.700475	4.866183	13.92537
	CP	1.704366	0.610073	2.009218	5.497898	15.0441

5.5 Discussion on fragility curves

The probability of exceedance for 3 limits states of IO, LS and CP can be read from fragility curves given in Figure 5.4 to Figure 5.5. These curves are discussed at spectral acceleration value of 0.40g. The basis for using 0.40g is that for Indian scenario, 0.10g to 0.15g is average pga value. The amplification in pga is usually 2-3 times. Therefore the amplified acceleration value comes out between 0.30g to 0.45g. Hence 0.40g value is used for comparison. It can be observed that the low rise RC frame structure considered in this study has approximately 50% and 60% probability of exceedance of IO at 0.40g of spectral acceleration in Y and X direction respectively (Figure 5.4 and Figure 5.7). For LS, structure has approximately 40% and 50% probability of exceedance at 0.40g of spectral acceleration in Y and X direction respectively (Figure 5.5 and Figure 5.8).

Similarly for CP, structure show 38% and 45% probability of exceedance at 0.40g of spectral acceleration in Y and X direction respectively (Figure 5.6 and Figure 5.9).

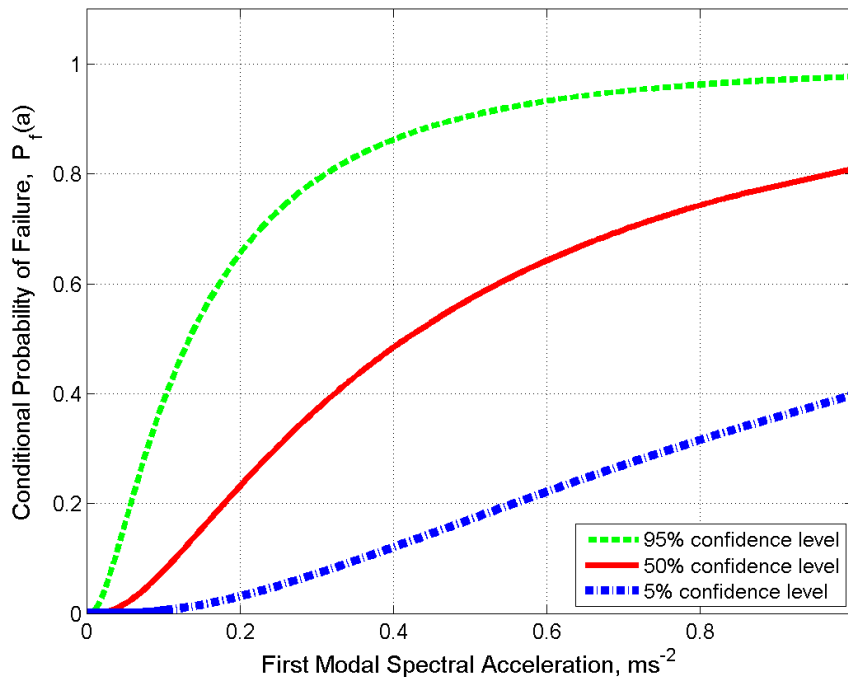


Figure 5.4: Fragility curves for Y direction for IO(2% drift)

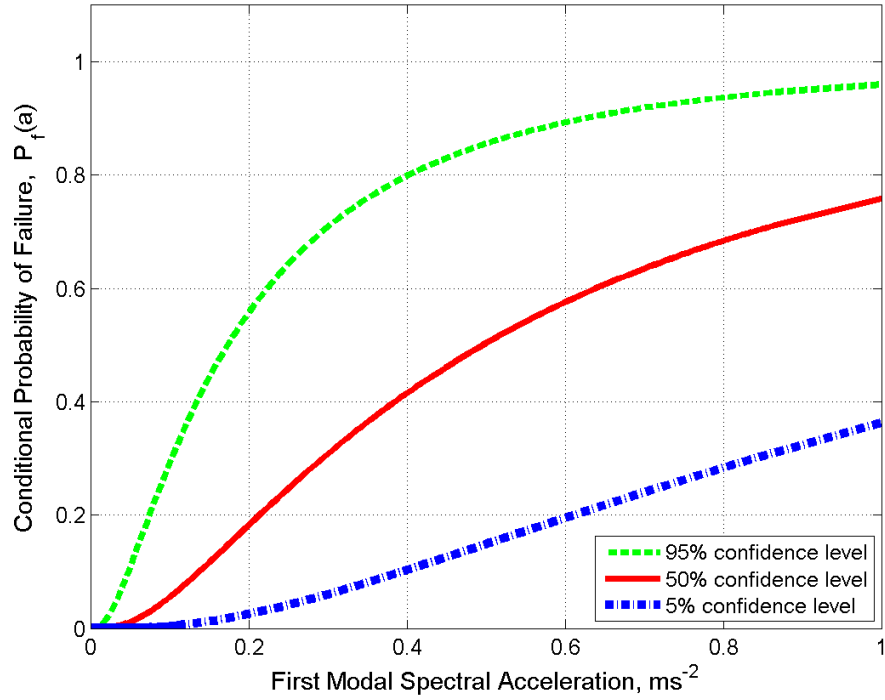


Figure 5.5: Fragility curves for Y direction for LS (4% drift)

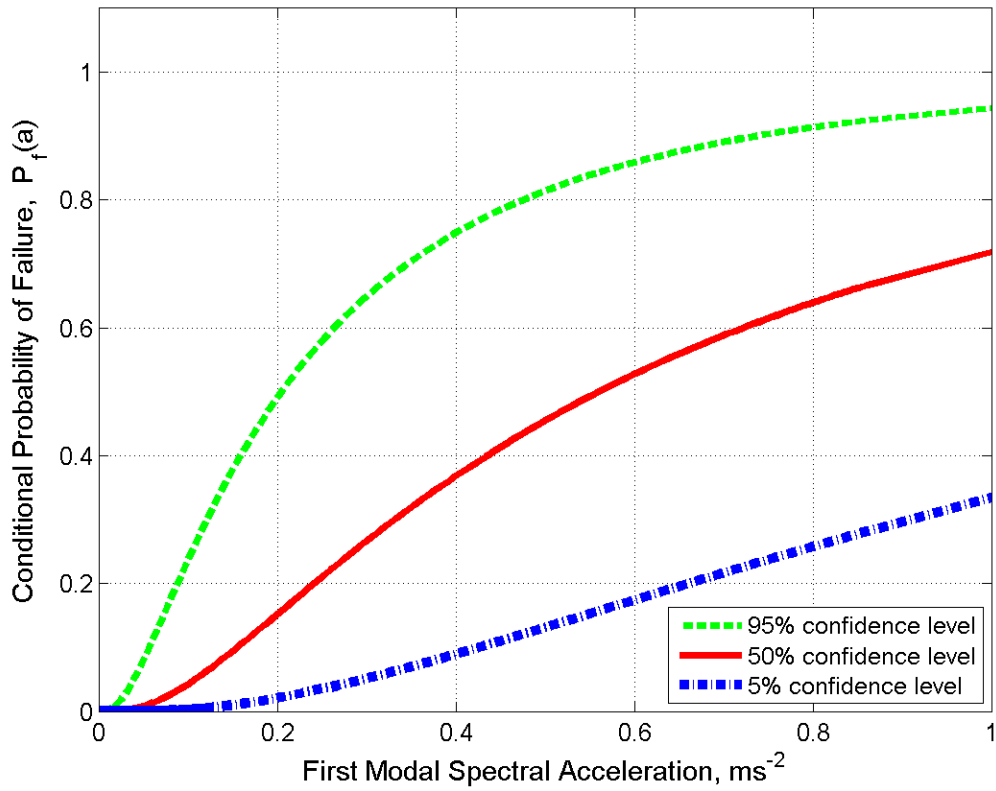


Figure 5.6: Fragility curves for Y direction for CP (6% drift)

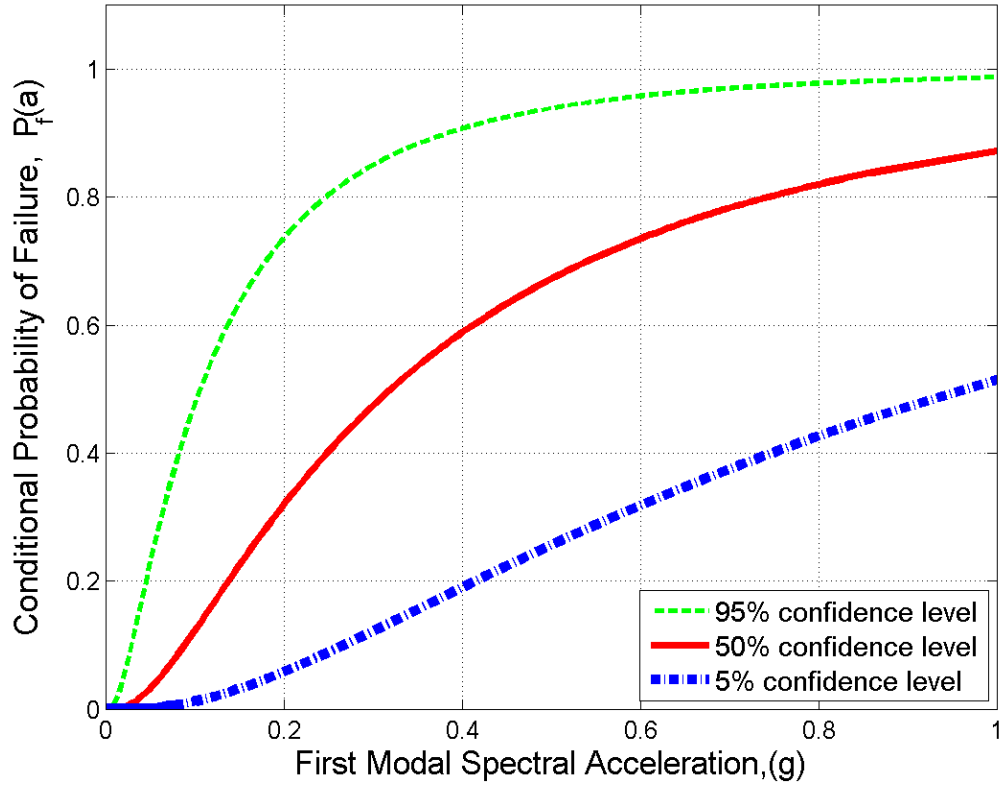


Figure 5.7: Fragility curves for X direction for IO(2% drift)

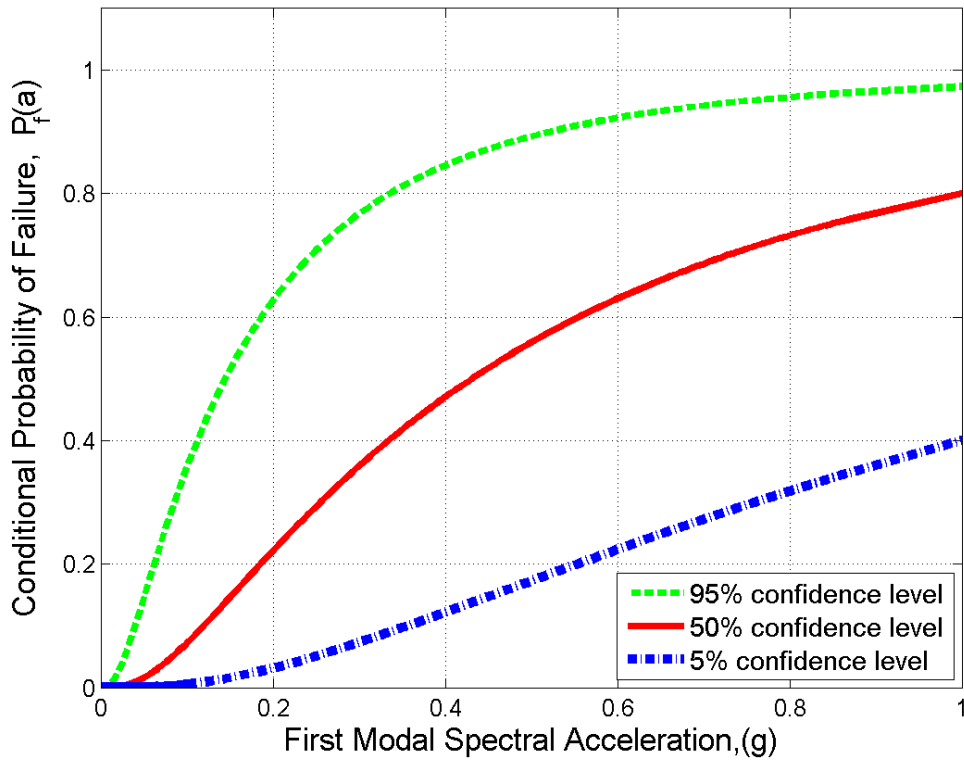


Figure 5.8: Fragility curves for X direction for LS(4% drift)

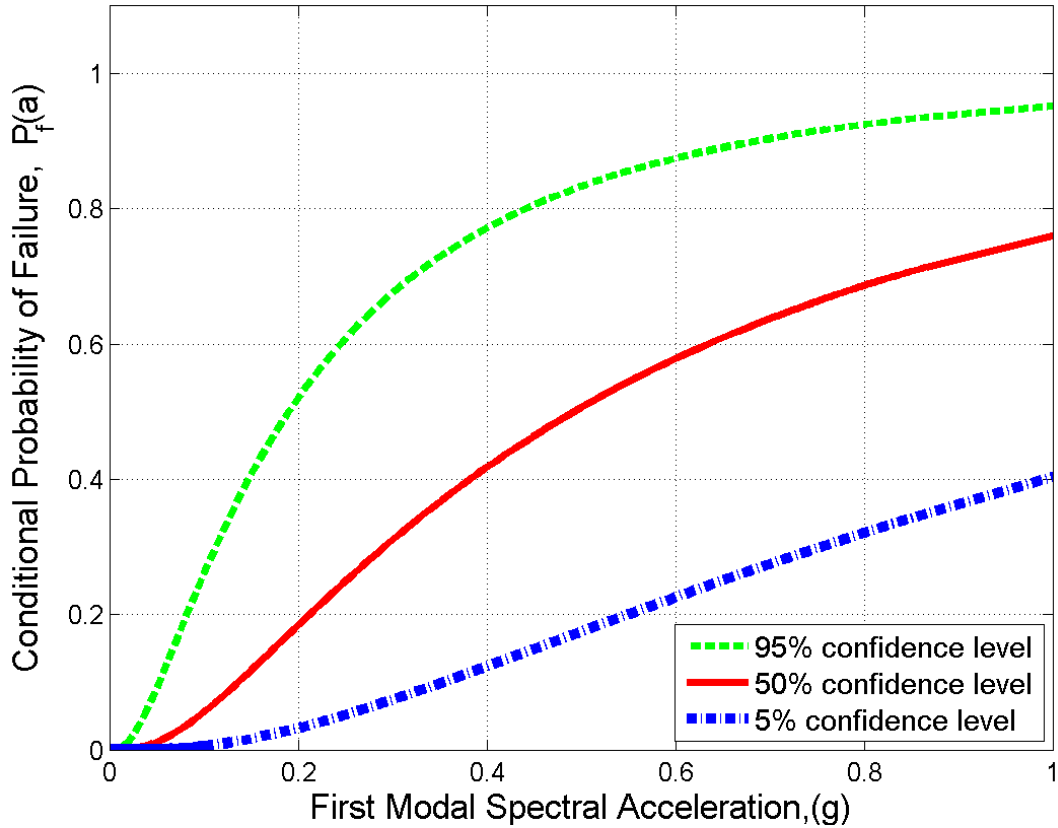


Figure 5.9: Fragility curves for X direction for CP(6% drift)

5.6 Concluding remarks on fragility curves

Fragility curves are developed for confidence levels of 5%, 50 % and 95 % for each performance level. It is observed that the high confidence of low probability of failure value of acceleration for the structure is 0.06g. This acceleration is very low as the structure is an experimental structure and is designed taking into consideration that the structure will deform nonlinearly during high seismic excitation of the region. Moreover, another structure having same dimensions and design reinforcement is placed on base isolators which will be transferring very low acceleration to the structure of the order of 0.05g. Thus purpose of the experiments is to compare the performance of

the two RCC structures, one founded on normal isolated footings and other on isolators when subjected to high seismic excitation of the region.

While obtaining incremental dynamic analysis curves same properties of a given model are considered for entire ground motion record suites and variation in only damping and soil structure interaction is considered. Fragility curves are developed by considering only these uncertainties. Effect of model parameter uncertainties on the seismic performance of the structure is not considered. If these uncertainties like variation in yield load, yield curvature and other hinge properties of the structure are considered then the sample size will be too large. Variability in ground acceleration capacity has been calculated by assuming that when one variable parameter is varied, then other variable parameters are at their mean values. However, for realistic estimation of fragility parameters “Latin Hypercube Sampling (LHS)” would be an efficient sampling technique as compared to the proposed estimation of variability in ground acceleration capacity because it allows the spatial variation of random variables simultaneously. This LHS method can be used in future studies.

6 CONCLUSION

Fragility curves for three storied RC framed structure subjected to real earthquake accelerograms are developed in this study. The Incremental dynamic analysis to be performed for generation of fragility curves is carried out using nonlinear dynamic analysis with pivot hysteretic model for RC structures. The variation in the parameters considered for obtaining IDA curves are uncertainty in ground motion records, variation in structural damping and the soil uncertainty, The results from IDA are compared at different limit states of Immediate occupancy, Life safety and collapse prevention specified by FEMA 356 [10] to develop fragility curves. The following conclusions are derived from the present work:

1. The stiffness of the structures with infill walls is higher than that of the structures without infill and the frequency of the structures with infill is 1.73 times than that of the structures without infill. In the present work the structures with infill are considered. Infills are assumed not to fail by providing measures like steel strips such that out of plane failure can be avoided.
2. The IDA curves for different real earthquakes show different characteristic patterns. IDA curves for El Centro earthquake show weaving behavior in the start and then elasto-plastic behavior. For Northridge earthquake the curve shows almost linear behavior in the start and then sudden softening. In case of Whittier Narrows TH the IDA shows continuous hardening softening behavior. IDA curve of Loma Gilroy2 earthquake shows softening just after 1% drift and then continuous hardening till 9 % drift. Finally, all IDA curves start softening again, showing ever decreasing slopes and then the structure has reached instability can be concluded.

3. It is observed from the IDA curves that the demand of S_a for 7% damping is lower than 5% which in turn is lower than 4% IDA curves. However, there are some regions in curve where the demand is not following this pattern. It is because, hysteretic energy dissipation is different for different damping curves at higher acceleration. At 4 % damping the hysteretic energy dissipated is slightly more than that at 7 % damping and hence the Spectral acceleration attracted at 4 % damping will be lesser than that at 7 % damping.
4. The demand of S_a for different support conditions is not following a fixed pattern. However, for some curves the demand for fixed support case is observed to be higher than spring supports and for other cases the curves have no appreciable difference. In few cases the demand on spring support is coming higher than fixed support case.
5. The structure considered in the study has high probability around 65 % in Y direction and 70% in X direction for reaching performance level of CP at approximately 0.80g spectral acceleration. It can be observed that the low-rise RC frame structure considered in this study has approximately 50% and 60% probability of exceedance of IO at 0.40g of spectral acceleration in Y and X direction respectively.

7 FUTURE WORK

The seismic structural fragilities obtained from conventional IDA has not accurately represented realistic scenario. IDA involves multiplying accelerograms by a scalar factor. However, as per probabilistic seismic hazard analysis (PSHA), the characteristics of ground motion records such as spectral shape etc. vary with IM level. Hence, further research on proper scaling effect to obtain more realistic incremental dynamic analysis curves is to be carried out.

REFERENCES

- [1] ASCE/SEI 4-16, Seismic Analysis of Safety-Related Nuclear Structures.
- [2] D. Vamvatsikos and C. A. Cornell, "Incremental dynamic analysis," *Earthquake Engng Struct. Dyn.*, vol. 31, pp. 31:491-514, 2002.
- [3] (ATC) Applied Technology Council (1985). ATC-13, Earthquake Damage Evaluation Data for California, Redwood City, CA, 492pp.
- [4] A. H. Barbat, M.EERI, F. Y. Moya and J. A. Canas, "Damage Scenarios Simulation for Seismic Risk Assessment in Urban Zones," *Earthquake Spectra*, vol. 12, no. 3, pp. 371-394, 1996.
- [5] S. Freeman, "The Capacity Spectrum Method as a Tool for Seismic Design," in *Eleventh European Conference on Earthquake Engineering*, Paris, 1998.
- [6] M. Shinozuka, M. Feng, T. Naganuma and J. Lee, "Statistical Analysis of Fragility Curves," *ASCE*, vol. 126, no. 12, pp. 1224-1225, 2000.
- [7] A. Abdelnaby, "Fragility curves for RC frames subjected to Tohoku mainshock-aftershocks sequences," *Eathquake Engg*, vol. 22, no. 5, 2016.
- [8] M. A. Erberik, "Fragility-based assessment of typical mid-rise and low-rise RC buildings in Turkey," *Engineering structures(30)*, pp. 1360-1374, 2008.
- [9] T. Rosettio and A. Elnashai, "A new analytical procedure for derivation of displacement based vulnerability curves for population of RC structures," *Engineering Structures*, vol. 27, no. 3, pp. 397-409, 2005.
- [10] FEMA 356, Federal Emergency Management Agency, "Seismic Rehabilitation of buildings," November, 2000.
- [11] FEMA-350, "Recommended Seismic Design Criteria for New Steel Moment-Frame prepared by the SAC Joint Venture for the Federal Emergency Management," Washington,DC, 2000.
- [12] H. Yalciner, S. Sensoy and O. Eren , "Effect of corrosion damage on the performance level of a 25-year-old reinforced concrete building," *Shock and Vibration 19*, pp. 891-902, 2012.
- [13] D. Vamvatsikos and C. A. Cornell, "Applied Incremental Dynamic Analysis," *Earthquake Spectra*, vol. 20, no. 2, pp. 523-553, 2004.
- [14] M. Dolsek, "Incremental dynamic analysis with consideration of modeling uncertainties," *Earthquake Engineering and Structural Dynamics*, vol. 38, no. 6, pp. 805-825, 2009.

- [15] D. Vamvatsikos and M. Fragiadakis, "Incremental dynamic analysis for estimating seismic performance sensitivity and uncertainty," *Earthquake Engineering and Structural Dynamics*, pp. 141-163, 2010.
- [16] A. Azarbakht and M. Dolsek, "Progressive Incremental Dynamic analysis of First mode dominated structures," *Journal of Structural Engineering ASCE*, vol. 137, no. 3, pp. 445-455, March 2011.
- [17] S. Zhu and C.-X. Qiu, "Incremental Dynamic Analysis of Highway Bridges with Novel Shape Memory Alloy Isolators," *Advances in Structural Engineering*, vol. 17, no. 3, pp. 429-438, 2014.
- [18] A. k. Banerjee, D. Pramanik and R. Roy, "Seismic structural fragilities: Proposals for improved methodology per spectral matching of accelerogram," *Engineering structures*, vol. 111, pp. 538-551, 2016.
- [19] F. Hosseinpour and A. Abdelnaby, "Fragility curves for RC frames under multiple earthquakes," *Soil Dynamics and Earthquake Engineering*, vol. 98, pp. 222-234, 2017.
- [20] M. A. Erberik and A. S. Elnashai, "Fragility Analysis of flat-slab structures," *Engineering Structures* 26, vol. 26, no. 7, pp. 937-948, 2004.
- [21] A. B. Liel, C. B. Haselton, G. G. Deierlein and J. W. Baker, "Incorporating modelling uncertainties in assessment of seismic collapse risk of buildings," *Structural safety*, vol. 31, no. 2, pp. 197-211, 2009.
- [22] B. Asgarian, M. Yahyai, M. Mirtaheri, H. R. Samani and P. Alanjari, "Incremental Dynamic Analysis of High Rise Towers," *The Structural Design of Tall and Special Buildings*, vol. 19, no. 8, pp. 922-934, 2010.
- [23] C.-L. Lee and R. K. L. su, "Fragility analysis of low rise masonry infilled reinforced concrete buildings by a coefficient based spectral acceleration method," *Earthquake Engineering and structural Dynamics*, pp. 697-713, 2012.
- [24] T. K. Mondal, S. Ghosh and N. N. Pujari, "Seismic Fragility analysis of typical Indian PHWR containment: Comparison of fragility models," *Structural Safety* 58, pp. 11-19, 2016.
- [25] T. Liu, Z. Chen, Y. Yuan and X. Shao, "Fragility analysis of a subway station structure by incremental dynamic analysis," *Advances in Structural Engineering*, vol. 20(7), pp. 1111-1124, 2017.
- [26] F. Basone, L. Cavaleri, F. D. Trapani and G. Muscolino, "Incremental dynamic based fragility assessment of reinforced concrete structures: Stationary vs. non-stationary artificial ground motions," *Soil Dynamics and Earthquake Engg.*, vol. 103, pp. 105-117, 2017.

- [27] D. S. Moon, Y.-J. Lee and S. Lee, "Fragility Analysis of Space Reinforced Concrete Frame Structures with Structural Irregularity in Plan," *Journal of Structural Engg*, vol. 144, no. 8, 2018.
- [28] M. Inel and H. B. Ozman, "Effects of plastic hinge properties in nonlinear analysis of reinforced concrete buildings," *Engineering structures*, vol. 28, no. 11, pp. 1494-1502, 2006.
- [29] ATC-40, "Seismic Evaluation and Retrofit of Concrete Buildings," California Seismic Safety Commission, California, 1996.
- [30] A. Sharma, G. Reddy, K. Vaze, A. Ghosh, H. Kushwaha and R. Eligehausen, "Experimental and Analytical Investigation on Behavior of Scaled Down Reinforced Concrete Framed Structure Under Monotonic Pushover Loads," BARC, 2008.
- [31] IS 456:2000, Indian Standard, Plain and Reinforced concrete- Code of Practise. Bureau of Indian Standards, New Delhi.
- [32] Kent, D.C and Park, "Flexural Mechanics with confined concrete," *ASCE, Vol.97*, pp. 1969-1990, 1971.
- [33] IS 1893 (Part 1): 2016, Indian Standard, Criteria for Earthquake Resistant Design of Structures, Bureau of Indian Standards, New Delhi.
- [34] G. Mondal and S. K. Jain, "Lateral stiffness of Masonry infilled RC frames with central opening," *Earthquake Spectra*, vol. 24, no. 3, pp. 701-723, 2008.
- [35] T. E. Kelly and J. D. Chambers, "Analysis Procedure for Performance Based Design," in *WCEE*, 2000.
- [36] T. Caughey and M. O'Kelly, "Classical Normal modes in Damped Linear Dynamic Systems," *J. Applied Mechanics*, vol. 32, no. 3, pp. 583-588, Sep, 1965.
- [37] A. Chopra, *Dynamics of Structures: Theory and Applications to Earthquake Engineering*, Prentice-Hall: Eaglewood Cliffs, NJ, 1995.
- [38] American Society of Civil Engineers (2005), *ASCE 7-05 Minimum Design Loads for Buildings*, Reston, VA..
- [39] E. Kalkan and A. K. Chopra, "Practical Guidelines to Select and Scale Earthquake records for Nonlinear Response History Analysis of Structures," EERI, 2010.
- [40] T. Takeda, M. Sozen and N. Nielsen, "Reinforced Concrete Response to Simulated Earthquakes," *J. Struct. Engrg. Div., ASCE, V.96, No.12*, pp. 2257-2573, 1970.
- [41] R. K. Dowell, F. Seible and E. L. Wilson, "Pivot Hysterisis Model for Reinforced Concrete Members," *ACI Structural Journal*, vol. 95, pp. 607-617, 1998.

- [42] A. Sharma, G. Reddy and K. Vaze, "Experimental and numerical investigations on as-built and retrofitted RC frames under Dynamic Earthquake loading," 2013.
- [43] N. Shome, A. Cornell, P. Bazurro and J. Carballo, "Earthquakes, records and non linear responses," *Earthquake Spectra*, vol. 14, no. 3, pp. 469-500, 1998.
- [44] "Methodology for developing Seismic Fragilities, EPRI TR-103959," Electrical Power Research Institute, Palo Alto, California, 1994.
- [45] D. Vamvatsikos and M. Fragiadakis, "Incremental dynamic analysis for seismic performance sensitivity and uncertainty," *Earthquake Engineering and Structural Dynamics*, vol. 39, no. 2, pp. 141-163, 2010.
- [46] M. Günay and K. Mosalam, "PEER Performance Based Earthquake Engineering Methodology, Revisited," *Journal of Earthquake Engineering*, vol. 17, no. 6, pp. 829-858, 2012.
- [47] P. Deng, S. Pei, J. W. V. d. Lindt, H. Liu and C. Zhang , "An approach to quantify the influence of ground motion uncertainty on elastoplastic system acceleration in incremental dynamic analysis," *Advances in structural Engineering*, vol. 20, no. 11, pp. 1744-1756, 2017.